Antigen Receptors and Accessory Molecules of T lymphocytes

Chp. 7 Cellular and Molecular Immunology

-Abul K. Abbas-

T cell receptor and accessory molecules

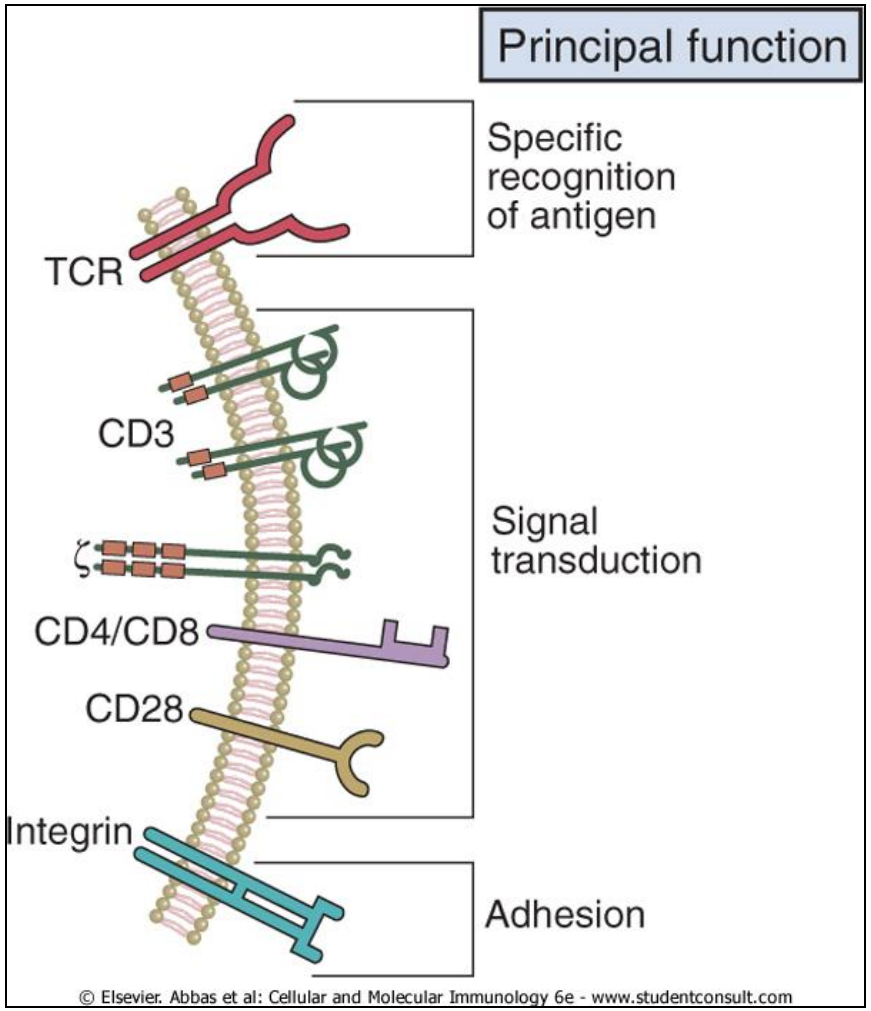

- TCR: polymorphic MHC (MHC restriction)
  peptides displayed by MHC
- CD3: non-covalent link to TCR
  signal transduction
  → form TCR complex

- Co-receptor: CD4 or CD8
- CD28 : second signal
- Adhesion molecules.

Antigen recognition and signaling function of lymphocyte antigen receptor

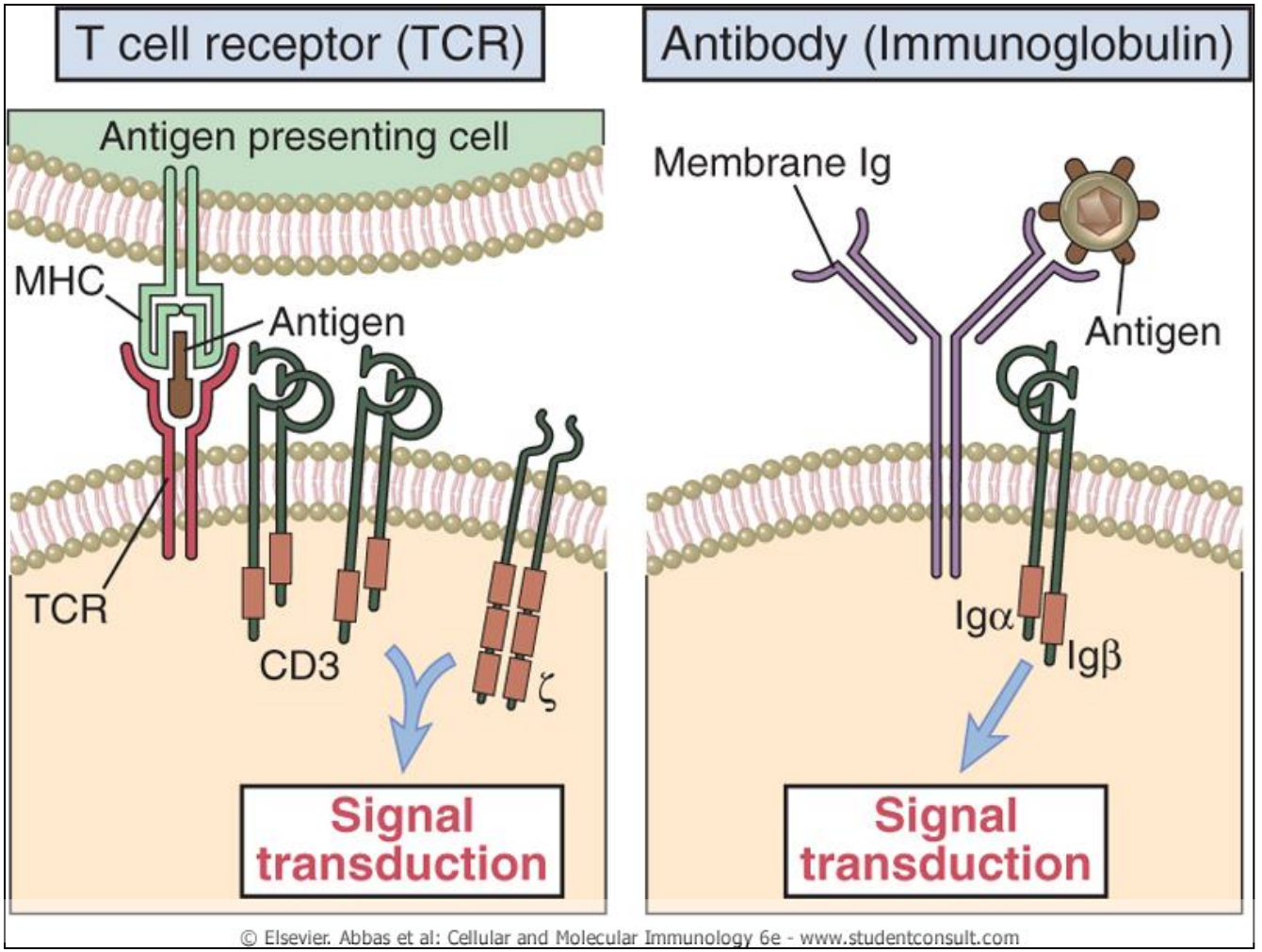

Identification of TCR

Purification of TCR molecule for biochemical studies

1. Generation of monoclonal T cell populations: all the cells express the same TCR
   : tumors derived from T lymphocytes
   : T-T hybridoma
   : antigen-specific T cell clones

2. Generation of antibody specific for idiotypic determinants of the TCR of clonal T cell population

→ Purification of TCR using the idiotypic antibody & amino acid sequencing

Identification of TCR

Cloning of the gene encoding TCRs
unique expression in T cells/ somatic recombination / homologous to Ig genes

1. Substractive hybridization: T cell specific genes
   cDNA from T cells
   → hybridization to B cell mRNA
   → separation of non-hybridized cDNAs
   → southern blotting : different structure in non- T cells than in T cells

2. Predicted amino acid sequence =the partial sequence obtained from putative TCR proteins purified from TCR-idotypic Ab

Crystallographic structure study
: provides insight into how TCR recognizes peptide/MHC complexes

Structure of the αβ TCR

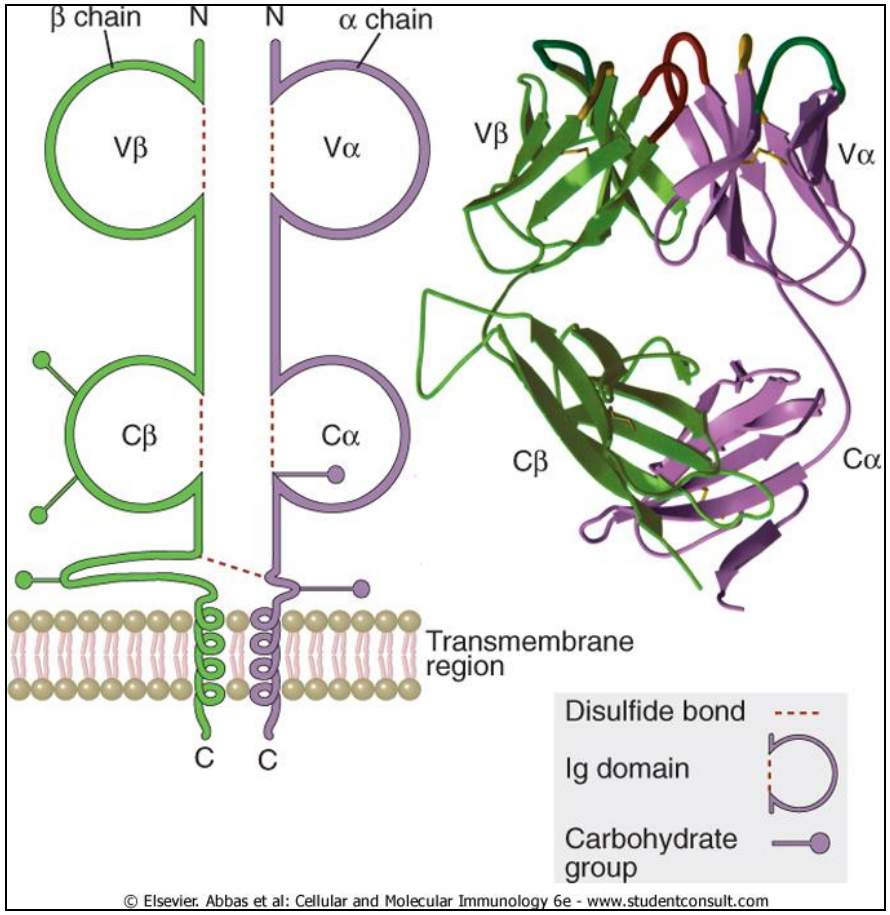

Heterodimeric complex
: α and β chains

Extracellular portion : one variable (V) domain + one constant domain

+ a hydrophobic transmembrane region
+ a short cytoplasmic region

Structure of the αβ TCR

•V regions of TCR α and β chains
: hypervariable region : complementary-determining regions (CDR 1,CDR2, CDR3)

→Juxtaposed to form contact region and recognizes peptide/MHC complexes

•CDR3 region : V-J and V-D-J
contain junctional sequence encoded by added nucelotides
(N regions & P nucleotides)
concentration of variability

Role of the αβ TCR in the Recognition of MHC-Peptide

Peptide/MHC recognition by CDRs formed by α and β chains of TCR
: participation of 6 CDRs of α and β chains of TCR

CDR1 loops of α and β chains ; positioned over the ends of bound peptide
CDR2 loops of α and β chains ; over the helices of the MHC molecule
CDR3 loops of α and β chains ; over the center of the MHC-assodiated peptide

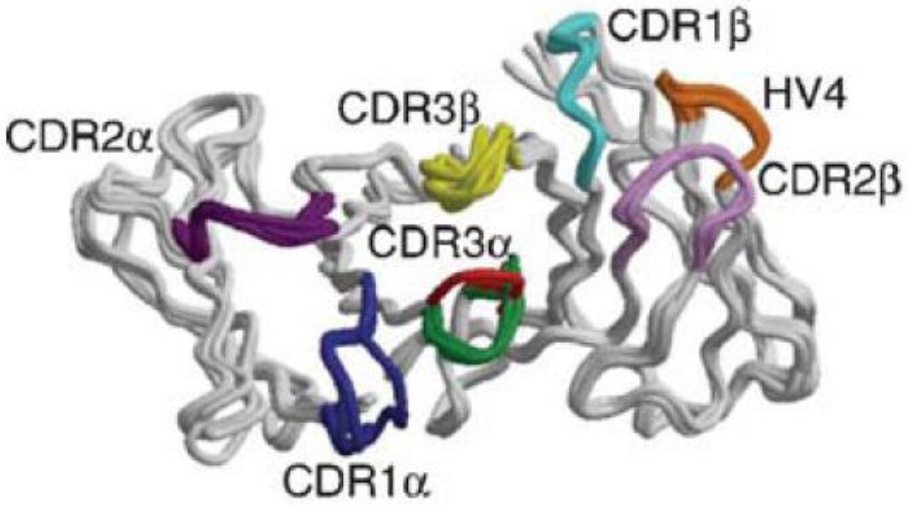

2C

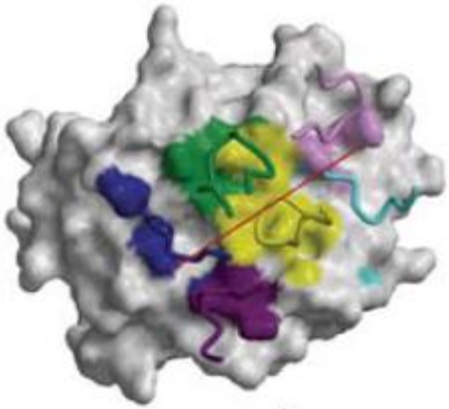

BM3.3/H-2K^{b}/VSV

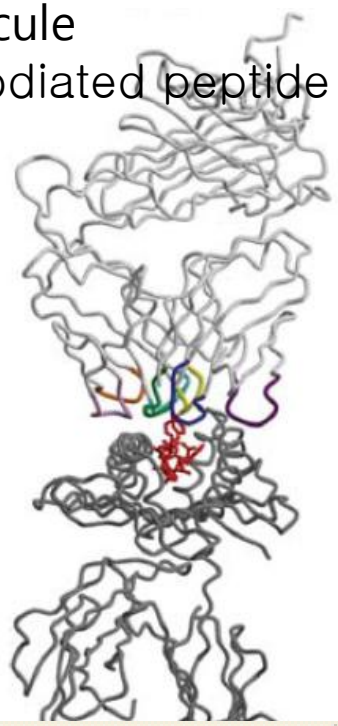

Annu. Rev. Immunol.
2006. 24:419–466

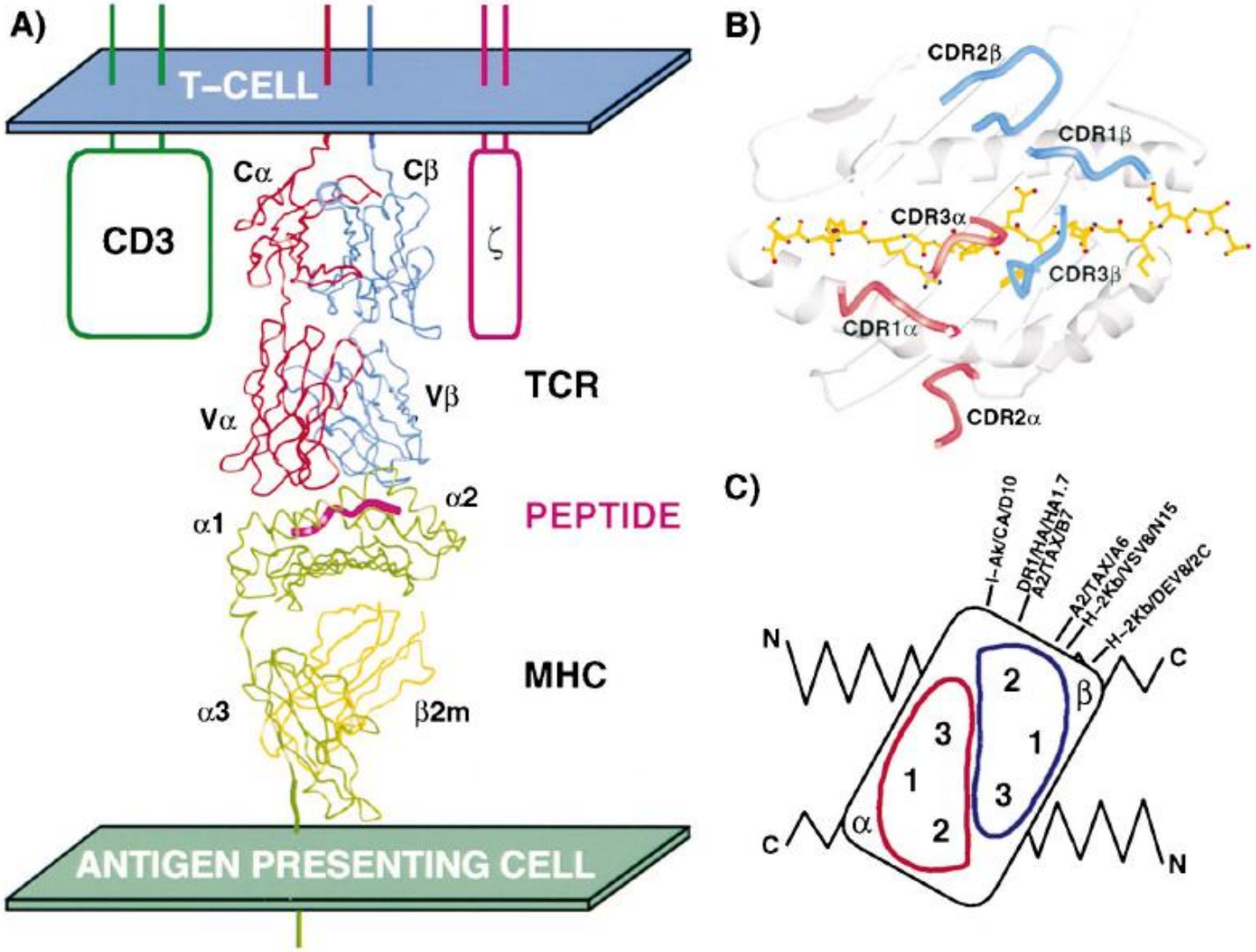

Figure 1. TCR/Peptide/MHC Complexes

(A) Overall view between cells (Garcia et al., 1998). (B) CDR placement over the peptide/MHC surface (Reinherz et al., 1999). (C) Range of TCR binding modes in TCR/peptide/MHC complexes. Short lines by the TCR labels indicate the angles at which each TCR binds across the peptide/MHC surface. (TCR counterclockwise: Garcia et al., 1998; Teng et al., 1998; Ding et al., 1998; Garboczi et al., 1996; Hennecke et al., 2000; Reinherz et al., 1999).

Structure of the αβ TCR

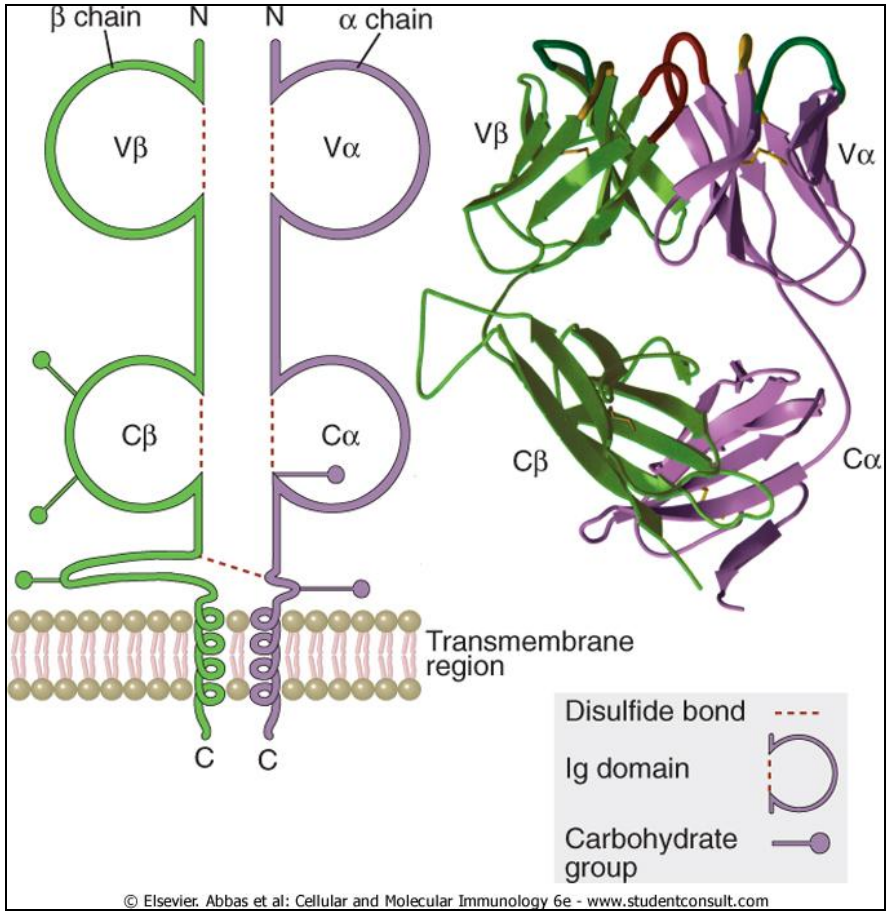

•C regions : cystein residue
→ disulfide bond

•TM region : lysine residue (α chain) and lysine and arginine residues (β chain) → interact with negatively charged CD3 chains

•Cytoplasmic region : 5 ~12 amino acid : too short for delivering signal

•Different from BCR
: no secretion of the TCR
no isotype switching of TCR
no Somatic mutations of TCR

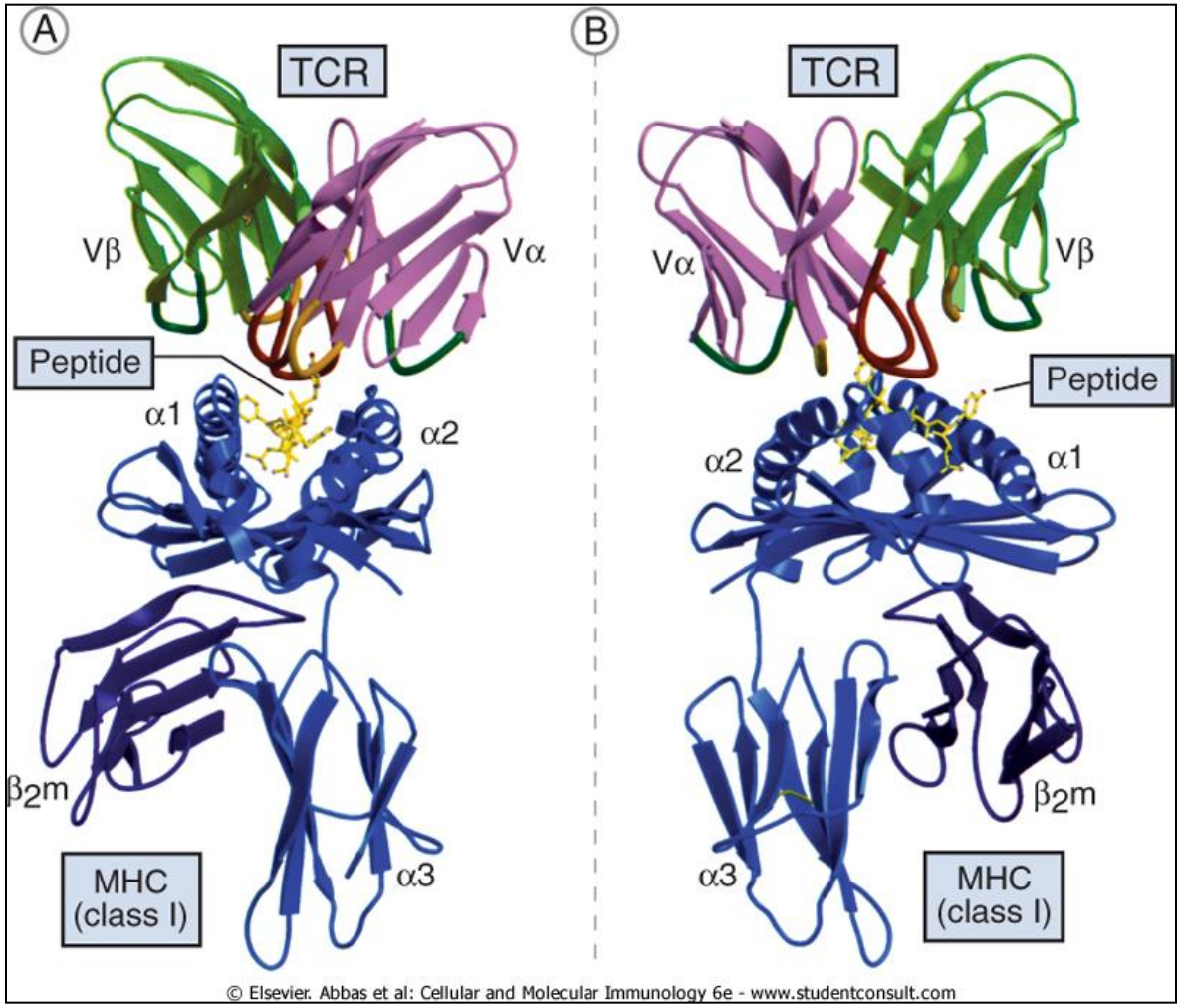

Binding of a TCR to a peptide/MHC complex

Role of the αβ TCR in the Recognition of MHC-Peptide

•Side chains of only **one or two** amino acid residues of the MHC-bound peptide make contact with the TCR

→Remarkable ability of T cells to distinguish among diverse antigens on the basis of very few amino acid differences

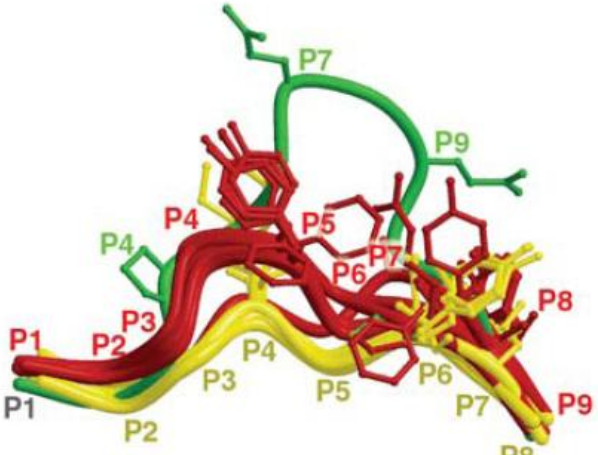

Peptides associated with MHC I

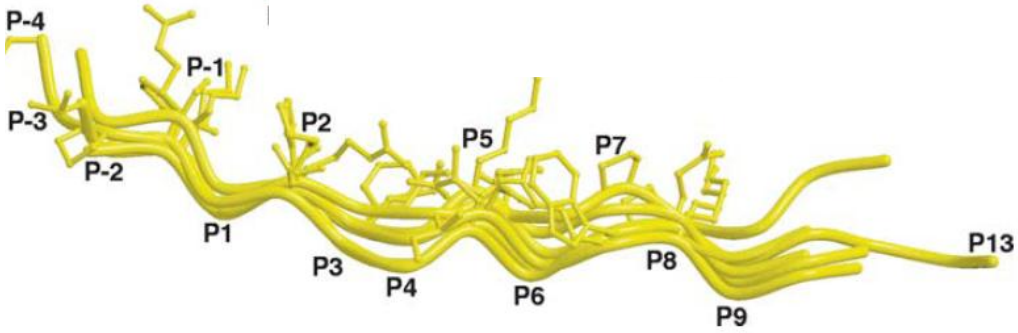

Peptides associated with MHC II

Annu. Rev. Immunol. 2006. 24:419–466

Role of the αβ TCR in the Recognition of MHC-Peptide

- Low affinity of TCR for peptide-MHC complexes
  : dissociation constant (K_d) in a range of 10^{-5} ~ 10^{-7}
  need of adhesion molecule for stable binding of T cells to APCs:
  prolonged or repeated engagement

- Immunological synapse
  TCR and accessory molecules in T cell mem - peptide/MHC in APCs
  supramolecular structure → regulate TCR-mediated signal transduction

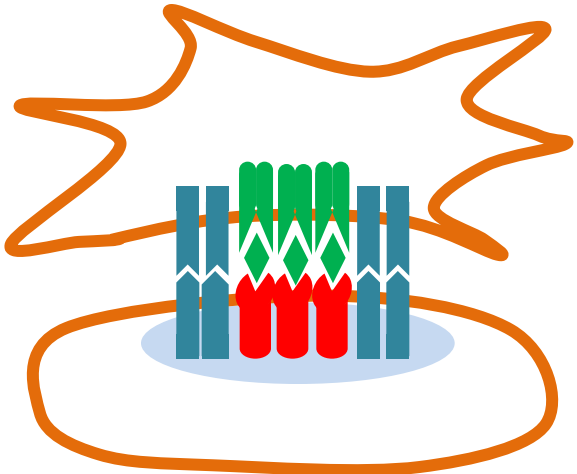

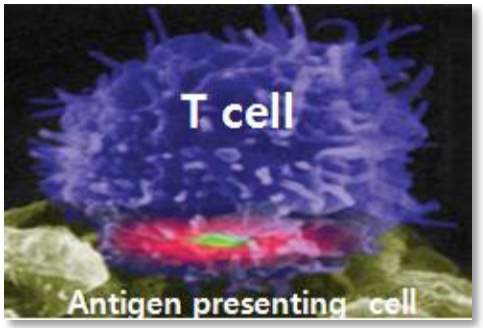

CD3 and ζ proteins in the TCR complex

- Noncovalently associated with TCR αβ heterodimer : CD3 γ ε– δ ε- ζζ
- transduce signals for T cell activation

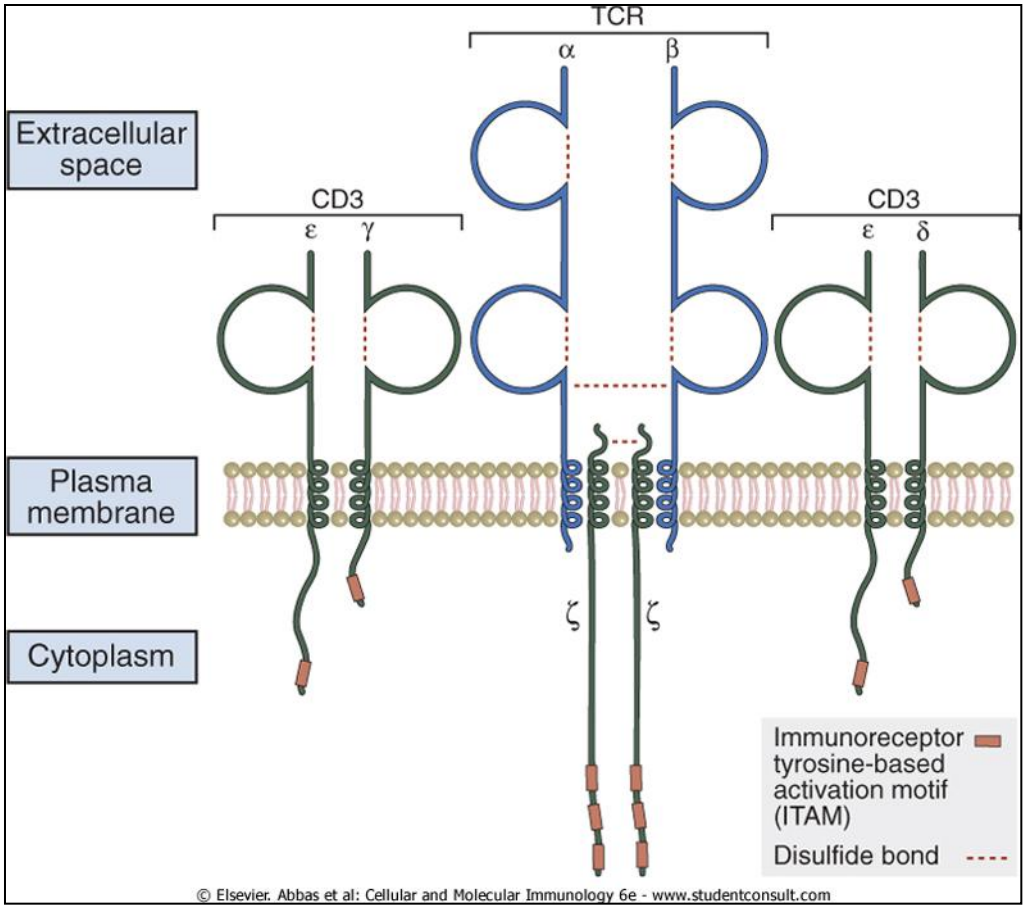

Structure and Association of CD3 and ζ proteins

- Ab against TCR αβ heterodimer or against CD3 any chain → coprecipitate each other from solubilized TCR plasma membrane
- Treatment of anti-CD3 or anti-TCR TCR αβ → endocytosis and disappearance of entire TCR complexes from the cell surface

Structure and Association of CD3 and ζ proteins

- All the CD3 proteins; negatively charged aspartic acid residue
  → binds to positively charged resides of TCR αβ at TM region

- ITAM : Immuereceptor Tyrosine-based Activation Motif
  YXXL/I $(X)_{6-8}$YXXL/I

- Cytoplasmic domain of CD3 γ δ ε ; 44 ~81 amino acid residues long
  one copy of ITAM motif
- Cytoplasmic domain of CD3ζ : 113 amino acid & three copy of ITAM

Structure and Association of CD3 and ζ proteins

- **The expression of TCR complex requires synthesis of all its components**

- During T cell development in the thymus

Synthesis of CD3 and ζ proteins → TCR TCR αβ expression

Retain individual members of TCR complex in the ER before the complex is fully assembled : Calnexin (chaperon)

- In Mature T cells

Entire TCR complex is assembled in the ER and transported to the cell surface

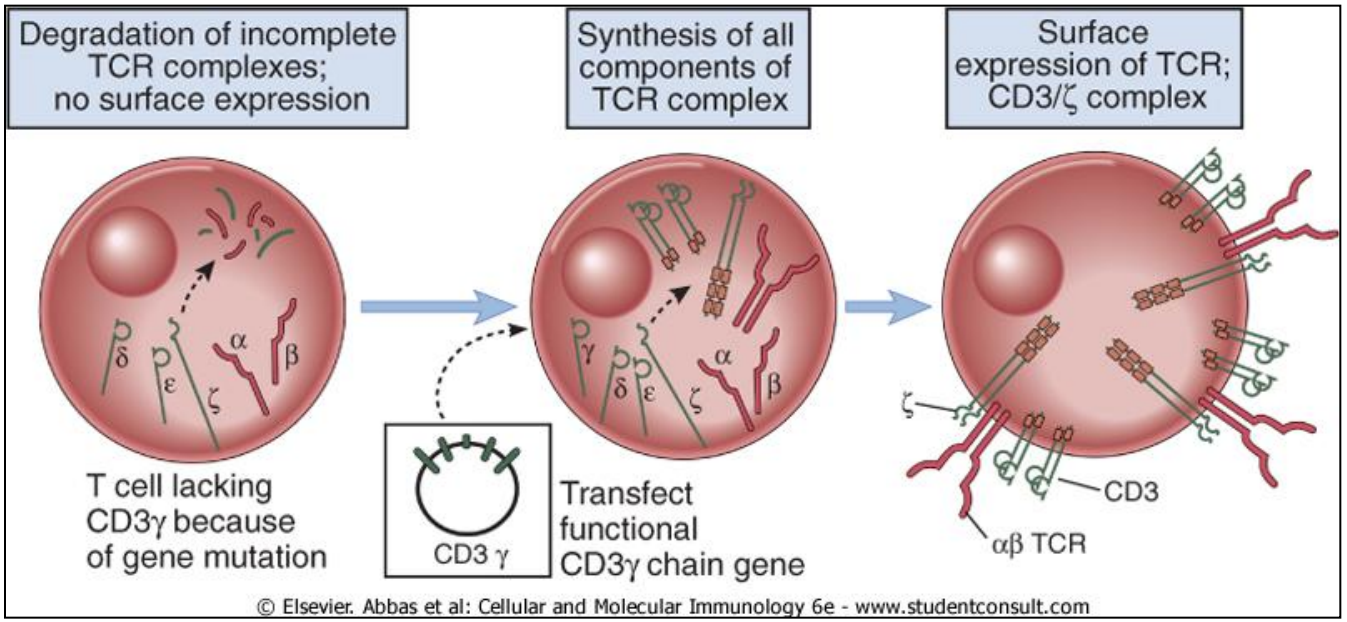

Assembly and surface expression of the TCR complex

Function of CD3 and ζ proteins

- link antigen recognition by TCR – biochemical events leading to functional activation of T cells
- Anti-CD3 Abs stimulate T cell functional response : polyclonal activator of T cells
- Cytoplsmic tail of either CD3 ε or the ζ protein is sufficient to transduce signals necessary for T cell activation : genetically engineered chimeric molecules containing cytoplsmic protion of CD3 ε or the ζ protein

Coreceptors and Costimulatory Receptors in T cells

- Coreceptor

: membrane proteins that enhance TCR signaling

can bind to MHC molecules and recognize a part of the same ligand (peptide/MHC complexes)

- Costimulatory receptors

: deliver activating signals to T cells

recognize molecules on APCs that are not part of the pep/MHC

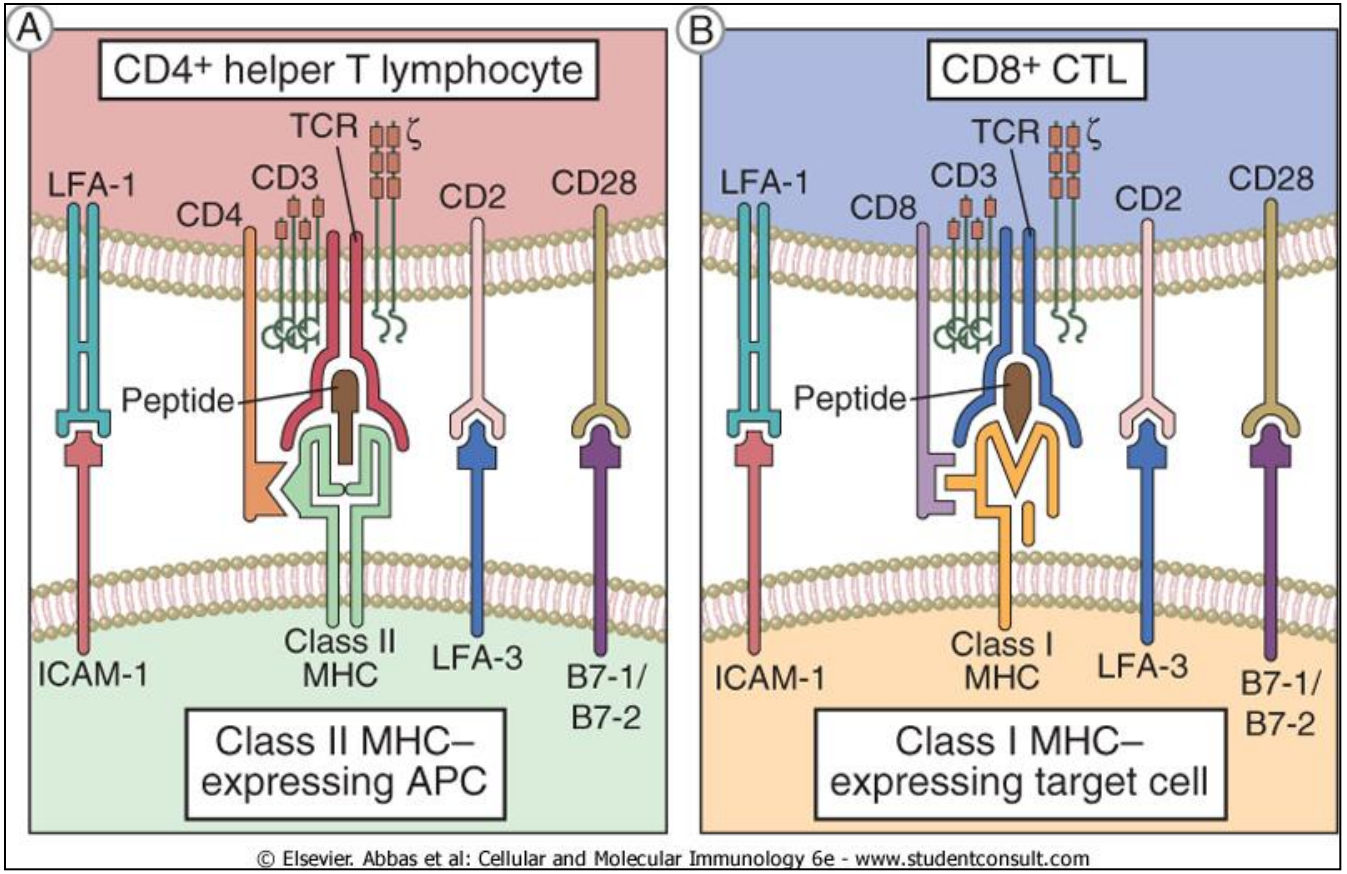

Accessory molecules of T lymphocytes

CD4 and CD8
: Coreceptors involved in MHC-restricted T cell activation

- Bind to nonpolymorphic regions of MHC molecules & facilitate signaling by the TCR complex
- Strengthen the binding of T cells to APCs
- CD4 bind to MHC II / CD8 to MHC I

Structure of CD4 and CD8

- Both : Ig superfamily transmembrane glycoprotein

- **CD4 :** monomer

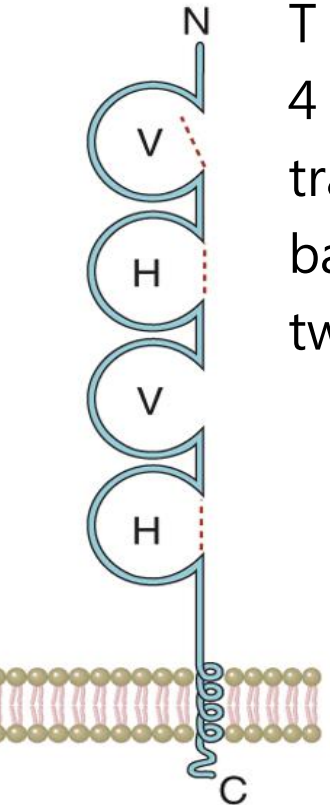

  T cells, thymocytes, mononuclear phagocytes, DC
  4 extracellular Ig-like domains
  transmembrane region
  basic cytoplasmic tail with 38 amino acid
  two Ig-like domain bind to nonpolymophic β2 domain of MHC II

Structure of CD4 and CD8

- **CD8:** disulfide-linked α β heterodimer
  single extracellular Ig domain
  hydrophobic transmembrane
  basic cytoplasmic tail with 25 amino acid
  Ig-like domain binds to nonpolymophic α3 domain of MHC I

- Some CD8 T cells express α α homodimers

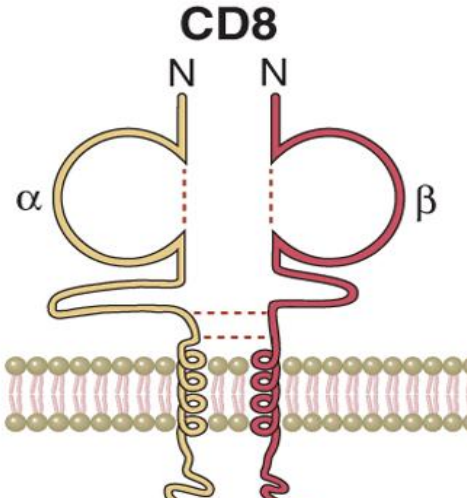

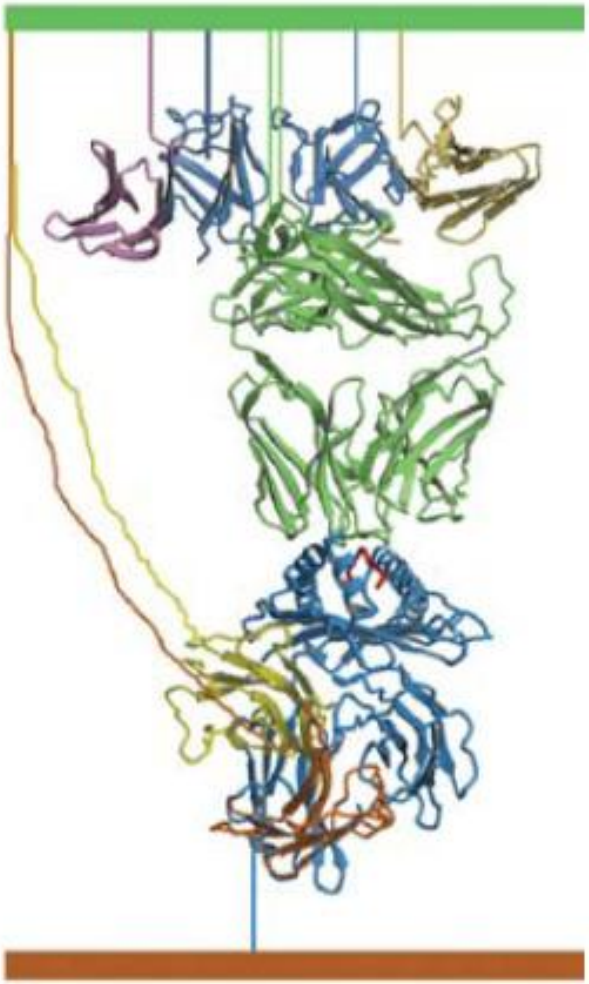

Annu. Rev. Immunol.
2006. 24:419–466

Hypothetical TCR/pMHC/CD3εδ/CD3εγ/CD8 complex. The TCR/pMHC-CD8αα and putative CD8αβ interaction is modeled by superimposing two structures, the HLA-A2/CD8αα complex (1akj) and the TCR A6/HLA-A2/TaxP6A complex (1qrn) on their MHC residues α1–180, with TCR (*green*), MHC (*dark blue*), peptide (*red*) and CD8 (*yellow* and *orange*). The CD3εδ (1xiw, *pink* and *blue*) and CD3εγ (1sy6, *gold* and *blue*) are shown "docked" at the top of the figure, with the common ε-chains colored in blue. This "docking" merely represents placing of the CD3 structures in the vicinity of where they are thought to bind, roughly following the cartoon diagram in Reference 125. Lines are drawn in to depict tethers connecting the different subunits to the TCR cell membrane (*top*, *green*) or the antigen-presenting cell membrane (*brown*, *bottom*).

Functions of CD4 and CD8

Selective binding to MHC molecules

- CD4 binding to MHC II : CD4 T cell binds to MHC II expressed on APCs
- CD8 binding to MHC I : CD8 T cell binds to MHC I expressed on APCs

- Anti-CD4 Ab selectively block the stimulation of MHC II-restricted T cells by APCs
- Anti-CD8 Ab selectively block killing of target cells by MHC I-restricted CTLs
- Transfection of TCR α and β genes into CD4 negative T cells → non-responsive to relevant MHC II-peptide
- CD4 binding or CD8 binding domain mutant of MHC II or MHCI : unable to activate corresponding T cells
- CD4 or CD8 KO mouse do not contain mature MHC II or MHC I-restricted T cells

Functions of CD4 and CD8

Participation in early events of TCR signaling

- Lck association with CD4 and CD8 cytoplasmic domain
- Lck KO → thymic development arrest
- CD4 KO mouse → re-introduction of WT CD4 vs mutant CD4
- Simultaneous binding of CD4 or CD8 to MHC molecules
  → Lck gets close to TCR complex
  → phosphorylation of ITAMs of CD3 molecules

Costimulatory and Inhibitory Receptors of the CD28 family

- CD28 : signal 2
  90% of CD4 T cells and 50% of CD8 T cells
  disulfide-linked homodimers
- CD28 ←→ CD80 and CD86 on DC, macrophage and B cells
  deliver signals to T cells : anti-apoptotic proteins
  growth factors and cytokines
  proliferation and differentiation
  second signal for T cell activation

- CTLA-4 (CD152) : recently activated CD4 and CD8 T cells
- CTLA-4 ←→ CD80 and CD86
  inhibit T cell activation

Costimulatory and Inhibitory Receptors of the CD28 family

Activation

- CD28
- ICOS (inducible costimulator)

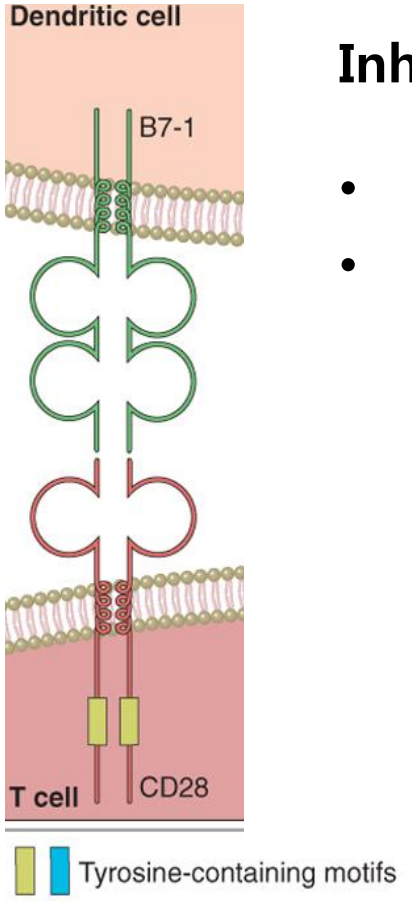

Inhibition

- CTLA-4
- PD-1

CD2 and the SLAM Family of Costimulatory Receptors

- **CD2:** 90% of mature T cells, 50 ~70% of thymocytes and NK cells
  two extracellular Ig like domain
  interact with LFA-3 (CD58) in human / CD48 in mouse
  intercellular adhesion and signal transducer

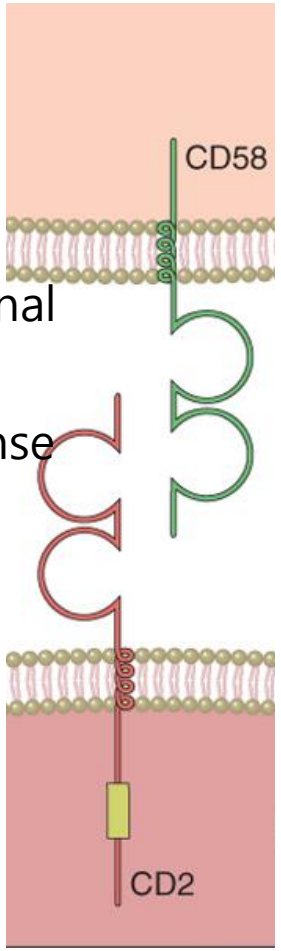

Anti-CD2 Ab treat → cytokine secretion increase, enhance TCR signal
→ block cellular conjugate formation
→ inhibit CTL function and helper T cell response

Double KO of CD2 and CD28 :
more profound defect in T cell response than single KO
redundant function

CD2 and the SLAM Family of Costimulatory Receptors

SLAM (singnaling lymphocytic activation molecule)

two extracellular Ig like domain

in cytoplasmic tail : ITSM (immunoreceptor tyrosin-based switch motif) like ITIM

- homophilic interaction : SLAM on T ←→ SLAM on DC
- SAP (SLAM-associated protein) : ITSM down stream

  SH2 domain: bridge between SLAM and Fyn

  mutation→ XLP (X-linked lymphoproliferative syndrom)
- Costimulatory

- **2B4 (CD48) :** ligand for CD2
- ITSM motif, binds to SAP, recruit Fyn
- deficiency → XLP patients

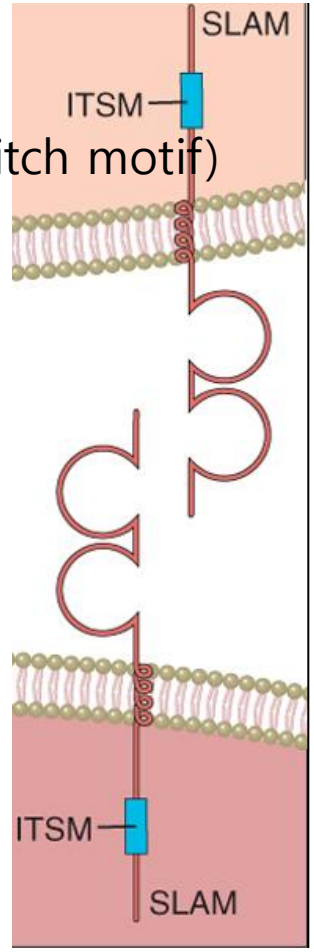

Other Accessory Molecules on T cells

- involved in T cell activation, migration, effector functions, regulation

- **CD44:** acidic sulfated membrane glycoprotein
  alternatively spliced and variably glycosylated forms
  recently activated T and memory T
  binds hyaluronate
  responsible for retention of T cells in extravascular tissues at infection sites
  binding of activated and memory T cells to endothelium at inflammation sites

- **CD40L :** activated CD4 T cells
  trimeric surface protein of TNF family
  binds to CD40 on B, macrophage, DC, endothelial cells
  helper function for B cell stimulation, DC activation, macrophage activation

Other Accessory Molecules on T cells

- **Fas L** : on activated T cells, trimeric molecule
  lignd of CD95 (Fas)
  apoptosis of T cells
  elimination of repeatedly stimulated T cells

- Activated T cells: secret cytokine→ growth and differentiation factor
  express cytokine receptor

How TCRs Bind MHCs, Peptides, and Coreceptors

Markus G. Rudolph,[1] Robyn L. Stanfield,[2] and Ian A. Wilson[2,3]

[1]Department of Molecular Structural Biology, University of Göttingen, 37077 Göttingen, Germany; email: mrudolp2@gwdg.de

[2]Department of Molecular Biology, The Scripps Research Institute, and [3]The Skaggs Institute for Chemical Biology, La Jolla, California 92037; email: robyn@scripps.edu, wilson@scripps.edu

Annu. Rev. Immunol.
2006. 24:419–466

First published online as a Review in Advance on January 16, 2006

The *Annual Review of Immunology* is online at immunol.annualreviews.org

This article's doi:
10.1146/annurev.immunol.23.021704.115658

0732-0582/06/0423-0419$20.00

Key Words

T cell receptor, major histocompatibility complex, protein-protein interaction, crystal structure, immunological synapse

Abstract

Since the first crystal structure determinations of αβ T cell receptors (TCRs) bound to class I MHC-peptide (pMHC) antigens in 1996, a sizable database of 24 class I and class II TCR/pMHC complexes has been accumulated that now defines a substantial degree of structural variability in TCR/pMHC recognition. Recent determination of free and bound γδ TCR structures has enabled comparisons of the modes of antigen recognition by αβ and γδ T cells and antibodies. Crystal structures of TCR accessory (CD4, CD8) and coreceptor molecules (CD3εδ, CD3εγ) have further advanced our structural understanding of most of the components that constitute the TCR signaling complex. Despite all these efforts, the structural basis for MHC restriction and signaling remains elusive as no structural features that define a common binding mode or signaling mechanism have yet been gleaned from the current set of TCR/pMHC complexes. Notwithstanding, the impressive array of self, foreign (microbial), and autoimmune TCR complexes have uncovered the diverse ways in which antigens can be specifically recognized by TCRs.

INTRODUCTION

Humoral (antibody-mediated) and cellular (T cell–mediated) immunity are the two main lines of defense that higher organisms rely on for combating microbial pathogens. While antibodies recognize intact antigens, T cells distinguish foreign material from self through presentation of fragments of the antigen by the MHC cell surface receptors. Only if an MHC molecule presents an appropriate antigenic peptide will a cellular immune response be triggered. The orchestration of recognition and signaling events, from the initial recognition of antigenic peptides to the lysis of the target cell, is performed in a localized environment on the T cell, called the immunological synapse, and requires the coordinated activities of several TCR-associated molecules, including coreceptors CD3 and CD8 or CD4, and other costimulatory receptors.

Insights into TCR structure have come from crystallized TCR fragments and individual chains (1–6), intact TCR ectodomains (7–10), and TCR/pMHC complexes (7, 11–31) (**Figure 1**). Analysis of the current database of 24 TCR/pMHC complexes has resolved many pressing questions in cellular immunity, but other issues have not yet been clarified, particularly in regard to what constitutes the structural basis of MHC restriction and its implications for positive and negative selection. Further, how do TCRs distinguish between agonist, partial agonist, and antagonist ligands in order to produce different signaling outcomes? One serious obstacle remaining is the generation of sufficient quantities of soluble TCR/pMHC complexes for crystallographic structure determination. Despite the presence of multiple disulfide bonds in these heterodimeric complexes, many TCRs and MHCs have been produced and refolded from *Escherichia coli* inclusion bodies (**Table 1**). Some MHCs have been produced in insect cells, such as *Drosophila melanogaster* (K-2K^b, HLA-DR1, HLA-DR4, I-A^u) or *Spodoptera frugiperda* (HLA-DR2), and TCRs have been produced in *D. melanogaster* (2C), *Trichoplusia ni* ($\gamma\delta$ TCR), and *S. frugiperda* (Ob.1A12) systems (**Table 1**). Mammalian myeloma cells enabled production of the scBM3.3 and scKB5-C20 TCRs. To increase peptide affinities and to reduce the unfavorable change in entropy during complex formation, stable complexes have also been engineered by covalently attaching the antigenic peptide to either the N terminus of the β-chain of class II MHC (15) or the N terminus of the TCR β-chain (18, 27, 29).

In this review, we discuss the recent advances in our understanding of TCR/pMHC recognition and signaling (via associated coreceptors) and outline some important questions that remain unanswered. For other notable previous reviews on this topic, see References 32–38.

ARCHITECTURE OF MHCs AND TCRs

Structural Variation and Functional Promiscuity of the MHC Fold

In the cellular immune response, antigens, generally peptides, are displayed to $\alpha\beta$ T cells in complex with class I or class II MHC molecules. Both classes of MHC are heterodimers with similar architectures and are composed of three domains, one α-helix/β-sheet ($\alpha\beta$) superdomain that forms the peptide-binding site and two Ig-like domains. In class I MHC molecules, the peptide-binding site (called the $\alpha_1\alpha_2$ domain) is constructed from the heavy chain only, and an additional light chain subunit, β_2-microglobulin (β_2m), associates with α_3 of the heavy chain. In contrast, the class II MHC peptide-binding site is assembled from two heavy chains ($\alpha_1\beta_1$). Notwithstanding, in both MHC classes, the overall architecture is the same where a seven-stranded β-sheet represents the floor of the binding groove, and the sides are formed by two long α-helices (or continuous α-helical segments in the α_2- or β_1-helices) that straddle the

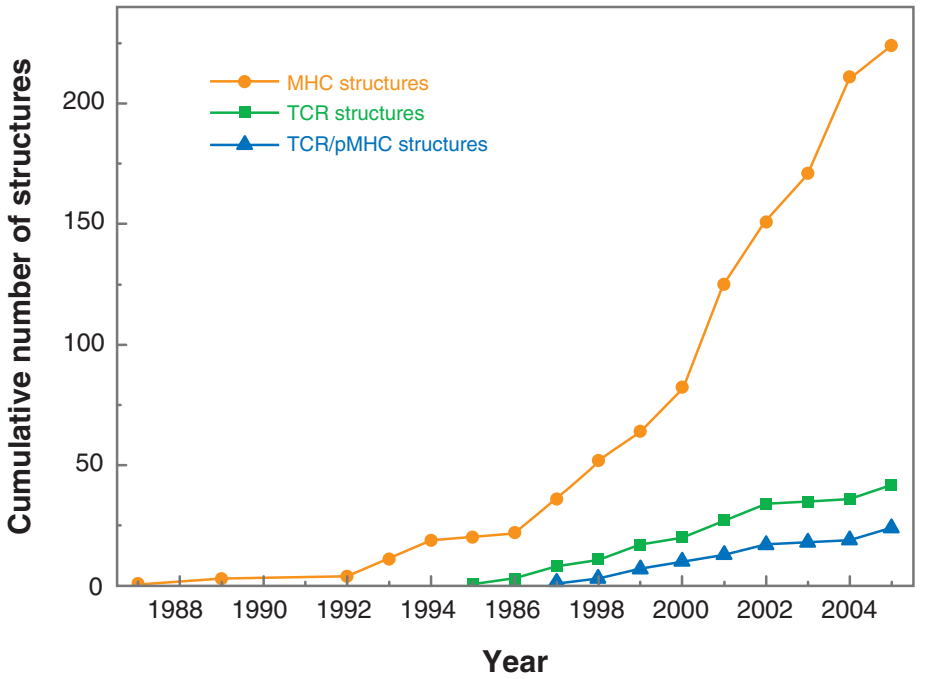

Figure 1

Cumulative number of pMHC [unliganded or with ligand (peptide, superantigen, etc.)], TCR (unliganded or with ligand other than pMHC), and TCR/pMHC complex crystal structures. The number of structures is plotted as a function of their deposition year in the Protein Data Bank (PDB) (151). The plot does not contain structures that were superseded by redetermination at higher resolution. However, MHC and TCR complexes with other molecules, such as superantigens or antibodies, were included. For the TCRs, all fragments and constructs (such as single chains), which were determined by either X-ray diffraction or NMR spectroscopy, are included. The first MHC crystal structure was determined in 1987 (152), and after an approximately five-year lag, the number of MHC structures increased drastically, with 39 structures added to the PDB in 2004. Since the first TCR and TCR/pMHC structures in 1996, no such dramatic increase has yet been seen in the annual output of new TCR or TCR/pMHC structures.

β-sheet (**Figure 2*a*,*b***). Polymorphic residues cluster within and around the binding groove in order to provide the required variation in shape and chemical properties that accounts for the specific peptide-binding motifs identified for each MHC allele (39–41).

Class I MHC molecules usually bind peptides of 8–10 residues length (on average 9-mers, P1–P9) (**Figure 3**) in an extended conformation with the termini and the so-called anchor residues buried in specificity pockets that differ from allele to allele (42, 43). This binding mode leaves the upward-pointing peptide side chains available for direct interaction with the TCR (**Figure 3**). Longer peptides can either bind by extension at the C terminus (44) or, due to the fixing of their termini, bulge out of the binding groove, providing additional surface area for TCR recognition (22, 45). In class II MHC, the groove is open at either end, and the peptide termini are not fixed so that bound peptides are usually significantly longer than in MHC class I (**Figure 3**). The peptide backbone in class II MHC is confined mainly to a polyproline type II conformation (44) and resides slightly deeper in the binding groove. Thus, the bound peptide (P1–P9) is more accessible for TCR inspection in MHC class I due to its ability to bulge out of the groove, even for

Table 1 Overview of TCR/pMHC complex structures, 1996–2005

Complex	Peptide activity	Constructs and expression systems	Reference
MHC class I			
2C/H-2K^b/dEV8	Weak agonist	*D. melanogaster*, acidic/basic leucine zipper for specific TCR chain-pairing	(12)
2C/H-2K^b/SIYR	Superagonist	As above	(17)
2C/H-2K^{bm3}/dEV8	Weak agonist	As above	(19)
scBM3.3/H-2K^b/pBM1	Agonist (naturally processed)	Myeloma cells for TCR, *E. coli* for MHC (refolded from inclusion bodies)	(16)
scBM3.3/H-2K^b/VSV8	Agonist	As above	(30)
scKB5-C20/H-2K^b/pKB1	Agonist (naturally processed)	Myeloma cells for TCR, *E. coli* for MHC (refolded from inclusion bodies)	(31)
B7/HLA-A2/Tax	Strong agonist	*E. coli*, refolded from inclusion bodies	(13)
A6/HLA-A2/Tax	Strong agonist	*E. coli*, refolded from inclusion bodies	(11)
A6/HLA-A2/TaxP6A	Weak antagonist	As above	(14)
A6/HLA-A2/TaxV7R	Weak agonist	As above	(14)
A6/HLA-A2/TaxY8A	Weak antagonist	As above	(14)
JM22/HLA-A2/MP	Agonist	*E. coli*, refolded from inclusion bodies. C-terminal extension of TCR chains coding for a cysteine to promote disulfide formation	(21)
1G4/HLA-A2/ESO9V	Agonist	*E. coli*, refolded from inclusion bodies	(25)
1G4/HLA-A2/ESO9C	Agonist	As above	(25)
AHIII12.2/HLA-A2.1/p1049	Agonist (xenoreactive)	*E. coli*, refolded from inclusion bodies	(20)
SB27/HLA-B3508/EBV	Agonist	*E. coli*, refolded from inclusion bodies	(23)
LC13/HLA-B8/FLR	Agonist (immuno-dominant)	*E. coli*, refolded from inclusion bodies	(24)
MHC class II			
scD10/I-A^k/CA	Agonist	*E. coli* for TCR, refolded from inclusion bodies; CHO cells for MHC. Peptide covalently connected to the MHC.	(15)
HA1.7/HLA-DR1/HA	Agonist	*E. coli* for TCR, refolded from inclusion bodies; *D. melanogaster* for MHC. Peptide covalently connected to the TCR β-chain.	(18)
HA1.7/HLA-DR4/HA	Agonist	As above	(153)
Ob.1A12/HLA-DR2b/MBP	Agonist (autoreactive self-peptide)	Baculovirus-infected *S. frugiperda* cells for both HLA-DR2 and TCR. Peptide covalently attached to the N terminus of the TCR β-chain. Jun/Fos leucine zipper for specific TCR chain-pairing.	(27)
sc172.10/I-A^u/MBP	Agonist (autoreactive self-peptide)	*E. coli* periplasm for TCR, *D. melanogaster* for MHC	(28)
3A6/HLA-DR2a/MBP	Agonist (autoreactive self-peptide)	*E. coli*, refolded from inclusion bodies for MHC and TCR; peptide covalently connected to the N terminus of the TCR β-chain.	(29)
γδ TCR/H2-T22	—	Baculovirus-infected *Trichoplusia ni* cells, acidic/basic leucine zipper for specific TCR chain-pairing	(102)

αβ class I, class II, and γδ TCR complexes are separated by horizontal lines. (Abbreviations: sc, single chain Fv fragment of the TCR.)

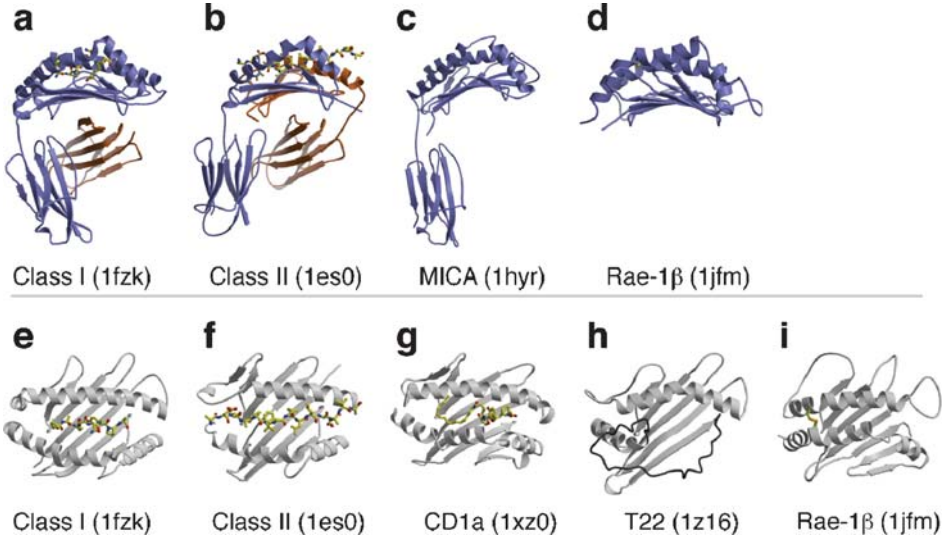

Figure 2

Architecture of MHC-like molecules. The top panel shows the domain organization of the MHC(-like) molecules and the lower panel focuses on the ligand and/or receptor binding sites. (*a*) Class I molecules consist of a heavy chain (*blue*) and a light β_2m chain (*orange*). The peptide-binding site is formed exclusively by elements of the heavy chain, whereas in class II molecules (*b*), it is assembled from both subunits. (*c*) The nonclassical MHC-like molecule MICA, which is a ligand for the natural killer (NK) cell receptor NKG2D, is structurally analogous to a class I molecule but lacks the β_2m subunit. (*d*) The NKG2D ligand Rae-1β is formed solely by the $\alpha_1\alpha_2$ platform, so that the α_3 domain is expendable. (*e*) A view from the TCR perspective onto the class I peptide-binding site with the peptide drawn as a stick model and atoms colored according to atom type. The α_1- and α_2-helices close off the ends of the groove, fixing the N and C termini of the peptide in the A and F pockets, respectively. (*f*) In class II molecules, the helices bordering the peptide are shorter and less curved, allowing the peptide to protrude from the ends of the groove. (*g*) Closer proximity of the helices and a hydrophobic binding groove are the hallmarks of the CD1 binding pocket for binding lipids, glycolipids, and lipopeptides. (*h*) In the nonclassical MHC molecule T22, which is a γδ T cell ligand, part of the α_2-helix has unwound, exposing one end of the underlying β-sheet. The newly acquired loop region (shown in *dark gray*) apparently is flexible as judged by the very high B values of the structure in this region. (*i*) No small molecule ligand can be bound by Rae-1β as the distance between the helices is minimal, which permits formation of an interhelical disulfide bond.

9-mer peptides; however, in MHC class II, the termini, particularly the N-terminal extension (P-4 to P-1), can play a major role in the TCR interaction.

Apart from displaying peptides to TCRs, the MHC fold has garnered many other functions during evolution that impact its domain organization and flexibility, as well as its substrate specificity. For instance, in the nonclassical MHC molecule CD1, the ligand-binding groove is deeper, narrower, and more hydrophobic than in class I MHCs, such that lipid tails of glycolipids and lipopeptides are bound in the groove and their polar moieties presented to T cells (46–55) (**Figure 2*g***). Other MHC-like molecules do not seem to present any antigen, such as γδ TCR ligands T10 (56) and T22 (57). In these structures, a 13-residue sequence deletion results in the partial unfolding of the α_2-helix and a concomitant exposure of the β-sheet floor of the $\alpha_1\alpha_2$ domain (**Figure 2*h***). This "rupture" of the ligand-binding site appears to account for the loss of peptide or other small molecule ligand-binding capability, although, initially, questions arose whether this disordered loop

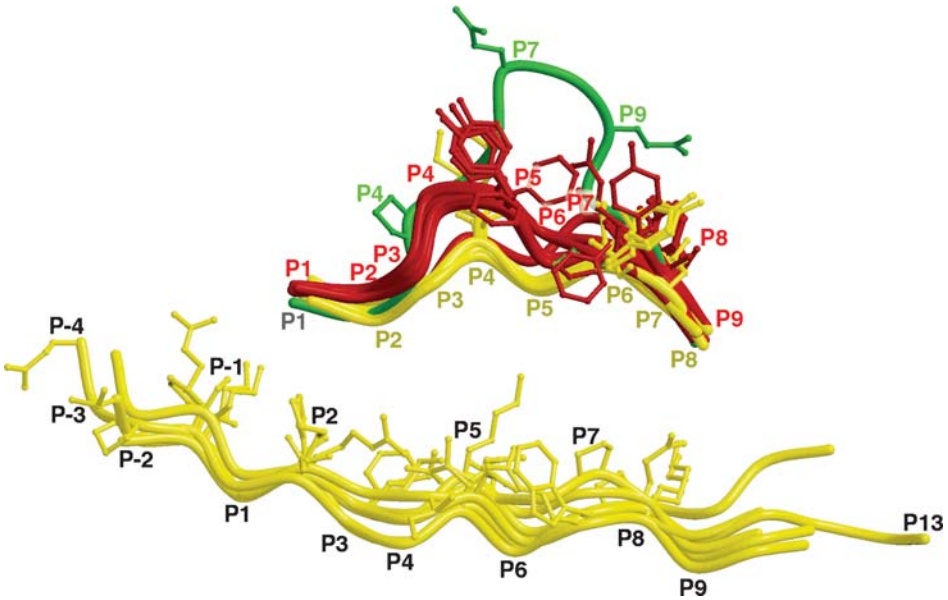

Figure 3

Comparison of peptide conformations as observed in class I (*top*) and class II (*bottom*) TCR/pMHC complexes. The Cα traces of the bound peptides (removed from their respective MHCs) are drawn as tubes with the TCR-contacting side chains (see **Table 3**) as stick representations. Class I–bound peptides of 8, 9, and 13 residues are colored yellow, red, and green, respectively. Peptides from class II complexes are colored yellow. The peptides are oriented with their TCR-contacting residues pointing upward. The β-sheet floors of the peptide-binding sites of the MHC molecules were superimposed to align the peptides. TCR interaction with the central P1–P9 residues is common to both class I and class II, but the bound peptides adopt substantially different conformations.

region would fold back into an α-helix upon TCR binding.

Yet another class of nonclassical MHC molecules that apparently lacks any affinity for small molecule antigens comprises ligands for the NK cell activating receptor NKG2D (58–61), i.e., human MICA, MICB, ULBP, and murine Rae1 and H60 (62). These cell surface receptors serve as general stress sensors and, as they do not present peptide antigens, are independent of transporter associated with antigen processing (TAPs) (63). Their expression levels are low and the receptors are displayed on fibroblast, epithelial, dendritic, and endothelial cells only in response to stress such as heat shock, oxidative stress, bacterial infection, and tumor growth (64, 65). Crystal structures of MICA (66) and Rae-1β (67) indicated that the loss of peptide, or any other ligand, binding was due to elimination of any binding groove because of the reduced distance between the α_1- and α_2-helices (**Figure 2*i***). In Rae-1β, these helices come close enough to permit formation of a noncanonical disulfide bond with a leucine-rich interface filling the former ligand-binding cavity. Thus, natural evolution of the MHC fold has taken nonclassical MHCs even further from the canonical MHC fold. In contrast to class I MHCs, MIC proteins do not associate with β_2m, and H60 and Rae-1β are even simpler modules as they dispense with an α_3 domain and exist only as an isolated $\alpha_1\alpha_2$ platform (**Figure 2**).

Receptor binding to MHCs is complemented by additional interaction events prior to T cell or killer cell activation. Coreceptors CD4 and CD8 bind not only to the underside

of the $\alpha_1\alpha_2$ platform and α_3 domain of pMHCs, but also to nonclassical MHCs, such as the thymic leukemia tumor antigen TL. TL modulates T cell activation through a moderate affinity ($K_d = 10$ μM) interaction with the CD8 coreceptor, but also does not serve as an antigen-presenting molecule, because its binding site is also occluded by close packing of the α_1- and α_2-helices (68).

αβ and γδ TCRs

TCRs are cell surface heterodimers consisting of either disulfide-linked α- and β- or γ- and δ-chains. Sequence analyses correctly predicted that TCRs would share a domain organization and binding mode similar to those of antibody Fab fragments (69, 70). Each TCR chain is composed of variable and constant Ig-like domains, followed by a transmembrane domain and a short cytoplasmic tail. The αβ TCRs bind pMHC with relatively low affinity (~1–100 μM) through complementarity-determining regions (CDRs) present in their variable domains.

Compared with αβ TCRs, where a variety of structures have been determined since 1996, much less is known about γδ TCRs. The only structure available until recently was that of a V_δ domain (71). This lack of structural information was paralleled by the ill-defined biological function of γδ T cells. γδ T cells appear to respond to bacterial and parasitic infections (72) and primarily recognize phosphate-containing antigens (phosphoantigens) from mycobacteria by an unknown mechanism (72, 73). Other identified ligands (74) for γδ T cells are few, with the exception of nonclassical MHC class Ib molecules T10 and T22, mouse MHC class II I-E^k, herpes simplex virus glycoprotein gI, and CD1 (75). However, the mechanism of engagement of the γδ TCR with these ligands was not understood until recently.

The crystal structure of the G115 $V_\gamma 9$-$V_\delta 2$ TCR has addressed some of these issues (76). As expected, the overall architecture of the γδ TCR closely resembles that of αβ TCRs and antibodies (**Figure 4**). The most striking observation is an acute V_γ/C_γ interdomain angle of 42°, which defines an unusually small elbow angle of 110°. Whether this is indeed a general feature of all γδ TCRs or represents an extreme example must await further determination of γδ TCR structures. The corresponding elbow angles of αβ TCRs have so far been restricted to a slightly narrower range (140°–210°) than those seen for antibodies (125°–225°), presumably due to the smaller database of αβ TCR structures. The requirement of αβ and γδ TCRs to interact with the common CD3 components might restrict flexibility for the V-C domain, but no structural data are available for any TCR/CD3 complexes to elucidate this requirement.

The γδ TCR structure also raises further questions about CD3 recognition in the TCR complex. Comparison of the C domain surfaces of both γδ and αβ TCRs revealed no apparent similarities (76) that could explain the dual binding specificity of CD3 for these different classes of TCRs; only a few solvent-exposed residues are structurally conserved. The striking distinctions between the exposed surfaces of γδ and αβ TCRs are corroborated by the large differences of the respective proposed CD3ε-binding FG loops of Cβ and Cγ, and the very different secondary structural features of Cα and Cδ. Cα shows a secondary structure unlike the normal Ig-fold in the outer β-sheet, as opposed to Cδ, which has the regular, canonical three-stranded β-sheet. Thus, the possibility of two very distinct TCR/CD3 signaling complexes exists, the biological significance of which is unclear. Alternatively, the main driving force for TCR/CD3 complex formation may not come from specific interaction of the extracellular domains, but may stem, at least in the primary stages of complex formation, from ionic interactions with the TCR stalk regions or through their transmembrane segments.

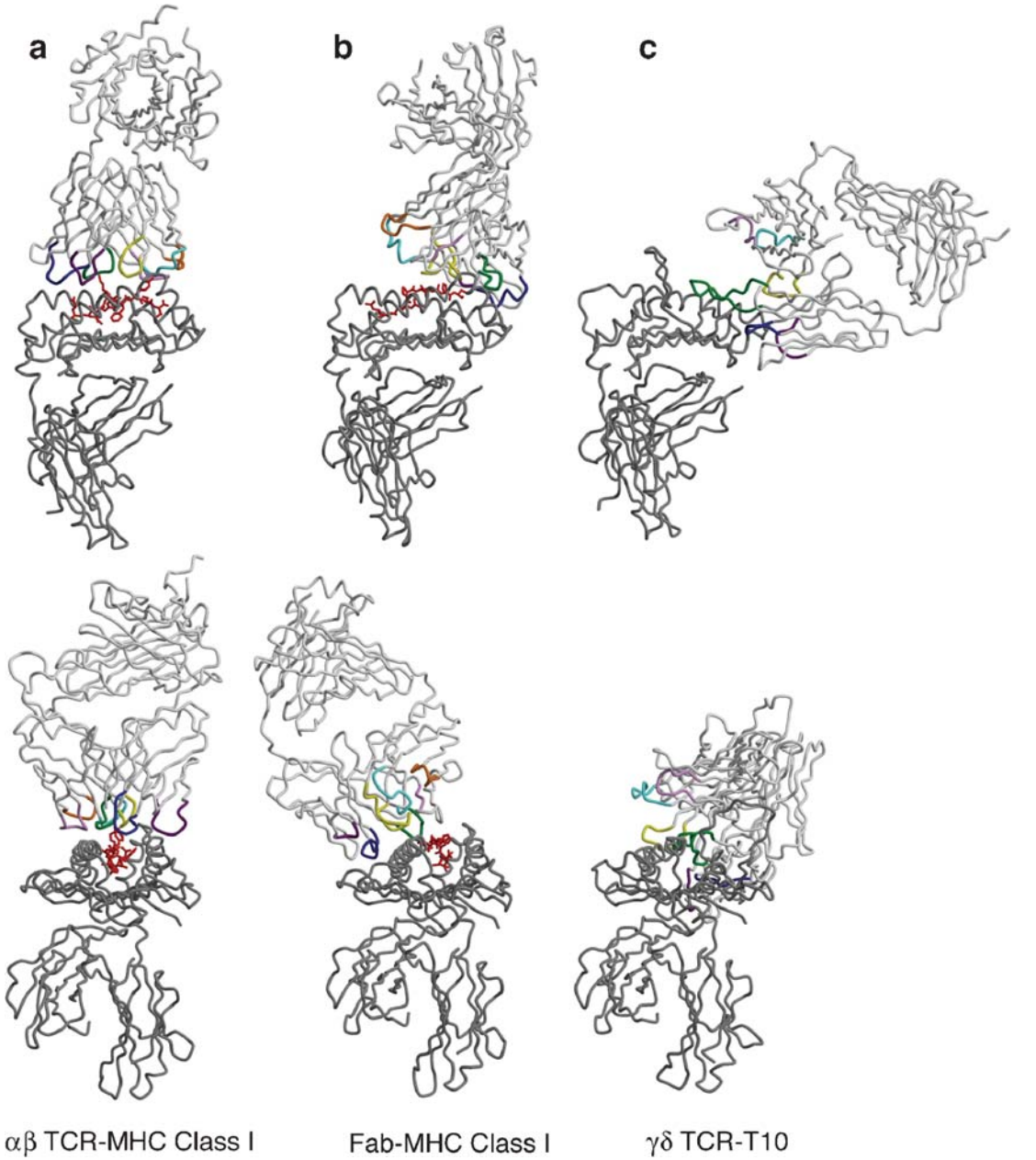

Figure 4

Overall comparison of the anatomy of complexes formed between MHC(-like) proteins and αβ TCR (*a*), Fab (*b*), and γδ TCR (*c*). The bottom panel is rotated 90° around the horizontal axis. Only one representative structure is shown for each type. The Cα trace of the TCR or Fab is on top in light gray with colored CDR loops and the MHC in dark gray below. The peptides in the αβ and Fab complexes are drawn as red ball-and-stick representations, while the CDR loops are colored as follows: CDR1 $\alpha_{(24-31)}$: dark blue, CDR2 $\alpha_{(48-55)}$: magenta, CDR3 $\alpha_{(93-104)}$: green, CDR1 $\beta_{(26-31)}$: cyan, CDR2 $\beta_{(48-55)}$: pink, CDR3 $\beta_{(95-107)}$: yellow, and HV4$_{(69-74)}$: orange. This color scheme is continued through **Figures 5** and **7**.

Structures of αβ TCR and Peptide-MHC Complexes

Clonotypic αβ TCRs recognize peptides presented by either class I or class II MHCs. Class II MHCs present peptides that originate from proteolysis of extracellular antigens in endosomal-type compartments, whereas class I MHCs present peptides primarily derived from intracellular degradation of proteins in the cytosol. TCRs that recognize these MHCs are found on two distinct cytotoxic and T-helper cell lineages, depending on the class of the MHC to which they are restricted. A current debate in class I MHC antigen presentation is over "cross-priming" of T cells for activation of CD8 T cells by transfer of peptide antigen or other substrates from a donor cell containing viral or tumor antigens to an acceptor cell (77–79). Peptide transfer is achieved by either (*a*) uptake of cell-derived proteins by receptor-mediated (LOX-1, CD91, and Toll-like receptors) endocytosis or (*b*) fusion of phagocytotic vesicles that contain material from apoptotic or necrotic cells with endoplasmic reticulum membranes. The proteasome is assumed to further degrade the proteins to peptides, which are then bound to chaperones, such as glycoprotein 69, HSP90, HSP70, and calreticulin before they are transferred to their new MHC hosts by an as yet unknown mechanism (78).

Class I and class II MHCs both present peptides in an extended conformation in a vice-like groove, with two flanking α-helices and a floor composed of antiparallel β-strands (**Figure 2**). Although the ends of the peptide-binding groove are occluded in class I MHC molecules, they are open in class II molecules; therefore, class II MHCs can accommodate peptides significantly longer than can those of class I MHCs. The first two turns of the class I MHC α_1-helix are replaced in class II MHCs by a β-strand. Whereas both classes of MHCs are composed of two noncovalently linked, polypeptide chains, in class I MHCs, the peptide-binding site is formed by the heavy chain only and, in class II MHCs, the α- and β-chains assemble into a similar fold that constitutes the peptide-binding groove.

Given the biological and structural divergence between these two MHC classes, it is of interest to compare and contrast the interactions with their cognate TCRs (**Figure 5**). **Tables 2–4** provide a detailed analysis of the TCR/pMHC interface that includes buried surface areas, relative contributions of CDR loops, shape complementarities, hydrogen bonds, salt bridges, and van der Waals' contacts. These tables have been updated from our previous analyses (36, 37) to include all complexes determined from 1996 to 2005. In the following section, we focus mainly on structures determined since 2002 and on new insights gained from this substantially increased database of TCR/pMHC complexes.

TCR/pMHC BINDING GEOMETRY

Several techniques have been used in various laboratories to define the relative TCR binding orientation on pMHC. These diverse methods of calculation often result in dissimilar values for this "crossing angle," making comparison of structures from multiple laboratories difficult and confusing. Hence, we outline simple, reproducible, and easy-to-use methods to describe the TCR-to-pMHC binding orientation and to calculate buried surface area.

We do not suggest that other proposed methods are incorrect, but only that TCR complexes should be compared using a standard method. It is the relative rather than the absolute values in these calculations that are important here for defining general principles of TCR/pMHC recognition. The MHC-TCR crossing angle has been described previously in our laboratory by the angle between the MHC binding platform helices or MHC-bound peptide and an axis drawn approximately through the center of the α- and β-chain TCR CDR loops. Unsatisfied with the general applicability of this method, we

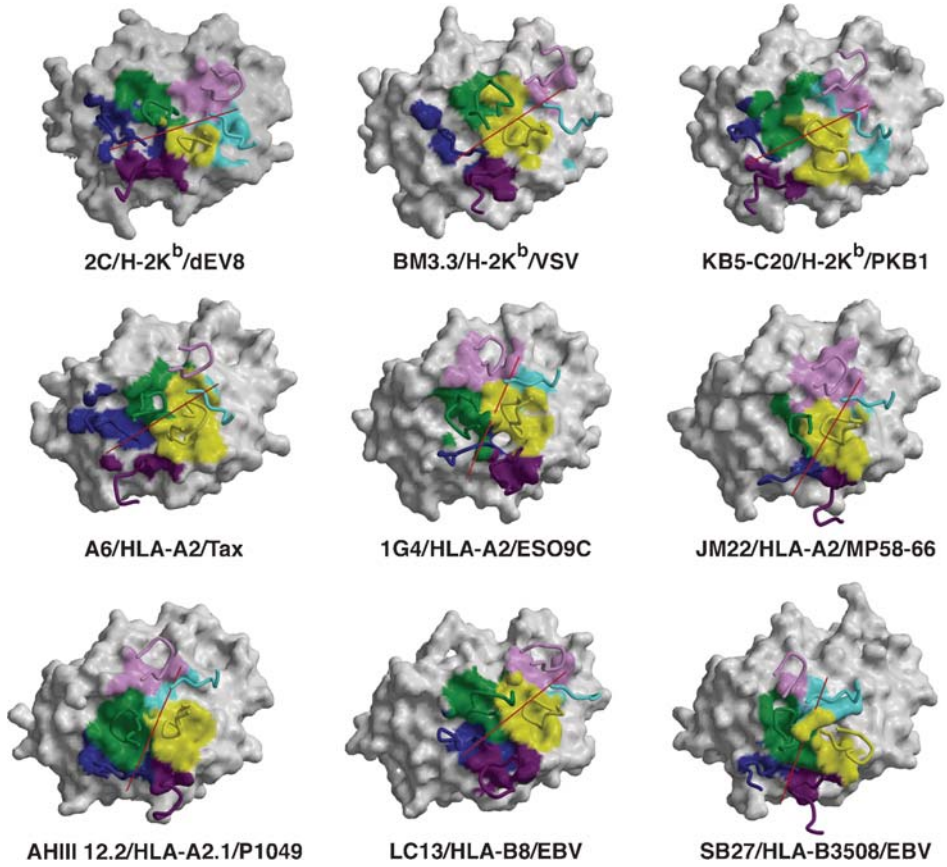

Figure 5

Footprints of TCR/pMHC complexes. The top surface of the MHC is colored in gray where it is not contacted by the TCR. Surface areas buried by TCR are colored by their contributions from each CDR loop, as in **Figure 3**. The red line represents a vector between the conserved disulfides in the α/β (or $\gamma\delta$ or light/heavy) chains, which has been translated to the center of gravity of the CDR loops, and indicates the relative orientation of the TCR onto the MHC. At this level of analysis, substantial variation is seen in the fine specificity of the TCR on the pMHC. Class I and II complexes are labeled in black and green, respectively. A corresponding view of the $\gamma\delta$ TCR/T22 complex (*red label*) and the Fab/HLA-A1 (*blue label*) complex is shown on the bottom row, with the δ, γ, light, and heavy chain CDRs colored correspondingly.

have experimented with several other ways to calculate this angle and now conclude that the method described here is optimal. We have now recalculated the crossing angles for all TCR/pMHC complexes, as listed in **Tables 2** and **3**, and the vectors representing the TCR are shown in **Figure 5**. We encourage other labs to adopt this method so that crossing angles for different complexes will be more easily comparable.

In our current algorithm, the vector along the MHC helix axis is calculated as the best-fit straight line through the Cα atoms from the two MHC helices. For class I MHC, we use Cα atoms A50–A86 and A140–A176, for class II MHC A46–78, B54–64, and B67–91, and for the nonclassical MHC T22 (which has only one ordered helix) Cα atoms A61–A82. The vector describing the long axis of the TCR binding site is calculated by

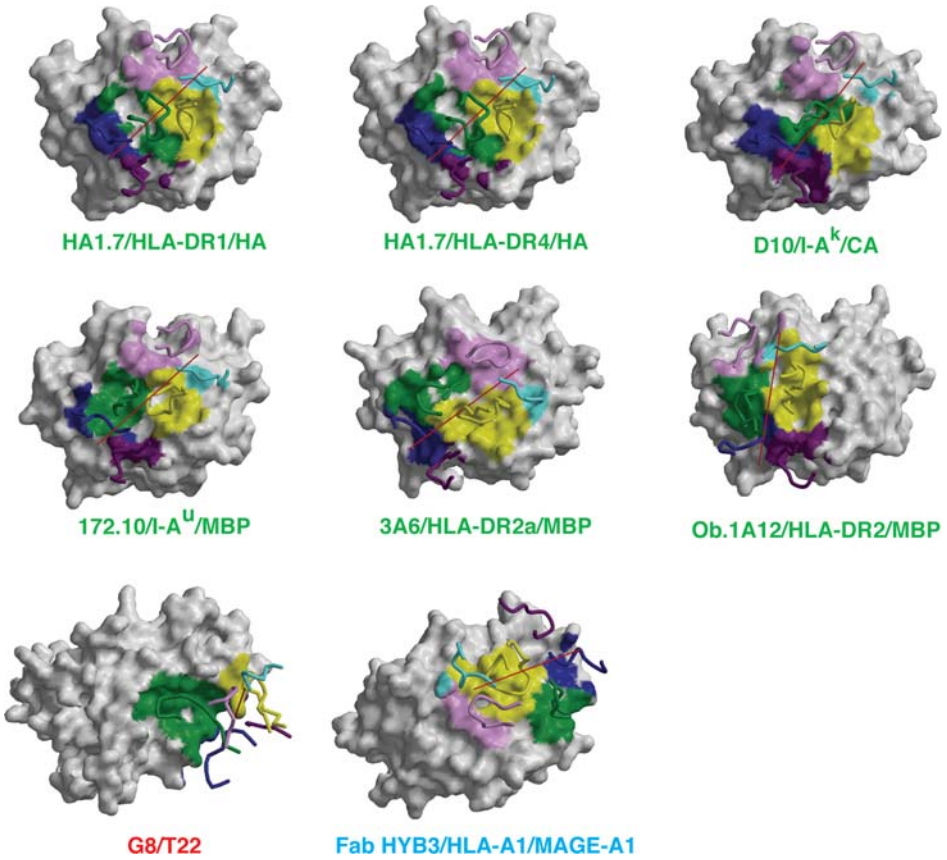

Figure 5

(*Continued*)

constructing a vector between the centroids of the conserved Ig disulfide-forming sulfur atoms in the light and heavy chains (Sγ atoms from L22–L90 and H23–H92 for $\alpha\beta$ TCRs and L22–L88 and H21–H94 for $\delta\gamma$TCRs). The angle between the MHC and TCR vectors is then the dot product of the two vectors. For graphic visualization, the vector between the disulfides is translated to the center of gravity of the TCR CDR loops.

Buried surface areas (see **Tables 2** and **3**) are calculated using the molecular surface from the program MS (80) with a 1.7 Å probe radius (a value historically used for most antibody-antigen analyses). The use of a solvent accessible, rather than molecular surface, for estimating the buried surface will give erroneous results, especially for more concave/convex binding regions.

Generally, the TCR heterodimer is oriented approximately diagonally relative to the long axis of the MHC peptide-binding groove (7, 11). The V_α domain is poised above the N-terminal half of the peptide, whereas the V_β domain is located over the C-terminal portion of the peptide (**Figures 4, 5**). Peptide contacts are made primarily through the CDR3 loops, which exhibit the greatest degree of genetic variability. The preponderance of generally conserved contacts with the MHC α-helices are mediated through CDRs 1 and 2 (32), particularly for V_α, with the CDR3 loops

Table 2 Analysis of TCR/pMHC class I complexes

TCR	2C	2C	2C	scBM3.3	scBM3.3	scKB5-C20	B7
MHC	H-2K^b	H-2K^b	H-2K^{bm3}	H-2K^b	H-2K^b	H-2K^b	HLA-A2
Peptide	dEV8	SIYR	dEV8	pBM1	VSV8	pKB1	Tax
Resolution	3.0/32.2	2.8/32.7	2.4/31.3	2.5/27.6	2.7/29.8	2.7/27.8	2.5/31.2
PDB ID	2ckb	1g6r	1mwa	1fo0	1nam	1kj2	1bd2
Reference	(12)	(17)	(19)	(16)	(30)	(31)	(13)
TCR/pMHC crossing angle (°)	22	23	23	41	40	31	48
Buried surface area[a] /K_d (μM)	1842/83	1795/54	1878/56.5	1239/2.6	1444/114	1678/>100	1697/-
TCR/pMHC (Å^2)	907/935	847/948	900/978	597/642	675/769	825/853	813/884
MHC/peptide (%)	76/24	76/24	75/25	79/21	81/19	79/21	69/31
V_α (Å^2) / (%)	490/54	438/52	469/52	221/37	348/52	371/45	552/68
CDR1/CDR2/ CDR3 (%)	23/13/16/1	18/16/16/1	20/14/17/1	14/17/6	17/13/21	9/9/25/1	27/13/22/2
V_β (Å^2) / (%)	417/46	409/48	431/48	376/63	327/48	454/55	261/32
CDR1/CDR2/ CDR3/HV4 (%)	16/19/10/1	15/19/12/3	19/18/11/1	10/14/39/1	6/14/27/2	18/12/24/0	1/10/21/0
S_c[b]	0.41	0.49	0.62	0.61	0.60	0.55	0.64
HB/salt links/vdW contacts[c]	4/1/80	5/0/69	6/0/107	8/0/83	3/0/78	5/3/84	4/3/99
V_α	4/1/63	4/0/36	4/0/46	1/0/27	3/0/49	3/2/47	3/3/66
CDR1$_{(24-31)}$	2/0/21	2/0/17	1/0/13	1/0/10	1/0/11	0/2/3	1/0/24
CDR2$_{(48-55)}$	0/0/17	0/0/1	1/0/12	0/0/15	0/0/10	0/0/5	1/0/17
CDR3$_{(93-104)}$	2/0/24	2/0/18	2/0/21	0/0/2	2/0/28	3/0/39	1/3/25
HV4$_{(68-74)}$	0/1/1	0/0/0	0/0/0	0/0/0	0/0/0	0/0/0	0/0/0
V_β	0/0/17	1/0/33	2/0/61	7/0/56	0/0/29	2/1/37	1/0/33
CDR1$_{(26-31)}$	0/0/7	1/0/15	2/0/35	0/0/1	0/0/3	0/0/11	0/0/0
CDR2$_{(48-55)}$	0/0/6	0/0/3	0/0/12	1/0/8	0/0/7	1/1/2	0/0/3
CDR3$_{(95-107)}$	0/0/4	0/0/15	0/0/14	6/0/47	0/0/19	1/0/23	1/0/30
HV4$_{(69-74)}$	0/0/0	0/0/0	0/0/0	0/0/0	0/0/0	0/0/0	0/0/0
MHC	2/1/59	2/0/37	3/0/69	3/0/54	3/0/60	3/2/73	1/3/42
Peptide	2/0/21	3/0/32	3/0/38	5/0/29	0/0/18	2/1/11	3/0/57

[a]Calculated with MS (80) using 1.7Å probe radius.
[b]Calculated with S_c (154) using a 1.7Å probe radius.
[c]Number of hydrogen bonds (HB), salt links and van der Waals (vdW) interactions calculated with HBPLUS (155) and CONTACSYM (156). Only the first molecule in the asymmetric unit in all complexes was analyzed.

Table 2 (*Continued*)

A6	A6	A6	A6	JM22	LC13	1G4	1G4	AHIII 12.2	SB27
HLA-A2	HLA-A2	HLA-A2	HLA-A2	HLA-A2	HLA-B8	HLA-A2	HLA-A2	HLA-A2.1	HLA-B3508
Tax	TaxP6A	TaxV7R	TaxY8A	MP58–66	EBV	ESO 9C	ESO 9V	p1049	EBV
2.6/32.0	2.8/27.3	2.8/29.0	2.8/28.6	1.4/23.1	2.5/28.8	1.9/26.0	1.7/25.3	2.0/25.3	2.5/27.9
1ao7	1qrn	1qse	1qsf	1oga	1mi5	2bnr	2bnq	1lp9	2ak4
(13)	(14)	(14)	(14)	(21)	(24)	(25)	(25)	(20)	(23)
34	32	36	34	62	42	69	69	67	70
1816/0.9	1768/-	1752/7.2	1666/-	1471/5.6	2020/10	1916/13.3	1924/5.7	1838/11.3	1752/9.9
908/908	851/917	838/914	810/856	738/733	1008/1012	979/936	979/945	943/895	827/925
66/34	67/33	66/34	73/27	72/28	80/20	65/35	64/36	73/27	60/40
587/65	561/66	536/64	598/74	241/33	573/57	465/47	470/48	550/58	474/57
24/10/24/5	23/13/25/6	23/10/26/5	29/12/27/5	11/6/13/3	17/18/22/0	8/12/27/0	8/13/27/0	16/13/27/1	10/17/31/0
321/35	290/34	302/36	211/26	496/67	435/43	515/53	509/52	393/42	354/43
2/1/33/0	2/1/31/0	2/0/34/0	0/0/26/0	5/34/27/1	3/17/22/0	9/20/19/5	9/19/20/4	6/16/20/0	19/5/18/1
0.64	0.61	0.66	0.61	0.63	0.61	0.72	0.75	0.70	0.73
11/4/105	10/1/120	7/2/136	6/1/102	8/0/92	8/1/122	10/0/178	10/0/184	5/1/147	11/0/106
7/3/60	7/1/86	4/2/81	6/1/78	0/0/29	3/0/62	5/0/100	5/0/109	4/0/99	5/0/58
3/0/21	3/0/20	2/0/19	2/0/21	0/0/9	2/0/18	0/0/41	0/0/40	0/0/27	1/0/7
0/0/3	0/0/4	0/0/8	1/0/8	0/0/10	0/0/12	1/0/7	2/0/18	0/0/23	1/0/6
3/2/33	3/1/53	2/2/49	2/1/43	0/0/10	1/0/32	4/0/52	3/0/51	4/0/49	3/0/45
1/1/2	1/0/9	0/0/5	1/0/6	0/0/0	0/0/0	0/0/0	0/0/0	0/0/0	0/0/0
4/1/45	3/0/34	3/0/55	0/0/24	8/0/63	5/1/60	5/0/78	5/0/75	1/0/48	6/0/48
1/1/2	1/0/3	1/0/3	0/0/0	1/0/4	0/0/1	1/0/16	1/0/14	1/0/2	5/0/32
0/0/0	0/0/0	0/0/0	0/0/0	2/0/23	1/1/15	1/0/23	1/0/21	0/0/11	0/0/1
3/0/43	2/0/31	2/0/52	0/0/24	5/0/33	4/0/44	2/0/33	2/0/37	0/0/31	0/0/12
0/0/0	0/0/0	0/0/0	0/0/0	0/0/0	0/0/0	1/0/3	1/0/2	0/0/0	0/0/0
4/4/65	3/1/67	1/2/84	3/1/75	4/0/67	6/1/96	5/0/73	6/0/73	2/1/94	2/0/40
7/0/40	7/0/53	6/0/52	3/0/27	4/0/25	2/0/26	5/0/105	4/0/111	3/0/53	9/0/66

contributing fewer conserved MHC contacts. The first crystal structures of TCRs with class I molecules led to proposals that the TCR orientation is approximately diagonal with a mean around 35° (36). By contrast, in the first class II complexes, the orientation was described as being closer to perpendicular (15, 18), suggesting a different binding mode between the MHC classes (81). However, we calculated this angle to be 50°, which is still roughly diagonal. Furthermore, the recent crystal structure determination of class I HLA-A2 in complex with the xenoreactive AHIII 12.2 TCR (20) showed a TCR/pMHC binding orientation of 67°, arguing against any real differences in receptor orientation between class I and class II complexes. In very low-affinity interactions (<10 μM), such as in the TCR/pMHC system, there is always a danger of stabilizing nonproductive conformations during the crystallization process that are not representative of those most populated in solution, or those that represent only one snapshot of the possible complex orientations. Nevertheless, the key questions are still how many ways can the TCR dock on the pMHC and what controls the docking, the TCR or the pMHC.

To partially address these questions, an antibody Fab/pMHC crystal structure was determined whereby the Fab Hyb3 serves as a TCR surrogate for binding to its antigen HLA-A1 complexed with a melanoma-associated human leukocyte peptide (82). In this complex, the Fab adopts a diagonal orientation of 41°, close to the range found in class I TCR/pMHC complexes (21°–70°), but the binding is shifted toward the C-terminal half of the peptide-binding site. The Fab binds with its heavy chain over the central part and the light chain over the C-terminal part of the peptide, respectively, which suggests that, although the structurally equivalent antibody can dock in a similar binding orientation on the pMHC, antibodies can still display a much more promiscuous binding mode toward their antigens, as they are not required to signal nor read out the peptide content, but only to bind with high affinity. Why then do TCRs generally dock on the pMHC in a generally diagonal orientation over the center of the binding groove?

The contacts of the individual TCR CDR loops with the pMHC are quite diverse and still do not allow definitive conclusions as to their contributions in determining the docking angle. The current database of TCR/pMHC crystal structures supports a scenario in which the TCR approaches the pMHC in a roughly diagonal manner, driven by either long-range electrostatic steering or through a low-affinity binding event, and then uses the conformational plasticity inherent in the CDR loops to maximally mold to and contact the pMHC, which then determines the final docking outcome (**Figure 6**). However, the rotational freedom of the TCR has been somewhat limited in that no 180° flip of the TCR has been observed to date that would poise the V_α (rather than V_β) domain over the C-terminal half of the peptide or vice versa, although such a scenario has been predicted (83). Because the docking angle dictated by the TCR/pMHC interface influences the disposition of the TCR constant domains relative to other components of the TCR signaling complex, such as CD4 or CD8, it is likely also to influence T cell signaling. However, in the absence of a ternary TCR/pMHC/CD3 or TCR/pMHC/CD8 complex structure, no conclusions can yet be drawn as to the precise role or restrictions that the TCR/pMHC docking geometry plays in coreceptor binding and downstream signaling. What is known is that ligand engagement of the TCR/CD3 complex induces a conformational change in CD3ε, which exposes a C-terminal proline-rich sequence in its cytoplasmic tail that recruits the adapter molecule Nck for downstream signaling via binding of its SH3 domain (84). In addition, comparison of the crystal structures of free and pMHC-bound LC13 TCR has revealed a conformational change in the AB-loop of the TCRα constant domain, which is predicted to be close to the CD3ε binding site (24). Furthermore, a

Table 3 Analysis of TCR/pMHC class II and nonclassical complexes

TCR	scD10	HA1.7	HA1.7	Ob.1A12	172.10	3A6	G8
MHC	I-A^k	HLA-DR1	HLA-DR4	HLA-DR2b	I-A^u	HLA-DR2a	T22
Peptide	CA	HA	HA	MBP	MBP	MBP	—
Resolution/R_{free}	3.2/29.3	2.6/25.5	2.4/24.6	3.5/31.8	2.42/27.4	2.8/32.9	3.40/33.0
PDB ID	1d9k	1fyt	1j8h	1ymm	1u3h	1zgl	1ypz
Reference	(15)	(18)	(26)	(27)	(28)	(29)	(102)
TCR/pMHC crossing angle (°)	53	47	49	84	43	40	87
Buried surface area/ K_d (μM)	1734/1-2	1945/-	1934/-	1916/-	1697/8.8	1984/≤500	1750/-
TCR/pMHC ($Å^2$)	868/866	975/970	975/959	968/948	866/831	953/1032	845/905
MHC/peptide (%)	77/23	67/33	68/32	60/40	76/24	66/34	100/0
V_α ($Å^2$)/(%)	530/61	456/47	471/48	473/49	459/53	394/41	755/89
CDR1/CDR2/ CDR3 (%)	22/15/22/2	15/8/23/0	15/9/23/0	6/19/24/0	14/14/25/1	17/4/19/0	15/5/61/4
V_β ($Å^2$)/(%)	338/39	519/53	504/52	495/51	408/47	558/59	90/11
CDR1/CDR2/ CDR3/HV4 (%)	3/20/16/0	8/22/22/1	8/19/23/1	5/11/32/2	5/19/23/0	6/24/28/0	0/0/11/0
S_c	0.71	0.56	0.56	0.52	0.62	0.63	0.66
HB/salt links/vdW contacts	6/3/119	4/4/104	2/5/101	4/0/116	5/0/110	8/1/127	3/0/116
V_α/V_δ	1/2/64	0/1/41	1/1/45	2/0/65	1/0/37	6/0/60	3/0/113
$CDR1_{(24-31)}$	1/1/24	0/0/13	0/0/16	0/0/9	0/0/6	1/0/39	0/0/30
$CDR2_{(48-55)}$	0/0/16	0/0/2	1/0/4	0/0/18	0/0/7	0/0/0	0/0/2
$CDR3_{(93-104)}$	0/0/24	0/1/26	0/1/25	2/0/38	1/0/24	5/0/21	3/0/68
$HV4_{(68-74)}$	0/1/0	0/0/0	0/0/0	0/0/0	0/0/0	0/0/0	0/0/4
V_β/V_γ	5/1/55	3/3/63	1/4/56	2/0/51	4/0/73	2/1/67	0/0/3
$CDR1_{(26-31)}$	0/0/0	0/2/10	0/2/8	1/0/6	1/0/5	1/0/11	0/0/0
$CDR2_{(48-55)}$	2/0/29	1/1/25	0/1/15	0/0/0	1/0/28	0/0/29	0/0/0
$CDR3_{(95-107)}$	3/0/21	2/0/20	1/0/24	1/0/40	2/0/34	1/1/23	0/0/3
$HV4_{(69-74)}$	0/0/0	0/0/0	0/0/1	0/0/0	0/0/0	0/0/0	0/0/0
MHC	5/3/86	2/1/79	1/2/77	2/0/69	3/0/89	4/1/86	3/0/116
Peptide	1/0/33	2/3/25	1/3/24	2/0/47	2/0/21	4/0/41	n.a.

n.a., not applicable.

similar AB-loop conformation has been found in the B7/HLA-A2/Tax complex structure (13), which, as for LC13, is free of crystal contacts in this region. A similar conformational change has not been observed for the 2C system, but here crystal contacts may have reduced the conformational freedom of the AB-loop. However, these data are still not compelling, and the necessity and extent of any conformational changes in the TCR/CD3 complex required for signaling must await a TCR/CD3 complex crystal structure or analysis by other biophysical methods, such as FRET.

One pertinent analysis of these TCR/pMHC docking orientations has resulted in grouping of the available TCR/pMHC complexes according to the positioning of their V_α domains with respect to the MHC-bound peptide (20). Four TCRs with their V_α

Table 4 Interactions of the peptide component of the pMHC with the TCR

TCR/MHC/peptide	# peptide residues	Peptide residue (P) and # contacts per residue																		# Total contacts
Peptide side-chain contacts with TCR																				
Human/mouse class I							P1	P2	P3		P4	P5	P6	P7	P8					
KB5-C20/H-2K^b/pKB1 (1kj2)	8						1	0	0		7	0	1	5	0					14
2C/H-2K^b/dEV8 (2ckb)	8						0	0	0		19	0	4	2	0					25
BM3.3/H-2K^b/pBM1 (1fo0)	8						0	0	0		1	0	24	6	0					31
2C-H-2K^b-SIYR (1g6r)	8						0	0	0		15	0	22	0	0					37
2C-H-2K^{bm3}-dEV8 (1mwa)	8						0	0	0		16	0	24	1	0					41
BM3.3-H-2K-VSV8 (1nam)	8						0	0	0		22	0	7	0	0					29
							P1	P2	P3	P4	P5	P6	P7	P8	P9					
A6/HLA-A2/Tax (1ao7)	9						1	0	0	0	16	1	5	11	0					34
B7/HLA-A2/Tax (1bd2)	9						4	0	0	0	29	0	4	10	0					47
AHIII12.2/HLA-A2.1/p1049 (1lp9)	9						0	0	4	0	13	12	2	6	0					37
JM22/HLA-A2/MP58–66 (1oga)	9						0	0	0	0	5	3	2	6	0					16
LC13/HLA-B8/EBV (1mi5)	9						0	0	0	0	0	3	17	0	0					20
A6-HLA-A2-TaxP6A (1qrn)	9						0	0	0	0	26	0	5	12	0					43
A6-HLA-A2-TaxV7R (1qse)	9						1	0	0	0	19	0	12	14	0					46
A6-HLA-A2-TaxY8A (1qsf)	9						4	0	0	0	15	0	1	0	0					20
1G4-HLA-A2-ESO9C (2bnr)	9						0	0	0	24[1]	56	2	8	10	0					100
1G4-HLA-A2-ESO9V (2bnq)	9						0	0	0	24	60	2	9	10	0					105
							P1	P2	P3	P4	P5[2]	P10	P11	P12	P13					
SB27-HLA-B3508-EBV (2ak4)	13						0	0	0	8	32	0	0	0	0					40
Human/mouse class II		P-4	P-3	P-2	P-1	P1	P2	P3	P4		P5	P6	P7	P8	P9	P10	P11	P12	P13	
172.10/I-A^u/MBP (1u3h)	12			0	2	0	0	0	0		8	0	5	1	0	0				16
HA1.7/HLA-DR4/HA (1j8h)	13			0	4	0	2	7	0		3	0	0	9	0	0	0			25
HA1.7/HLA-DR1/HA (1fyt)	13			0	6	0	2	4	0		7	0	0	9	0	0	0			28
Ob.1A12/HLA-DR2b/MBP (1ymm)	14	2	0	2	9	0	7	10	0		9	0	0	0	0	0				39
3A6-HLA-DR2a-MBP (1zgl)	14		6	0	3	0	10	0	1		2	0	9	0	0	1	0			32
scD10/I-A^k/CA (1d9k)	16		0	0	1	0	11	0	0		9	0	4	7	0	0	0	0		32

Peptide main-chain contacts with TCR

Human/mouse class I							P1	P2	P3		P4	P5	P6	P7	P8					
KB5-C20/H-2K^{b}/pKB1 (1kj2)	8						0	1	1		0	0	0	0	0					2
2C/H-2K^{b}/dEV8 (2ckb)	8						0	0	0		0	0	0	0	0					0
BM3.3/H-2K^{b}/pBM1 (1fo0)	8						0	0	0		0	1	1	5	0					7
2C-H-2K^{b}-SIYR (1g6r)	8						0	0	0		0	0	0	0	0					0
2C-H-2K^{bm3}-dEV8 (1mwa)	8						0	0	0		0	0	0	2	0					2
BM3.3-H-2K^{b}-VSV8 (1nam)	8						0	0	0		0	0	0	0	0					0
							P1	P2	P3	P4	P5	P6	P7	P8	P9					
A6/HLA-A2/Tax (1ao7)	9						0	1	0	10	0	1	1	1	0					14
B7/HLA-A2/Tax (1bd2)	9						0	0	0	5	0	1	4	3	0					13
AHIII12.2/HLA-A2.1/p1049 (1lp9)	9						0	0	0	15	3	1	2	0	0					20
JM22/HLA-A2/MP58–66 (1oga)	9						0	0	0	10	2	2	0	0	0					14
LC13/HLA-B8/EBV (1mi5)	9						0	0	0	0	0	7	0	1	0					8
A6-HLA-A2-TaxP6A (1qrn)	9						0	1	0	11	0	2	1	1	0					16
A6-HLA-A2-TaxV7R (1qse)	9						0	1	0	10	1	0	0	1	0					13
A6-HLA-A2-TaxY8A (1qsf)	9						0	1	0	9	0	0	0	0	0					10
1G4-HLA-A2-ESO9C (2bnr)	9						0	0	0	5	2	5	0	0	0					12
1G4-HLA-A2-ESO9V (2bnq)	9						0	0	0	5	2	6	0	0	0					13
							P1	P2	P3	P4	P5[3]	P10	P11	P12	P13					
SB27-HLA-B3508-EBV (2ak4)	13						0	0	0	0	39									39
Human/mouse class II		P-4	P-3	P-2	P-1	P1	P2	P3	P4		P5	P6	P7	P8	P9	P10	P11	P12	P13	
172.10/I-A^{u}/MBP (1u3h)	12			0	0	0	8	2	0		0	0	1	0	0	0				11
HA1.7/HLA-DR4/HA (1j8h)	13			0	0	0	0	0	0		0	1	2	4	0	0	0			7
HA1.7/HLA-DR1/HA (1fyt)	13			0	0	0	0	0	0		1	3	1	3	0	0	0			8
Ob.1A12/HLA-DR2b/MBP (1ymm)	14	3	0	3	1	0	0	3	0		0	0	0	0	0	0				10
3A6-HLA-DR2a-MBP (1zgl)	14		8	2	3	0	0	0	0		0	0	0	1	0	0	0			14
scD10/I-A^{k}/CA (1d9k)	16		0	0	0	0	0	0	0		0	1	1	1	0	0	0	0		3

[1] P4 is a Met and P5 is a Trp in the 1G4 structures; P4 is a Gly in the other 9-mer structures, and P5 is a Tyr, Phe, or Arg in the other 9-mer structures. This explains the high number of contacts at this position for the 1G4 structures.

[2] P5 is a P5, P6, P7, P8, P9 insert, with 3,0,16,0,13 contacts for these residues.

[3] P5 is a P5, P6, P7, P8, P9 insert, with 8,4,8,16,3 contacts for these residues.

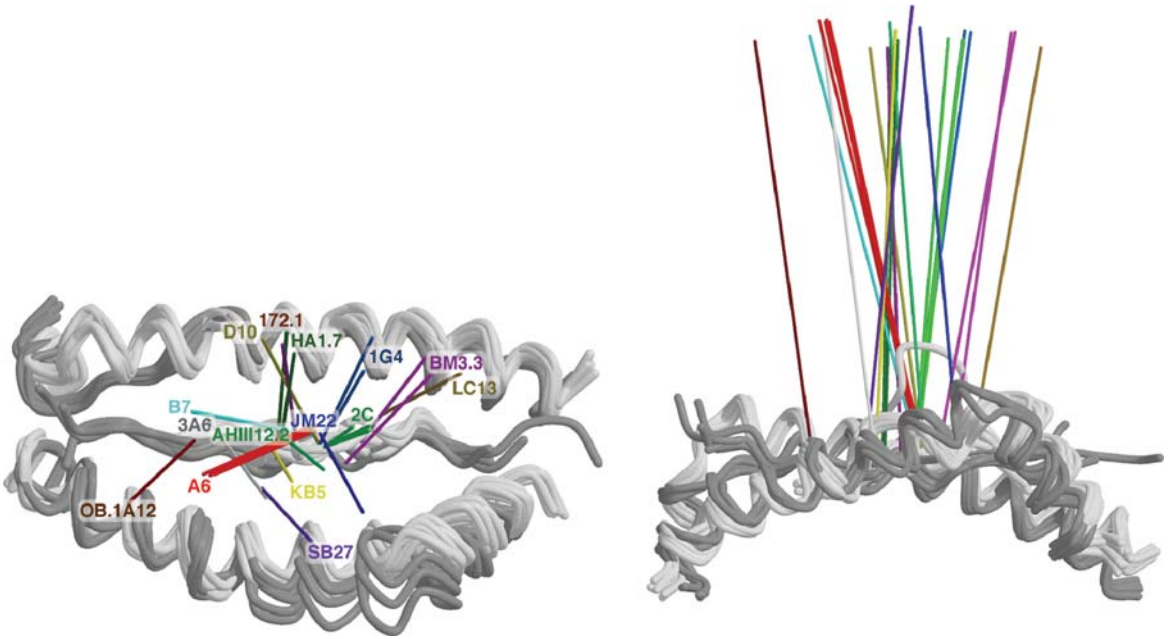

Figure 6

Variation in the tilt and roll of the TCR on top of the MHC. The left and right views are related by a 90° rotation about a horizontal axis. The MHC peptide backbones and the MHC helices are shown as gray tubes. The orientation axes are colored individually for each TCR. For 15 individual TCRs, the pseudo-twofold axes that relate the V_α and V_β domains of the TCRs to each other are shown, giving a good estimate of the inclination (roll, tilt) of the TCR on top of the MHC. The TCR twofold axes tend to cluster around P4-P6 at the center of the interface. Labels are placed at the top of each axis. The figure also indicates any shifts of the TCR along the peptide where the Ob.1A12 and LC13 TCRs mark the extremes, centered around P1 and P6, respectively. 3A6 and SB27 also are outliers at present where they are centered on one half of the peptide.

domains located closer to the N terminus of the peptide exhibited CD8-dependent signaling, whereas another four TCRs in which their V_α domains were closer to the C terminus of the peptide acted independently of CD8. A geometric model was put forward to explain this correlation of V_α domain positioning with the CD8-dependence: A diagonal orientation of the TCR with the V_α domain over the N terminus of the peptide would allow efficient recruitment of CD8, whereas the TCR/pMHC docking mode with the V_α domain closer to the C terminus of the peptide would require high TCR/pMHC affinity to initiate CD8-independent signaling. Thus, it was speculated that CD8-independent TCRs would generally exhibit a higher affinity for pMHCs, which in turn raised the question why these TCRs survived negative selection in the thymus that would be biased against high-affinity self-recognition. To reconcile this apparent discrepancy, a very different docking orientation was proposed during TCR selection compared to T cell/APC engagement, in contrast to other views that dispute any such global rearrangement of TCRs once they have engaged pMHC (16, 85, 86). Furthermore, in the H-$2K^b$ system, the BM3.3 TCR requires CD8 for signaling when engaging H-$2K^b$/VSV8, but can signal independently of CD8 when bound to a different peptide (pBM1) in the context of the same MHC (87), yet crystal structures of the two complexes do not show

any significant differences in their docking geometries (16, 30).

TCR-INDUCED FIT

Insight into the structural changes that accompany TCR/antigen engagement (i.e., induced fit) must include crystal structures of the same TCR in its free and bound forms or of the same TCR bound to different pMHCs. Until recently, only two well-studied systems, the 2C and A6 TCRs, fulfilled these requirements. The 2C system allowed comparison of the free 2C TCR (7) with an agonist (12) and a superagonist peptide (17) in complex with the same H-2K^b MHC (**Figure 7*a***). This comparison disclosed a functional hotspot between the CDR3 loops in the 2C TCR that finely discriminated between side chains and conformations of centrally located peptide residues through increased complementarity and additional hydrogen bonds. In the A6 system (13, 14), altered peptide ligands (APLs), i.e., peptides of slightly different sequence than the natural ligand, induced only subtle conformational changes in the TCR (**Figure 7*b***). In both the 2C and A6 systems, conformational changes are restricted mainly to the CDR3 loop regions, and the largest conformational differences were observed when comparing free versus bound TCR (36).

Recently, two crystal structures of the BM3.3 TCR bound to different peptides (pBM1 and VSV8) in complex with the class I MHC H-2K^b (30, 31) provided another system for study of conformational changes (**Figure 7*c***). The BM3.3 TCR not only recognizes the naturally processed, allogeneic pBM1 peptide presented by H-2K^b, but also cross-reacts with an H-2K^b-bound peptide from vesicular stomatitis virus (VSV8). The BM3.3 TCR rotates 5° and shifts by 1.2 Å when contacting the VSV8 peptide compared to the pBM1 peptide, which is comparatively small given the complete absence of any sequence homology between the two peptides. The $\alpha_1\alpha_2$-helices move slightly, in synchronization with peptide conformational changes, but similar changes have already been seen within unliganded pMHC complexes (88) and, hence, are not necessarily attributable to TCR binding. Large differences between the two complexes are, however, seen in the CDR3 conformations, which allow the BM3.3 TCR to adapt to different peptides bound to the same H-2K^b MHC. In the allogeneic BM3.3/H-2K^b/pBM1 pMHC complex, the CDR3α loop flares away from the peptide, leaving a large, water-filled cavity between the pMHC and the TCR. In the BM3.3/H-2K^b/VSV8 complex, the CDR3α loop adopts a very different conformation with a maximum displacement of >5 Å for the Tyr97 Cα atom (**Figure 7*c***). This movement results in burial of a larger surface area (~16%) for this complex due to closer proximity of CDR3α to the pMHC interface (**Table 2**). This altered CDR3α conformation can explain the cross-reactive properties of this TCR, but also raises the question of how reasonable specificity is maintained given the large loop movements in CDR3α. The affinity of the self BM3.3/H-2K^b/pBM1 complex is 44-fold higher than for the VSV8 complex (K_d at 298 K of 2.6 μM and 114 μM, respectively) despite the buried surface area being smaller. The TCR conformational changes led to increased V_β interaction (56 versus 29 contacts), but decreased V_α contacts (27 versus 49) in the allogeneic complex compared with the self-syngeneic complex, although slightly more overall TCR-peptide contacts (83 versus 78) are made in the self complex (**Table 2**). Although this affinity difference amounts only to 9.4 kJ/mol at 298 K, which is equivalent to a single hydrogen bond, it is significant, and the nonconformity with the size of the buried surface area is somewhat unexpected. The antidromic behavior of affinity and buried surface may result from unfavorable entropic contributions due to conformational changes of CDR3α during BM3.3 binding to H-2K^b/pBM1.

The KB5-C20 TCR has also been determined in its free form (8) and bound to the

pKB1 peptide presented by H-2K$^{b(31)}$. In the free form, the unusually long CDR3β loop of 13 residues is packed tightly against the CDR3α loop, leaving no pocket for binding of pMHC. Thus, this unliganded KB5-C20 structure indicated that a large conformational change of at least CDR3β must accompany pMHC engagement, which was indeed found in the KB5-C20/H-2K^{b}/pKB1 complex (31). Although the other CDRs displayed

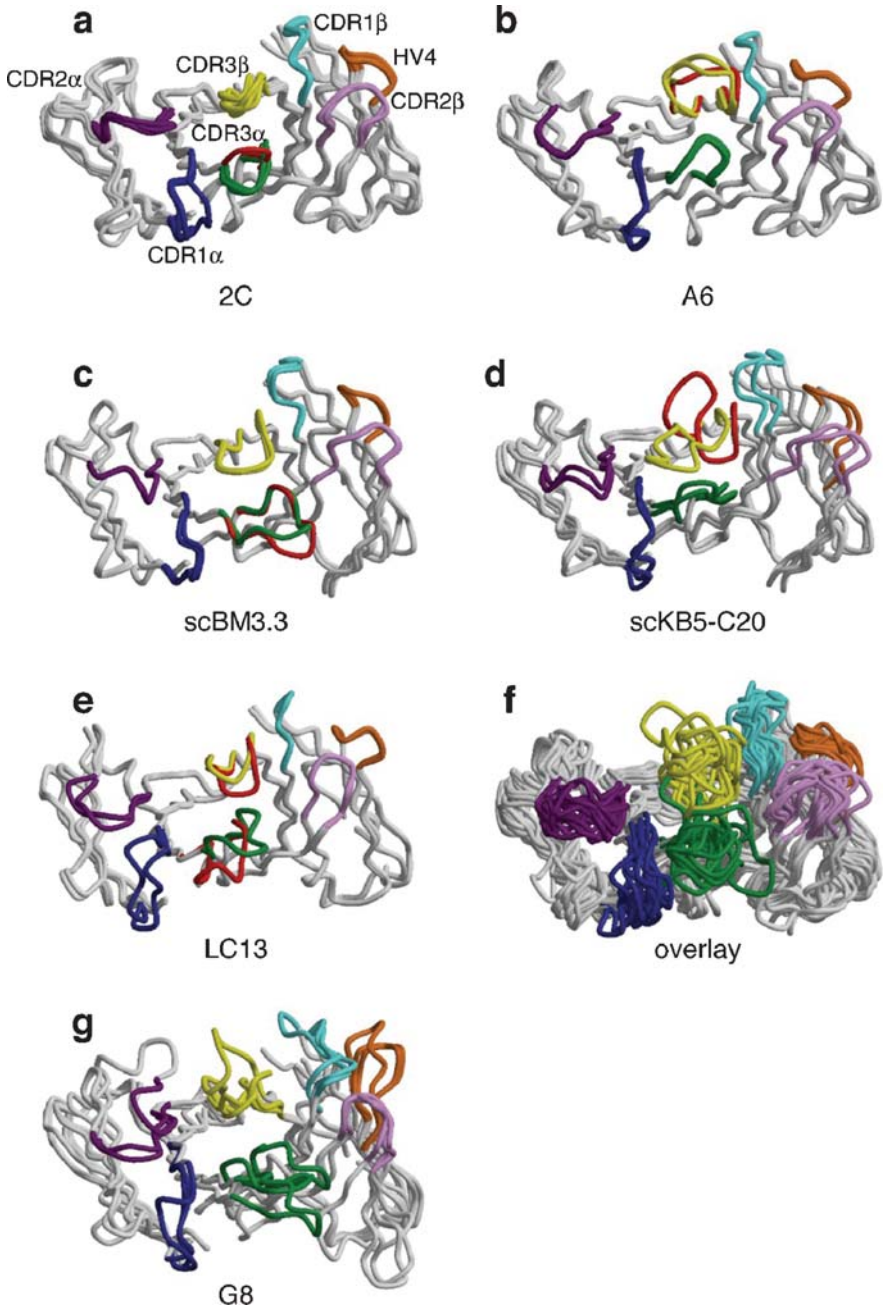

only minor hinge movements upon pMHC complex formation, the apex of CDR3β underwent a large shift of 15 Å, concomitant with a complete reorganization of its loop structure (**Figure 7*d***).

In these four examples described above, the majority of CDR conformational changes were limited to either CDR3α or CDR3β, but in a recent complex between the "public" LC13 TCR and its immunodominant Epstein Barr virus (EBV) peptide antigen in complex with HLA-B8, both CDR3 loops, as well as CDR1α and CDR2α, underwent large conformational changes when free and bound TCRs were compared (10, 24) (**Figure 7*e***). Apparently, the dominant LC13 TCR response represents the optimal immunological answer to persistent EBV infection, as it is selected by unrelated individuals, and thus termed public. One hallmark of this TCR is a ~7–10 Å translational shift (calculated after overlapping the HLA-A2 MHC molecules in the B7, A6, JM22, and 1G4 complexes) toward the EBV peptide C terminus (**Figure 5**), contacting peptide residues P6 and P7 rather than the more common peptide contact residue P5 (**Table 4**). However, the marked lateral shift of the LC13 TCR is peculiar to this complex and not a general characteristic of HLA-B MHC complexes as the SB27/HLAB3508/EBV complex (23) does not show this feature (**Figure 5**). Of the three C-terminal peptide residues, the Tyr-P7 side chain (17 contacts plus two water-mediated hydrogen bonds to LC13 residues His33α and His48α) dominates the TCR contact area. Mutation of this tyrosine to phenylalanine reduces CTL recognition by a factor of 10 (which would translate into a K_d value of ~100 μM) (24), similar to a functional hotspot described for the 2C system, where mutation of a lysine to an arginine residue in the dEV8 peptide converts an agonist into a superagonist with ~1000-fold increase in cytotoxicity (17). Comparison of free and bound LC13 TCRs reveals a 2.5 Å rigid body shift and rotation by 38° of CDR3β, which displaces individual loop residues (Gln98β, Ala99β, Tyr100β) by up to 5 Å and maximizes the peptide readout by increasing the shape complementarity (S_c). More drastic changes of up to 8 Å are found for CDR3α, which switches from a mobile, extended structure in the unliganded LC13 to a crumpled structure (89) that makes extensive contacts with the HLA-B8 α_1-helix. Pro93 appears to

Figure 7

Conformational variation and induced fit in the TCR CDR loops. The TCR V_α- and V_β-chains are shown in light gray looking down onto their antigen-binding site (MHC view). Their CDR loops are colored as in **Figure 3**. The central CDR3 loops are the most structurally diverse and recognize mainly peptide, whereas the CDR1 and CDR2 loops recognize the mostly conserved helical structural features on the MHC. (*a*) Overlay of the unliganded 2C TCR with three pMHC-liganded structures. The unliganded 2C TCR structure shows significant conformational differences of its CDR3α (*red*) and CDR1α loops (*dark blue*). (*b*) Overlay of four liganded A6 TCR structures. The only A6 CDR loop showing conformational variability in response to the different Tax peptide mutants in the HLA-A2 complexes is CDR3β (*red* for the wild-type Tax complex, *yellow* for all others). (*c*) Comparison of the BM3.3 conformation when bound to H-2K^b carrying either the pBM1 or the VSV8 peptide. The CDR3α loop flares away from the peptide in the pBM1 complex (*red*), interacting with the MHC α_1-helix, while it is closer to the peptide in the VSV8 complex, where it also buries a larger surface area of the pMHC compared to the pBM1 complex. (*d*) Comparison of the unliganded KB5-C20 TCR and its structure in the H-2K^b/pKB1 complex. The large conformational change of the CDR3β loop (*yellow* in the unliganded form) is highlighted in red for the H-2K^b/pKB1 complex. (*e*) Comparison of the unliganded class II LC13 TCR and its structure in the HLA-B8/EBV complex. The large conformational changes of the CDR3α and CDR3β loops are highlighted in red for the complex. (*f*) Overlay of all TCRs, free and bound, to show the degree of variation in the CDR loop regions. The Cα atoms of the variable domains were used to generate the alignment. (*g*) Comparison of the G8 (102) and the $V_\gamma 9/V_\delta 2$ γδ (76) TCRs. Both molecules in the asymmetric unit of the G8 receptor are shown.

mediate this radical change in CDR3α conformation, as it is present in six different HLA-B8-restricted CTL clones (90) and is encoded by an N-region addition, indicating that somatically derived TCR residues may be important for specifying cognate interactions. When complexed to HLA-B8/EBV, CDR1α and CDR2α deviate strongly from the canonical conformations (91) that they adopt in the unbound state. Both rigid body shifts and structural crumpling lead to maximum displacements of up to 7 Å in each loop. Such large changes were not apparent in the 2C and KB5-C20 systems, where nonrigid body conformational changes were confined to the CDR3 loops (**Figure 7**).

FROM ALLOREACTIVITY TO XENOREACTIVITY

An impressive 1% to 10% of mature T cells recognize and respond to nonself MHC (92), a phenomenon termed alloreactivity, which is the molecular reason for organ and skin graft rejection and, in immunocompromised individuals, graft-versus-host disease. As an exact tissue typing between donor and acceptor is not always possible, graft rejection poses a major obstacle for long-term stability of organ transplants in patients. Crystal structures of alloreactive TCR/pMHC complexes and comparison with their syngeneic counterparts have recently begun to shed light on the structural basis of alloreactivity. The alloreactive BM3.3/H-2K^b/pBM1 (16) and 2C/H-2K^{bm3}/dEV8 (19) complexes showed an increased propensity for TCR V_β interactions with the pMHC (**Table 2**). Although the syngeneic complex is still unavailable for BM3.3/H-2K^b/pBM1, the 2C/H-2K^{bm3}/dEV8 structure (19), which carries an alloreactive Asp77Ser mutation buried in the H-2K^{bm3} molecule, can be compared with the syngeneic 2C/H-2K^b/dEV8 complex (12). This analysis revealed a shift of the TCR/pMHC contacts from predominantly V_α contributions in 2C/H-2K^b/dEV8 to a preponderance of V_β interactions in 2C/H-2K^{bm3}/dEV8 (**Table 2**). In the 2C/H-2K^b/dEV8 complex, the V_α domain of the 2C TCR mediates 69 interactions (van der Waals and polar) with pMHC versus only 17 contacts by the V_β domain. Strikingly, the relative contribution of the variable domains in the 2C/H-2K^{bm3}/dEV8 interface was reversed to 50 V_α versus 63 V_β interactions. In the BM3.3/H-2K^b/pBM1 complex, the V_β interactions also dominate the TCR/pMHC interface (28 V_α versus 63 V_β interactions). However, this propensity for increased V_β interactions in alloreactive complexes was contradicted by another TCR/pMHC complex, KB5-C20/H-2K^b/pKB1 (31). The alloreactive murine TCR KB5-C20 arises from an H-2^k background and recognizes three different pKB peptides (pKB1–3) in complex with H-2K$^{b(87)}$. In the KB5-C20/H-2K^b/pKB1 complex, the V_α domain contributes 52 contacts to the pMHC, whereas only 40 contacts are mediated by the V_β domain (**Table 2**). However, we do not have the corresponding syngeneic complex for comparison.

In addition, a recent structure of a xenoreactive TCR/pMHC complex (20) showed a preponderance of V_α interactions. In xenoreactive complexes, a TCR selected in one species now exercises cross-species reactivity. Murine AHIII 12.2 TCR cross-reacts with human class I MHC HLA-A2 bound to peptide p1049 and acts in a CD8-independent manner, as mouse CD8 does not bind to human MHC. The crystal structure of this complex (20) provided some insight not only into the CD8-independence of T cell signaling (see below), but also on the structural basis of xenoreactivity. The TCR, again, is poised diagonally (67°) across the pMHC interface, with no obvious reorientation or other characteristics that would easily rationalize this biological distinctiveness. Thus, in this case, xenoreactivity is indistinguishable from self- and allorecognition at the overall TCR/pMHC structural level. V_α contributes twice as many interactions to the pMHC as V_β (103 V_α and 49 V_β interactions), again

suggesting that V_β interactions do not necessarily dominate in alloreactive or xenobiotic complexes.

Taken together, neither alloreactivity nor xenoreactivity seems distinguishable from syngeneic TCR recognition by analysis of the TCR/pMHC interfaces of their respective crystal structures. Apparently, alloreactivity is a natural consequence of the essential requirement for TCRs to be able to rapidly screen the repertoire of MHC/antigen complexes on the cell surface. A certain number of contacts must be made and/or landmarks recognized on the pMHC surface for the TCR to successfully interact and remain docked with its antigen. However, the TCR/pMHC associations selected in the thymus are of relatively low affinity (1–100 μM), creating opportunities for cross-reactivity in the periphery. Thymic selection cannot select for substantially higher or lower affinity or else too few (i.e., too highly restricted or too promiscuous, respectively) TCRs would emerge to combat the ever-changing antigenic repertoire of microorganisms.

TCR SELECTION, SELECTIVITY, CHAIN BIAS, AND CROSS-REACTIVITY

Certain antigens select a very restricted TCR repertoire, such as the immunodominant antigen derived from EBV. This virus causes persistent infections in up to 90% of adults (93), and an antigen derived from it is presented by HLA-B8. The conformational changes associated with binding of the LC13 TCR to the HLA-B8/EBV pMHC antigen have been described above and are on a scale similar to other changes seen between free TCRs and their complexes with pMHC. Also, the affinity of the LC13/HLA-B8/EBV complex (K_d ~10 μM) is within the range of most other TCR/pMHC systems (24). Why then, in this particular case, is chain bias so extreme that most CTLs use the LC13 TCR for combating EBV infections? The structural explanation for this immunodominance is proposed to be the induced fit of the CDRs, which included changes in the canonical structures of germ line–encoded CDRs 1α and 2α, that enhance complementarity with the pMHC. The TCR/pMHC interaction was then proposed to induce further conformational changes in the TCR Cα domain to enhance its interaction with CDR3ε (24). This specificity advantage of LC13 was then proposed to increase avidity of the expanded T cell lineages, or lead to superior signaling or more efficient formation of the immunological synapse. However, LC13 does not exhibit the highest complementarity seen so far as measured by the S_c index. LC13 has a S_c coefficient of 0.61, whereas in other TCR/pMHC complexes this value varies from 0.41 to 0.75, with several around 0.70 (**Table 1**). However, the buried surface area for the LC13 complex is among the largest at 2020 $Å^2$ compared with an average of 1791 $Å^2$. Furthermore, other TCRs undergo conformational changes, and only this TCR has the C_α-induced change.

Another example of immunodominance in TCR chain bias is the V_β17-V_α10.2 TCR (JM22) in complex with HLA-A2 that presents an influenza matrix protein antigen (21). In general, the anti-influenza response in HLA-A2-positive adults relies predominantly on TCRs containing V_β17 and is directed against the influenza matrix protein (M1) residues 56–66. The 1.4 Å-resolution structure of the complex is the highest-resolution TCR/pMHC crystal structure determined to date and notably defines four water molecules that are completely buried in the TCR/pMHC interface and strongly contribute to the overall shape complementarity ($S_c = 0.73$ in the presence and 0.63 in the absence of these water molecules), underscoring the essential role of solvent in immune recognition, as in antibody-antigen interfaces (94). The JM22/HLA-A2/MP58-66 structure indicates a more perpendicular orientation (62°) of the TCR with respect to the MHC that differs strongly from TCRs B7 (48°) or A6 (34°), but not from 1G4 (69°), that all

bind to the same MHC (**Table 2**, **Figure 5**). This TCR footprint is more focused on the C-terminal end of the pMHC groove, with substantially more V_β (71) than V_α (29) interactions. Thus, as in the examples of H-2K^b recognition by different TCRs (2C, BM3.3, KB5-C20), these HLA-A2 TCRs find different solutions to binding the same MHC, albeit with different peptides, such as has been found for different antibodies that bind to the same protein antigen (95).

Does the binding mode of JM22 to HLA-A2/MP58-66 then reveal the molecular reason for its immunodominance? Normally, the centrally located P5 peptide side chain in HLA-A2 complexes wedges into a notch between the CDR3α and CDR3β loops. In the JM22/HLA-A2/MP58-66 complex, this situation is reversed in that a large side chain from the TCR, CDR3β Arg89, now binds into a notch between peptide residue Phe-P5 and the MHC α_2-helix and establishes five hydrogen bonds. As CDR3β residues Arg89 and Ser99 are conserved in the majority of TCRs active against the HLA-A2/MB58-66 epitope (96, 97), this region is likely responsible for the immunodominance. Markedly more contacts to the pMHC are mediated by the TCR β-chain than by the α-chain (71 versus 29 contacts; **Table 2**), and all specific contacts to the peptide are made by the β-chain (21). In addition, CDR1β Asp32 and CDR2β Gln52 bind to the MP58-66 peptide, suggesting that these four residues apparently are sufficient for V_β17 chain bias. Selection of this particular TCR is probably reinforced by repeated influenza infections, as the V_β17 chain becomes dominant during the first years of life (98). The N-terminal domain of influenza matrix protein M1 (99), from which the antigen is derived, is composed of a dimer of two four-helix bundles, where the TCR epitope residues 56–66 form one of the central helices. Thus, this sequence may critically contribute to stability of M1 so that it is not easily mutable during influenza evolution, and may explain why this epitope would give such a conserved and durable cytotoxic response.

AUTOIMMUNE TCR/pMHC CLASS II COMPLEXES

In a recent class II TCR/pMHC complex, a novel docking mode was identified where the Ob.1A12 TCR slid along the binding groove toward the N-terminal region of the bound peptide (**Figure 5**). The crystal structure of the human autoimmune TCR Ob.1A12 in complex with HLA-DR2 and a self-peptide from myelin basic protein (MBP), which has been linked to multiple sclerosis, represented the second example of an autoimmune TCR/pMHC complex (27). It was suggested that this docking mode pertains to autoimmune complexes in general. The translation of the Ob.1A12 TCR along the groove indeed represents another facet of MHC restriction (100) in which the TCR has moved its center of mass to focus only on half of the available peptide epitope and binds in an orthogonal orientation (84°) (**Table 3**; **Figure 5**). As a consequence, only the N-terminal residues of the autoimmune MBP peptide (P-4, P-2, P-1, P2, P3, and P5) are contacted by the TCR, leaving the C-terminal half of the peptide unsurveyed, as far as the informational content is concerned (**Table 4**).

Why are such autoimmune TCRs not deleted via positive and negative selection? A possible explanation would be that in the thymus, the canonical diagonal docking geometry is used during the selection process for low-affinity interactions (MHC) to self pMHC. TCRs would then bind to pMHCs containing self-peptides in the periphery, but in a noncanonical, yet immunologically productive, manner, which would effectively undermine the selection process. In addition, coreceptor binding (CD4 or CD8) could aid in rescue of low-affinity complexes, such as the Ob.1A12 complex (27). Although the Ob.1A12/HLA-DR2/MBP complex certainly expands the

range of TCR/pMHC orientations and translations, its docking geometry is not the answer to this question of autoimmune TCR/pMHC recognition as a related complex, 172.10/I-A^u/MBP (28), docks canonically in a diagonal mode (60°) and in the center of the binding groove. Unlike Ob.1A12, which focuses on the N-terminal residues of MBP, the 172–10 TCR binds only to MBP residues at the C-terminal end of the groove. As for allogeneic complexes, V_β dominates the interaction. In this case, the preponderance of V_β interactions is due not to TCR translation along the groove but to a two-residue register shift of the bound peptide within the I-A^u groove (101). This shift places the first peptide residue in the P3 pocket of the MHC, and the peptide N terminus is now buried under the CDR3α loop, out of reach of CDRs 1α and 2α, and, as a consequence, the majority of the MBP peptide is accessible only to V_β (**Table 1**).

γδ TCR/NONCLASSICAL MHC COMPLEX

Although a database of αβ TCRs and αβ TCR/pMHC complexes has now been accumulated that is large enough to permit some general conclusions on TCR binding modes, the γδ lineage of TCRs was severely underrepresented until the first crystal structure of a human γδ TCR G155 (76). A recent crystal structure of the γδ TCR G8 bound to its ligand, the nonclassical MHC T22 (102), provided some indication of a ligand recognition strategy by γδ TCRs. Because γδ TCRs are normally stimulated by small molecule antigens, such as phosphoantigens derived from pathogens like *Mycobacteria* (72, 73), or by whole protein molecules, such as herpes simplex virus glycoprotein gI (74) and CD1 (75), the γδ TCR/T22 complex is an exception to the normal binding repertoire of γδ T cells, as this TCR is in complex with an MHC molecule. The most striking observation of this 3.4 Å-resolution complex structure is the severely tilted orientation of the γδ TCR with respect to its MHC-like ligand that by far exceeds the range of tilting angles seen in αβ TCRs (**Figure 4)** and is also slightly different within the two molecules present in the crystallographic asymmetric unit. The γδ TCR binding mode may then be more like those of antibodies rather than of αβ TCRs, which are restricted to MHC molecules. Indeed, structural comparison of the γδ TCR chains to antibodies and αβ TCR chains showed more antibody-like characteristics of the γδ TCR, which is also reflected in their diverse ligand specificities (103).

The CDR loops of the two γδ TCR molecules in the crystallographic asymmetric unit are coaligned such that they could recognize two T22 ligands on a target cell simultaneously. Multimerization for some αβ TCRs has been observed by quasi-elastic light scattering in solution upon ligand binding (104), but no crystallographic evidence yet supports this notion. Thus, other crystal structures of γδ TCR/ligand complexes are needed to verify any possible increased multimerization propensity for γδ TCRs compared to αβ TCRs.

The tilted orientation of the γδ TCR with respect to its ligand (**Figure 4**) almost entirely abolishes any contacts of the V_γ domain with T22; only two (complex 1) or four (complex 2) interactions between CDR3γ and T22 are present in the complex, whereas, surprisingly, the CDR1γ and CDR2γ loops are not utilized at all. The paucity of V_γ interactions (3 van der Waals contacts) is in stark contrast to the 116 V_δ interactions, in which the CDR3δ loop predominates (71 van der Waals contacts). CDR3δ loops in γδ TCRs are generally longer than in αβ TCRs and, owing to the sideways binding mode of G8, can fully access the exposed region of the T22 groove. The disordered α_2-helix region in the unliganded T22, which is also unstructured in T10 (56), does not become ordered upon TCR binding as might have been expected from comparison of an unrelated complex of the NK cell

receptor NKG2D with the nonclassical MHC MICA (105). In unliganded MICA, the partially unwound α_2-helix (66) refolds upon receptor binding, but this loop ordering is not observed with T22 as the γδ TCR does not engage this part of the MHC-like antigen.

Some docking flexibility of G8 with respect to ligand binding is apparent where the TCR pivots around CDR3δ, which leads to a rotation of 5° (V_δ) and 13° (V_γ) of the TCR domains when the two complexes in the asymmetric unit are compared with each other. Such TCR flexibility was also seen in a recent αβ TCR complex, where the SB27 TCR binds to a bulged 13-mer peptide derived from EBV that is presented by the class I MHC HLA-B3508 (23). As the peptide termini are fixed in the MHC class I groove, the additional central residues bulge outward and away from the MHC, limiting access of the TCR to the MHC α-helices; only two direct hydrogen bonds and 40 van der Waals contacts are present between the SB27 TCR and the HLA-B3508 MHC, whereas the peptide contributes 9 hydrogen bonds and 66 van der Waals contacts to the TCR/pMHC interface (**Tables 2, 4**). With the bulged peptide dominating the interface, the TCR "swivels" on top of the peptide, and the two copies of the TCR in this crystal form differ by a 12° rotation when compared with each other, as no other interactions with the MHC α-helices are observed that would restrict its orientation and docking angle (23).

Thus, the γδ TCR docking flexibility is not unique to this class of TCRs and does not seem to be a consequence of smaller buried surface area (1750 Å^2) or lower shape complementarity (S_c of 0.66), as both of these parameters are in the same range as αβ complexes (**Tables 2, 3**). In addition, as the precision of buried surface area and S_c calculations is also dependent on the resolution of the structure determination, more crystal structures of higher resolution and with different γδ TCRs are needed for statistically meaningful analyses on ligand recognition by γδ TCRs.

TCR ASSEMBLY AND SIGNALING

TCR/pMHC engagement is only the first step in the assembly of what is now referred to as the immunological synapse, wherein not only TCRs but also coreceptors (CD4 and CD8) and additional signaling modules (CD3) interact to form the signaling-competent, supramolecular complex. No structural information is available on the entire T cell receptor assembly, but steric restrictions imposed by the shape and properties of the individual domains and subcomplexes whose structures are known provide some essential limitations on the architecture of the complex.

CD4 AND CD8 CORECEPTORS AND THEIR MHC COMPLEXES

In addition to their cognate TCRs, class I and class II MHCs are recognized by their respective coreceptors CD8 and CD4. The current database for CD8 coreceptor consists of human CD8αα/HLA-A2 (106), murine CD8αα/H-2K^b (107) (**Figure 8*a***), and murine CD8αα/TL (68) structures. In all complexes, the CD8αα homodimer binds primarily to the α_3 domain of the MHC molecule in an antibody-like fashion, with the MHC α_3 CD loop wedged between two corresponding CDR-like loops from the CD8αα dimers (**Figure 8*a***). The structure and relative conformation of the C-terminal stalk region of CD8, which connects the coreceptor to the T cell surface, are still unclear, so the disposition of the TCR relative to the CD8αα/MHC scaffold is unresolved.

The determination of a crystal structure of a CD8αβ heterodimer has also been elusive. CD8αβ modeling based on CD8αα, mutagenesis, and the different stalk lengths of the α and β subunits have been used to predict the orientation of the CD8αβ heterodimer with respect to the MHC (**Figure 8**). The CD8αβ heterodimer is not simply a functional homolog of the CD8αα homodimer,

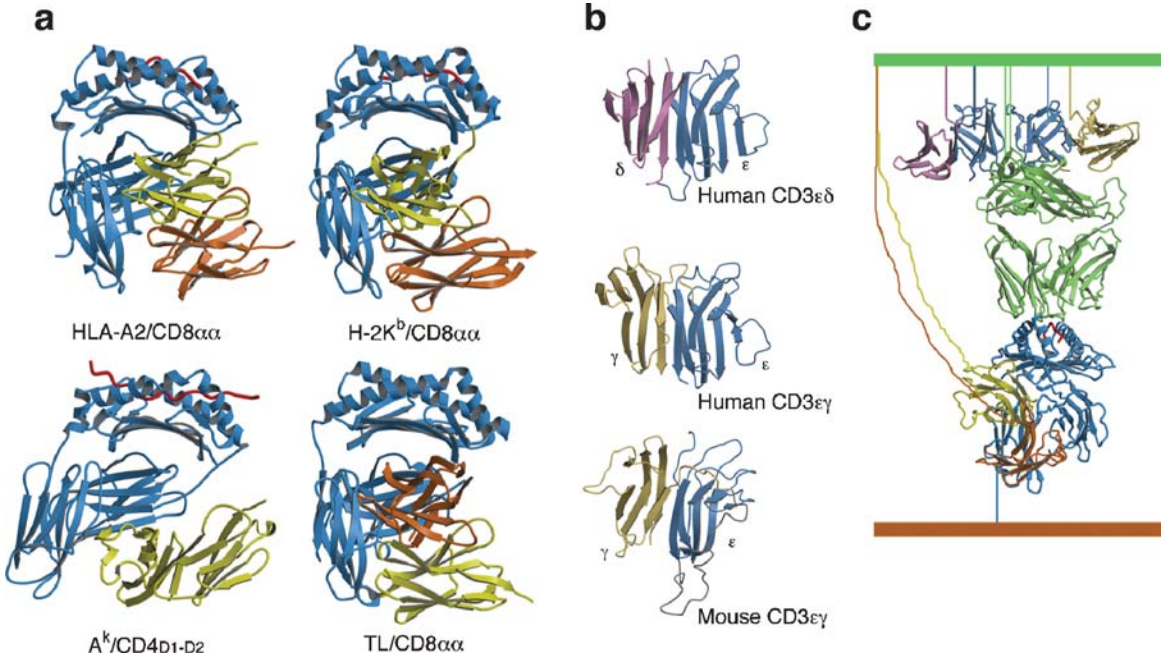

Figure 8

CD8 and CD4 coreceptor binding to class I and class II MHC. (*a*) The MHC is colored blue, CD8αα in yellow and orange. It is not yet known which of the domains of CD8αα homodimer correspond to the CD8αβ heterodimer (*upper* and *lower right panel*). The MHC is colored blue, and the CD4 (two N-terminal domains) is colored in yellow (*lower left panel*). (*b*) Human CD3εδ (*top*), human CD3εγ (*middle*), and mouse CD3εγ (*bottom*). In all three panels, the common ε-chain is colored in blue. (*c*) Hypothetical TCR/pMHC/CD3εδ/CD3εγ/CD8 complex. The TCR/pMHC-CD8αα and putative CD8αβ interaction is modeled by superimposing two structures, the HLA-A2/CD8αα complex (1akj) and the TCR A6/HLA-A2/TaxP6A complex (1qrn) on their MHC residues α1–180, with TCR (*green*), MHC (*dark blue*), peptide (*red*) and CD8 (*yellow* and *orange*). The CD3εδ (1xiw, *pink* and *blue*) and CD3εγ (1sy6, *gold* and *blue*) are shown "docked" at the top of the figure, with the common ε-chains colored in blue. This "docking" merely represents placing of the CD3 structures in the vicinity of where they are thought to bind, roughly following the cartoon diagram in Reference 125. Lines are drawn in to depict tethers connecting the different subunits to the TCR cell membrane (*top*, *green*) or the antigen-presenting cell membrane (*brown*, *bottom*).

as CD8αβ is the true αβ TCR coreceptor, whereas the main function of CD8αα on intraepithelial lymphocytes is to aid in adaptation and survival in the gut (108). Clearly, a CD8αβ structure in complex with pMHC is needed to derive the structural basis of why CD8αα cannot functionally replace or complement CD8αβ.

The low-resolution (4.3 Å) crystal structure of CD4 (domains 1 and 2) bound to I-A^k shows how the analogous coreceptor interaction is achieved in the MHC class II system (109). Whereas both domains of CD8 cooperate to bind class I MHCs, only one domain (the N-terminal variable-like region) of CD4 makes contact with the MHC with the second tandem CD4 domain being distal to the interface. Comparison of the CD4/pMHC and CD8/pMHC structures exposes a surprising structural dichotomy of the MHC class I and class II architectures, implying profoundly different modes of organization in their respective immunological synapses (**Figure 8**). As the complete, four-domain crystal

structure of human CD4 is also known (110), superposition of the MHC-proximal CD4 domains 1 and 2 permits assembly of a complete class II TCR/pMHC/CD4 model that suggests a V-shape with the T cell membrane-proximal ends of the TCR and CD4 separated by around 100 Å. This separation would exclude direct TCR/CD4 interactions, but leaves ample room for binding of CD3.

CD3 SIGNALING MODULES

CD3 consists of subunits δ, ε, γ, and ζ that noncovalently associate to form CD3ζζ homodimers and CD3εδ and CD3εγ heterodimers (111, 112). Whereas sustained T cell responses rely on coreceptor binding and TCR aggregation (113–116), early TCR signaling is independent of these events but may instead rely on conformational changes in the CD3ε subunit (84). In addition, stable cell surface expression and normal development of αβ TCRs rely on the presence of the CD3 components (117–119). Sequence comparisons predicted that the extracellular domains of the CD3ε- and CD3γ-chains would adopt an immunoglobulin fold (120). A cavity formed by the FG loop in the Cβ domain of αβ TCRs was suggested to host a binding site for such an Ig-domain (9), but other studies reported the dispensability of any Ig-domain residues in CDεδ for TCR α-chain binding, limiting the key residues to the conserved charged transmembrane residues on CD3 and the TCR (121). The first insights into these signaling modules came from an NMR structure in which the extracellular domains of the mouse CD3ε and -γ subunits that lacked the conserved RxCxxCxE stalk region motif, considered important for dimerization, were converted to a single-chain format by a 26-residue linker that ensured close proximity during folding from inclusion bodies (120) (**Figure 8*b***). The solution structure of this construct indeed revealed an Ig-fold of canonical type C2 (A Greek key motif) for the CD3ε and CD3γ subunits (122). The two subunits are connected via an intermolecular β-sheet, which would put the conserved RxCxxCxE stalk region motifs into close proximity to each other (**Figure 8*b***).

The crystal structure of the human CD3εγ heterodimer in complex with the therapeutic antibody Fab OKT3 (89) revealed a topology for CD3ε slightly different from that suggested by the solution structure (**Figure 8*b***). In the human CD3ε, an eight-residue sequence insertion between β-strands C′ and E adds an additional β-strand D on the surface of CD3ε. This β-strand is distal to the subunit interface and significantly alters the surface shape and electrostatic properties of CD3ε (see below). As a result of the additional β-strand, human CD3ε adopts a C1 Ig-fold rather than the C2 Ig-fold present in mouse CD3ε(122).

The higher precision of this crystal structure allowed reliable calculation of S_c values and buried surface areas (S_c of 0.76 and 1840 Å^2, respectively), which explains the high affinity of the subunits for each other and the fact that the cysteine-rich stalk region is not necessary for CD3εγ complex formation (123, 124). Comparison of the NMR and crystal structures indicated a 23° rotation of the domains about the pseudo-twofold axis relating the ε and γ subunits. Thus, variability in domain associations seems to arise among these accessory modules, as they do in other Ig proteins, such as TCRs and antibodies. Also, compared to mouse CD3ε, significant differences are present in the surface potential of human CD3ε, mainly due to the presence of the sequence Asp-Glu-Asp, which connects β-strands D and E and considerably increases the size of an electronegative patch that is also present in mouse CD3ε. Both CD3εγ structures, therefore, support a TCR binding model that is based mainly on electrostatic interactions, although their detailed interactions may vary.

In the human OKT3/CD3εγ complex, the antibody Fab binds at a site remote from the proposed TCR interacting surface of CD3εγ. Both antibody and TCR appear able to bind

the CD3εγ module if it is kinked. This kinking, as the authors speculate, could transduce a conformational change across the plasma membrane that could represent the molecular basis for the induction of early T cell signaling by OKT3.

The elusive human CD3εδ structure was recently determined in complex with the scFv fragment of the UCHT1 antibody (125) (**Figure 8*b***). In contrast to the CD3εγ structures, no linker was used in the production of a CD3εδ complex, and each domain included the conserved cysteine-rich stalk region. The ε and δ ectodomains were produced separately and refolded with the antibody scFv fragment. Similar to CD3γ, CD3δ adopts a C2 Ig-fold and pairs with CD3ε via an intersubunit β-sheet that buries a similar surface area (1740 Å^2) between the ectodomains as CD3εγ. Although the complete ectodomains were crystallized, no interpretable electron density was observed for the stalk regions containing the conserved CxxCxExD motif. The presence of a disulfide bond in the stalk region was detected in most of the material by nonreducing SDS-PAGE, which should nevertheless have reduced the flexibility of the stalk region. The earlier proposal (122) that pairing of the CD3 subunits via the G-strand should lead to ordering of this region is apparently not the case, at least for these crystal forms of CD3.

Although the interfaces of CD3εγ and CD3εδ are conserved, their molecular surfaces are quite different, with CD3δ being more electronegative than CD3γ (calculated pIs of 5 and 9, respectively). Of the 13 conserved surface residues in CD3δ, 11 are absent in CD3γ. Some of the conserved CD3δ residues (Glu9, Asp10, Arg11, and Lys41) form a charged patch on CD3δ that may constitute a TCR or coreceptor binding site (125). CD3δ and CD3γ are both N-glycosylated, with two sites each at residues 38, 74 and 52, 92, respectively, whereas CD3ε is not glycosylated.

Both the OKT3 and UCHT1 antibodies bind at sites distal from the proposed TCR-interaction sites, and their binding sites overlap. Thus, this binding site may constitute an immunodominant epitope (125). The larger buried surface area by UCHT1 (1790 Å^2) compared to OKT3 (1140 Å^2) may explain the higher affinity of UCHT1 for CD3 ($K_d = 0.5$ nM versus 2.6 μM). However, the mechanism of action of these antibodies seems to be the same, regardless of their affinities.

TCR/CD3 ASSEMBLY

The stoichiometry of the signaling-competent αβ TCR complex, as well as the sequence of its assembly and the chemical nature of the interactions between the subunits, has long been enigmatic. The early signaling TCR complex seems to consist of heterodimers of αβ TCR, CD3εγ, and CD3εδ, and a homodimer of CD3ζζ (121,126). Nine conserved charged residues in the transmembrane segments of the αβ TCR (three basic residues, an arginine and a lysine in the α-chain, and a lysine in the β-chain), CD3ε (aspartate), CD3γ (aspartate), CD3δ (glutamate), and CD3ζ (aspartate), could electrostatically steer docking of the subunits (127, 128). This electrostatic interaction would be stronger in the membrane than in water owing to the smaller dielectric constant in a membrane environment (129). How then are these charged residues shielded from the energetically unfavorable membrane environment in the absence of complex formation? Perturbation of the pKa's of the side chains could eliminate formal charges in the noncomplexed dimers but would still leave unsatisfied and, therefore, destabilizing membrane-inserted hydrogen bond donors and acceptors. The TCR α chain binds CD3εδ (130), which would allow CD3εγ to interact with the TCR β-chain (131), but no structural information is available for the transmembrane regions of these TCR components. If an α-helical conformation is assumed, which is likely given their

hydrophobic sequence propensities, the two basic residues in the transmembrane region of the TCR α-chain would lie on opposite faces, which could enable binding of the α-chain not only to CD3εδ, but also to CD3ζζ. The sequence of binding events to the TCR has been suggested to occur in the order CD3εδ, CD3εγ, and then CD3ζζ(127).

With almost all the extracellular domains of the αβ TCR signaling complex known, a tentative structural model can be put forward that contains all the αβ TCR, MHC, CD3εγ, CD3εδ, and CD8 components, lacking only the CD3ζζ-chains (**Figure 8*c***). In addition to stereochemical requirements, construction of this supramolecular assembly relies on the electrostatic interactions of the conserved residues in the transmembrane regions of the TCR and CD3s, and on the fact that carbohydrates generally do not participate in protein-protein interactions and, therefore, shield surfaces that do not participate in specific complex formation (132). A model proposed for a TCR/CD3εγ/CD3εδ complex (125) can be extended to include the CD8 coreceptor.

The main features of this model (125) include a compact TCR/CD3 complex with trimeric transmembrane contacts among all components (α-ε-δ, β-ε-γ, and α-ζ-ζ). To facilitate interactions between the transmembrane regions of the components, the bulky CD3 dimer ectodomains probably lie at an angle with respect to the membrane and the TCR globular domains. This notion is also supported by the shape of the membrane-proximal surface of the TCR, which would nicely fit the CD3 dimers. The CD3εγ and CD3εδ dimers would interact with conserved, nonglycosylated regions of the TCR surface. Although not present in any of the current TCR structures, the length of the peptide sequences connecting the TCR α- and β-chains to the membrane suggests that the TCR would be located further from the membrane than the CD3 dimers and, hence, sit "above" them (**Figure 8*c***).

MECHANISMS OF pMHC/TCR DOCKING

Not every engagement of a pMHC with its cognate TCR results in T cell activation. Indeed, antagonist peptides can inhibit T cell activation, and, similarly, engagement with a partial agonist elicits some, but not all, of the responses that characterize T cell activation by fully agonistic ligands. It was expected that, by examination of crystal structures of the respective altered peptide ligands (APL) TCR/pMHC complexes, this range of responses could be correlated with structural features, such as domain or CDR loop rearrangements. Thus far, the crystal structures do not explain the large biological differences or outcomes that can arise in T cell signaling from binding of APLs (14, 17) other than some minor changes in complementarity between the surfaces that can affect the half-life of the complexes. The crystal structures of TCR/pMHC complexes define the endpoints of the docking process. Most likely, this endpoint structure initiates TCR signaling. Interesting new results confirm that the overall dimensions of the TCR/pMHC complex dictate TCR triggering (133), where the relatively small TCR/pMHC complex brings the T cell and antigen-presenting cell membranes close enough together so that larger molecules such as the CD45 phosphatase are occluded, allowing the TCR-CD3 ITAMs to remain phosphorylated and thus to initiate downstream signaling events. But understanding of the early steps of TCR docking is also important because they define the antigen and TCR selection processes. The precise steps of this binding and signaling mechanism are largely unknown, despite extensive data on TCR-MHC complexation, including data on association and dissociation kinetics, half-life determination, and relative affinities (134–140). The sheer number of antigen complexes that have to be scanned by the TCR necessitates a rather cursory screen, i.e., a rapid mechanism to discriminate self from nonself in the periphery. Still, the scan needs to be

comprehensive enough to select reasonable affinity TCRs that allow for T cell activation. To this end, several hypotheses have been put forward to account for these requirements, including a two-step mechanism and electrostatic steering for TCR docking.

The two-step mechanism is based on forming an encounter complex of the TCR with the MHC α_1- and α_2-helices, followed by a more intensive sampling of the content of the MHC peptide-binding groove by the TCR CDR3 loops (141). Such a mechanism would generally be consistent with TCR/pMHC crystal structures, which show that the CDR1 and CDR2 loops primarily contact the MHC, whereas the highly diverse CDR3 loops mainly interact with the peptide (**Figure 9, 10**; **Tables 5–8**). For recognition of class II pMHC complexes, the two-step mechanism may be more appropriate, as the peptide lies deeper in the binding groove, so the first contact of the pMHC with the TCR would be dominated by encounter with the MHC α-helices. Indeed, using surface plasmon resonance, this mechanism has been supported by investigating the 2B4 TCR and its interactions with MHC class II I-E^k (141) containing a moth cytochrome C peptide. A two-step process in the class I system of B6 TCR Tax-HLA-A2 pMHC was detectable but less pronounced (142, 143).

This distinction of consecutive scanning and reading steps may be arbitrary where peptide bound to a class I MHC (45) bulges extensively out of the groove so that the TCR encounters the peptide and the MHC simultaneously (22, 23). In such a case, only long-range electrostatic steering could preorient the TCR relative to the MHC without direct antigen contact. However, these surfaces should also not be too highly charged or they would bind other counter-ions that would need to be removed and hence would compete with the TCR for interaction. Along these lines, some short-(salt bridges) to long-range (>4 Å distance) electrostatic interactions have been found in TCR/pMHC crystal structures, for example between TCR residue

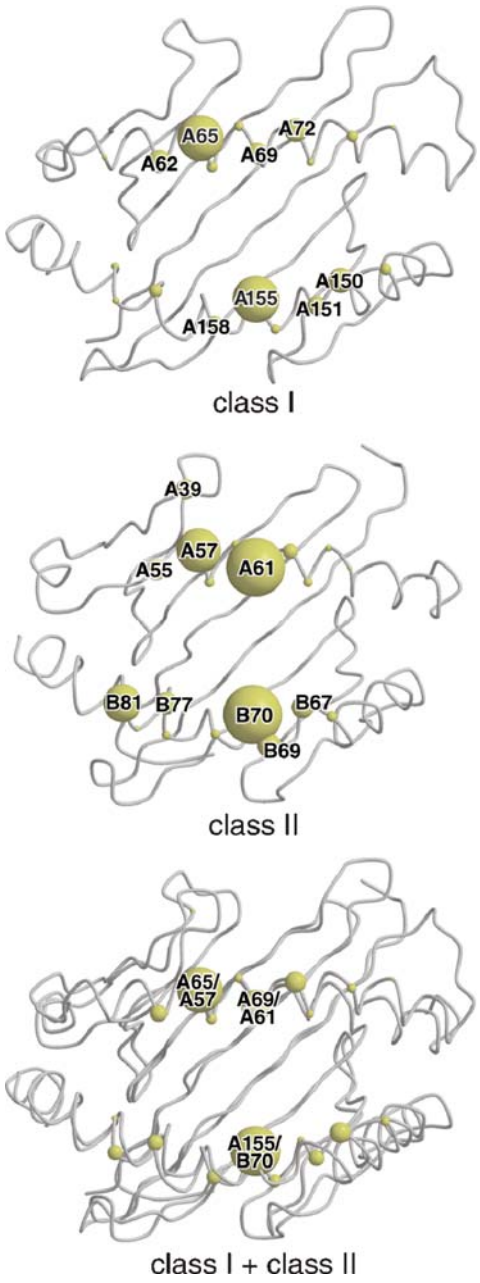

Figure 9

Conserved contacts formed between MHC class I and class II residues and αβ TCR. The MHC Cα backbone is shown for class I (*top*), class II (*middle*), and class I and II combined (*bottom*) in gray. On each backbone, spheres are placed at Cα positions of residues that contact TCR. The spheres are drawn so that their diameters are in proportion to their numbers of contacts to TCR (so that the large spheres represent residues with the most contacts). The numbers of contacts are listed in **Tables 5** and **6** for MHC residues and in **Tables 7** and **8** for TCR residues.

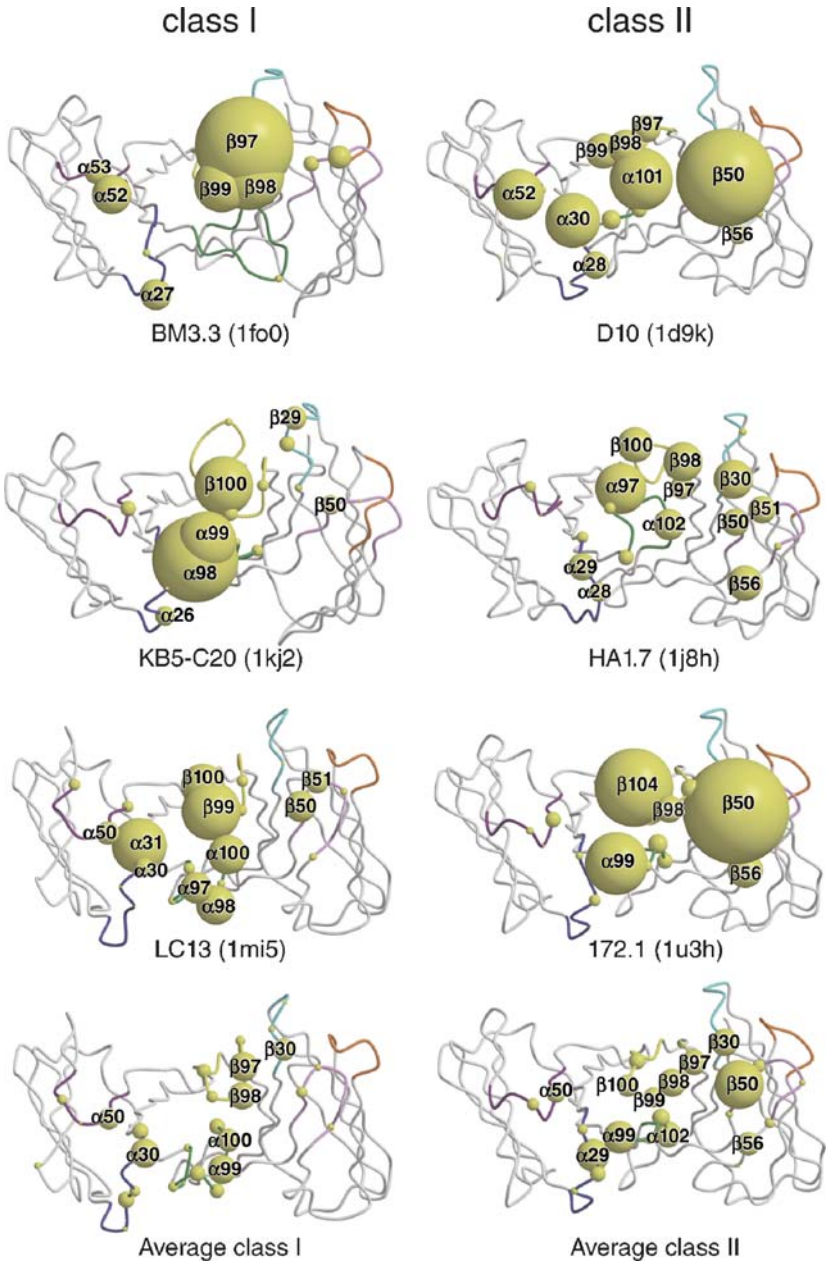

Figure 10

Conserved contacts formed between TCR residues and MHC. The TCR Cα backbone is shown for three different class I TCRs (*left column*) and three different class II TCRs (*right column*), with one TCR repeated on the bottom of each column. On each of the top three TCRs in each column, spheres are placed at Cα positions of residues that contact MHC. The spheres are drawn so that their diameters are in proportion to their actual numbers of contacts to TCR (thus, the large spheres represent residues with the most contacts). The numbers of contacts are listed in **Tables 7** and **8** for TCR residues. The "conserved" contacts for TCRs of each class are shown as spheres representing the average number of contacts for each residue (*bottom row*).

Table 5 Numbers of contacts made by class I MHC on TCR sorted by MHC residue

	PDB code																		
Residue #	1kj2	2ckb	1fo0	1g6r	1mwa	1nam	1ao7	1bd2	1lp9	1oga	1mi5	1qrn	1qse	1qsf	2bnr	2bnq	2ak4	Sum of contacts	Average
A58		6		2	2		9							1				20	1.2
A59								4										4	0.2
A62	28	14	8	8	13	10		1			3							85	5.0
A65	2	6	2	9	6	11	12	14	11	4	6	17	20	20	16	9	3	168	9.9
A66	7						4		4		6	4	4	5	4	3		41	2.4
A68							1		5			2	2	2	12	11		35	2.1
A69	2		7	1	1	11	8	1	2	3	10	9	9	6	4	4	1	79	4.7
A70			3			2												5	0.3
A72	2			1	4		3	1	5	6	17	4	7	5	16	15		86	5.1
A73			3	1	1	3				2	1	1	4		6	7		29	1.7
A75										1	1							2	0.1
A76	1	2	4		5	9				3	13				3	2		42	2.5
A79		4	6		1	1					8							20	1.2
A146	2	1	6	7	12	3			1		10							42	2.5
A147									1		2							3	0.2
A149	3				6		2			3								14	0.8
A150	6	2	1	4	4	1	15	1	8	15	3	4	2	11	6	7	1	91	5.4
A151							1		21	12	7	2	11		4	9	4	71	4.2
A152					1				2	5	1							9	0.5
A154			7		1	3			6	5	2	2	1		1	2	5	35	2.1
A155	16	24	9	7	9	11	5		7	15	16	3	10	9	9	13	8	171	10.1
A158	4	2	4	1	6	1	3	14	3		2	1	4	3			15	63	3.7
A159									1			1	1	1			3	7	0.4
A162	1	1			1			2	3									8	0.5
A163	6		2			2	2	2	15			9	4	4			4	50	2.9
A166		2			1		4		2			7	4	6				26	1.5
A167							5	6	1			7	5	5				29	1.7
A170							3					3	4	5				15	0.9

Table 6 Numbers of contacts made by class II MHC on αβTCR sorted by MHC residue

Residue #	PDB code						Sum of contacts	Average
	1u3h	1j8h	1fyt	1ymm	1zgl	1d9k		
A39	6	5	10			5	26	4.3
A54	1						1	0.2
A55	3			16	9		28	4.7
A57	13	6	12	6	4	16	57	9.5
A58			1	3	9		13	2.2
A60	2	2	1		2	3	10	1.7
A61	31	9	7	2	8	19	76	12.7
A62		1	1				2	0.3
A64	1	7	9		3		20	3.3
A65	1	2	5		4		12	2.0
A67	1	4	4				9	1.5
A68	3	2	1				6	1.0
B60					3	1	4	0.7
B61					1		1	0.2
B64		4	2			8	14	2.3
B66		1	2		6		9	1.5
B67	5	6	4		1	12	28	4.7
B69	3	4	1	15		8	31	5.2
B70	15	13	11	9	12	16	76	12.7
B72						4	4	0.7
B73	3			3		6	12	2.0
B76					10	1	11	1.8
B77	5	5	3	8	4	4	29	4.8
B80					8		8	1.3
B81	5	10	9	12	13		49	8.2
B84				3			3	0.5
B85				3			3	0.5

Lys68 in the HV4α loop and Asp76β in MHC class II or Glu166α in MHC class I (144). More examples include the electrostatic interaction in the MHC class I complex LC13/HLA-B8/EBV (24) between CDR2β residue Glu52 and HLA-B8 residue Arg79, and the interaction seen in two MHC class II complexes (HLA-DR1 and HLA-DR4) (18, 26), between Lys39α in a loop that projects up and away from the floor of the β-sheet and Glu56β of the HA1.7 TCR CDR2β. In a recent study, a single point mutation in the CDR3β loop of the 2C TCR (Gly95Arg) increased its affinity by a factor of 1000 to the QL9/L^d pMHC, most likely due to direct electrostatic interaction of the TCR arginine side chain with an aspartate residue at P8 (145). Thus, although such salt bridges and hydrogen bonds have not been conserved in all TCR/pMHC class I complexes, electrostatic effects, especially for orienting purposes, can work at a distance (146), so their influence on orienting the TCR relative to the pMHC at an early stage during antigen recognition must be considered. The glycan shield around these molecules may also influence the docking and help orient and exclude certain modes of binding (147).

Table 7 Numbers of contacts by TCR on class I MHC sorted by αβ TCR residue

Residue #	PDB code																	Sum of contacts	Average
	1kj2	2ckb	1fo0	1g6r	1mwa	1nam	1ao7	1bd2	1lp9	1oga	1mi5	1qrn	1qse	1qsf	2bnr	2bnq	2ak4		
α1							2											2	0.1
α26	5	7		1	4		7							1				25	1.5
α27		7	8	7	4	10	7	4				9	8	8				72	4.2
α28	1	4		2	4		1	10	16		1	1	2	5				47	2.8
α29			2			2			1		1						4	10	0.6
α30							5	6		9	5	8	6	6	41	40		126	7.4
α31		7	1	9	2	1	4	5	10		14	4	5	4			4	70	4.1
α48					1						3							4	0.2
α50	4	15		1	6		2	2	20	10	6	3	6	5	4	6	3	93	5.5
α51		2					1	5	3				2	2		3		18	1.1
α52	1		10			8	1	11				1		2	1	6	4	45	2.7
α53			6			2									3	8		19	1.1
α55											3							3	0.2
α68		2			1		4					11	6	7				31	1.8
α93		4		5	2		1	4	5			1	1		4	5	3	35	2.1
α94											3							3	0.2
α95								6									12	18	1.1
α96						4		5			2				5	5	24	45	2.7
α97						22			11		8				9	7	12	69	4.1
α98	22		2			3	2		9		10	3		4	4	4		63	3.7
α99	15	6		5	6	3	17		6	1	2	25	17	20	1	1		125	7.4
α100	2	9		9	10		8		2	3	10	10	11	7	9	10		100	5.9
α101		8		2	5		11		15	6		17	19	14	2			99	5.8
α102	3				1		1	1	7	2		3	5	3	21	22		69	4.1
α103								4										4	0.2
β27																	3	3	0.2

(*Continued*)

Table 7 (*Continued*)

Residue #	PDB code																	Sum of contacts	Average
	1kj2	2ckb	1fo0	1g6r	1mwa	1nam	1ao7	1bd2	1lp9	1oga	1mi5	1qrn	1qse	1qsf	2bnr	2bnq	2ak4		
β28		1		1	11										4	3		20	1.2
β29	6	3		2	7												11	29	1.7
β30	4	4		14	21		3		1	5	1	4	4		15	14	8	98	5.8
β31	2		1	1		3			2								6	15	0.9
β33																	4	4	0.2
β48								2	2		1				6	2		13	0.8
β50	5	2	4	2	7	6			5	8	8				1	1	1	50	2.9
β51	1		6		1				4	6	6				3	5		32	1.9
β52					1	1				2	2				3	3		12	0.7
β53										5								5	0.3
β54		3			1			1		3					12	11		31	1.8
β55											2							2	0.1
β56				1	2				6	4					5	1		19	1.1
β72															4	3		7	0.4
β95							1					2					5	8	0.5
β96	1	1	1	12	11			2		1	3		1		5	5		43	2.5
β97	3	3	25	4	3	9			23	20	3		1		16	16	1	127	7.5
β98			18			6	16	18	2	1	15	15	19	3			6	119	7.0
β99	4		14			6	1	1	1	5	11	2	6					51	3.0
β100	15						3	1	5	13	17	3	1	3				61	3.6
β101							7					4	4	9	6	8	1	39	2.3
β102	2						15					3	12		9	10		51	3.0
β103			2			1	5					6	13	10				37	2.2
β104								9								1		10	0.6

Table 8 Numbers of contacts made by αβTCR on class II MHC sorted by TCR residue

Residue #	PDB code						Sum of contacts	Average
	1u3h	1j8h	1fyt	1ymm	1zgl	1d9k		
α26	1					1	2	0.3
α27		1			10	1	12	2.0
α28	3	5	3		6	7	24	4.0
α29		7	8	9	25	1	50	8.3
α30	2					14	16	27.0
α31		3	2				5	0.8
α50	4	1		22		2	29	4.8
α51	1	1	1			1	4	0.7
α52	2	3	1			13	19	3.2
α68						1	1	0.2
α93						1	1	0.2
α94		4	6		5		15	2.5
α96		3	5				8	1.3
α97		13	13				26	4.3
α98				1			1	0.2
α99	16			16	13	5	50	8.3
α100	3			7		4	14	2.3
α101	5			1	5	16	27	4.5
α102	4	8	6	18	4		40	6.7
β28		2	2				4	0.7
β30	3	10	12	5	12		42	7.0
β31	3			2		1	6	1.0
β48	2		3			7	12	2.0
β50	27	7	10		6	25	75	12.5
β51		7	9		4		20	3.3
β52	1						1	0.2
β53					10		10	1.7
β54		2	2		1		5	0.8
β55		1	3		10	2	16	2.7
β56	9	9	10		3	5	36	6.0
β57				5	1	1	7	1.2
β72		1					1	0.2
β96	1					1	2	0.3
β97	5	6	11	10		7	39	6.5
β98	7	10	8	8	1	9	43	7.2
β99				5	17	9	31	5.2
β100	5	9	4	12	4		34	5.7
β101					6		6	1.0
β103				3			3	0.5
β104	20			5			25	4.2

Ionic interactions may also be implicated in the interaction of pMHC with the plasma membrane where the pMHC has been observed as being severely tilted with its long axis parallel to the membrane in a supine orientation (148). In addition, a kinked orientation of the CD3 modules relative to the T cell membrane was assumed to be an essential prerequisite for TCR binding (125). This "fourth dimension" in T cell signaling, which becomes available to any of the modules participating in the assembly of the TCR, may prove more important than suggested by the isolated crystal structures, particularly in light of the lipid rafts that have been implicated in membrane-regulated signaling events (149, 150).

So we must return again to the issue of MHC restriction. Detailed analyses of these 24 TCR/pMHC complexes do not readily identify a conserved set of interactions that would dictate a common binding orientation of the TCR on the pMHC. A variety of docking orientations from diagonal to near orthogonal (range 22°–87°), and some additional lateral mobility along the groove can displace some TCRs from their roughly central location over the middle of the peptide to either end of the binding groove (**Figure 5, 6**; **Tables 2–4**). If we list the contacts that each pMHC residue makes with TCR, no absolutely conserved interactions are made (**Table 7, 8**). However, trends develop when these complexes are considered as a whole. Most TCRs that recognize class I or class II MHCs clearly focus their binding interactions on the central regions of the α_1- and α_2/β_1-helices. Several MHC residues, such as α65 and α155 of class I and the corresponding α57 and β70 of class II, have the highest average number of contacts (**Figure 9**). These conserved contact residues also stand out when both classes are grouped together and correspond to α65/α57, α69/α61, and α155/β70 for class I/class II MHC. No such compelling picture arises from similar analyses of TCR contact residues (**Figure 10**). High variability in the location and number of contacts is found in each individual TCR that does not correlate well with average values. This finding is perhaps not unexpected because of the enormous repertoire of TCRs that can be produced against the very limited arsenal of MHCs. However, it might have been predicted that the germ line–encoded CDRs 1 and 2 would have the most conserved contacts. This prediction is true to some extent, but the data are not really convincing. Residues α30 (CDR1) and α50 (CDR2) make the most frequent contacts for TCRs to class I MHC, and, similarly, α29 and α50 for TCRs to class II MHC. Residue β30 (CDR1) is the only relatively conserved contact residue in the TCR β-chain, and some variation in the use of β50 (CDR2) as a contact residue is noted between TCRs interacting with class I and class II MHC. Several residues in CDRs 3α (α99) and 3β (β97, β98) have the most conserved contacts in both classes. What dictates this variable but still relatively conserved docking orientation? At present, we must fall back on overall shape complementarity, restricted orientation through interaction with coreceptors, and electrostatic steering.

CONCLUSIONS AND FUTURE PERSPECTIVES

More than 400 antibody structures have now been determined to delineate the full extent of antibody-antigen interactions and the general principles that governed antibody-antigen recognition. But even now, completely novel modes of binding and unexpected features continue to emerge from human and other antibody complexes. From the comparatively limited number of TCR/pMHC structures, we conclude that TCRs bind MHC class I and class II in a somewhat conserved way, but with some considerable structural variation in the details of the interaction. A common docking mode would enable the $\alpha\beta$ TCR to quickly survey the contents of the MHC binding groove. However, the 13 independent complex structures determined so far have not yet

revealed the basis for this conserved orientation and hence the basis for MHC restriction. The variability in the pitch, twist, and roll of the TCR indicates that individual solutions to the docking problem are found that differ substantially in their details. In many cases, the TCR V_α interactions with the pMHC seem to predominate and thus provide some basis for a conserved orientation. But in several alloreactive TCR/pMHC complexes, the β-chain seems to provide most of the interactions with pMHC.

Also unresolved is how the exceedingly small changes in the TCR/pMHC interface in response to different APLs can lead to such drastically different biological outcomes. The TCR itself seems to adapt to small changes in the pMHC ligand by small conformational changes or rearrangements of its central CDR loops. The complementarity, buried surface area, or number of contacts in agonist versus antagonist complexes are very similar and are difficult to reconcile with the substantial differences in T cell responses. Proposals that changes in the CDR conformations themselves through induced fit provide some discrimination (138) seem hard to reconcile. Therefore, differentiation of strong from weak agonists, or agonists from antagonists, by visual inspection of the crystal structures is not yet possible. The future direction still demands more TCR/pMHC complex structures to address these key issues and to garner the general principles that govern TCR/pMHC recognition.

So far, these soluble TCR/pMHC complexes are not in their native context on the membrane surface, nor are they surrounded by the other signaling components of the TCR, such as CD3, nor in the vicinity of their coreceptors or costimulatory receptors. Therefore, the most important breakthrough would be the determination of a complete αβ TCR signaling complex, including CD4/CD8 and the CD3γ-, δ-, ε-, and ζ-chains. This assembly would define the global changes that influence TCR signaling events. However, the lack of the membrane-anchoring domains in the constructs used for the current structure determinations will remain a problem until intact membrane proteins can be routinely crystallized. Meanwhile, models of the TCR/pMHC in complex with coreceptors (CD4/CD8) and signaling modules (CD3εγ and CD3εδ) can be assembled from the component pieces (**Figure 8*c***), but have to be interpreted with caution.

Notwithstanding, substantial advances have certainly been made in the past two years in our understanding of the recognition of MHC class I and class II by αβ TCRs, and now of antigen recognition by γδ TCRs, as well as obtaining structural insights into alloreactivity and graft rejection, response to APLs and bulged ligands, autoimmunity, and TCR selection and bias. Future studies should also deal with the extent to which other bulky ligands, especially glycolipids or lipopeptides in the case of CD1 (68), can be accommodated within the TCR/pMHC interface.

ACKNOWLEDGMENTS

We thank Christopher Garcia, Roy Mariuzza, and Jamie Rossjohn for providing coordinates prior to publication. The authors are supported by DFG SFB 523 (M.G.R.) and NIH grants CA-58896 and AI-42266 (R.L.S. and I.A.W.). This is manuscript #17589-MB from The Scripps Research Institute.

LITERATURE CITED

1. Fields BA, Ober B, Malchiodi EL, Lebedeva MI, Braden BC, et al. 1995. Crystal structure of the Vα domain of a T cell antigen receptor. *Science* 270:1821–24

2. Fields BA, Malchiodi EL, Li H, Ysern X, Stauffacher CV, et al. 1996. Crystal structure of a T-cell receptor β-chain complexed with a superantigen. *Nature* 384:188–92
3. Li H, Lebedeva MI, Ward ES, Mariuzza RA. 1997. Dual conformations of a T cell receptor Vα homodimer: implications for variability in Vα Vβ domain association. *J. Mol. Biol.* 269:385–94
4. Plaksin D, Chacko S, Navaza J, Margulies DH, Padlan EA. 1999. The X-ray crystal structure of a Vα2.6Jα38 mouse T cell receptor domain at 2.5 Å resolution: alternate modes of dimerization and crystal packing. *J. Mol. Biol.* 289:1153–61
5. Machius M, Cianga P, Deisenhofer J, Ward ES. 2001. Crystal structure of a T cell receptor Vα11 (AV11S5) domain: new canonical forms for the first and second complementarity determining regions. *J. Mol. Biol.* 310:689–98
6. Rudolph MG, Huang M, Teyton L, Wilson IA. 2001. Crystal structure of an isolated V_α domain of the 2C T-cell receptor. *J. Mol. Biol.* 314:1–8
7. Garcia KC, Degano M, Stanfield RL, Brunmark A, Jackson MR, et al. 1996. An αβ T cell receptor structure at 2.5 Å and its orientation in the TCR-MHC complex. *Science* 274:209–19
8. Housset D, Mazza G, Gregoire C, Piras C, Malissen B, Fontecilla-Camps JC. 1997. The three-dimensional structure of a T-cell antigen receptor VαVβ heterodimer reveals a novel arrangement of the Vβ domain. *EMBO J.* 16:4205–16
9. Wang J, Lim K, Smolyar A, Teng M, Liu J, et al. 1998. Atomic structure of an αβ T cell receptor (TCR) heterodimer in complex with an anti-TCR fab fragment derived from a mitogenic antibody. *EMBO J.* 17:10–26
10. Kjer-Nielsen L, Clements CS, Brooks AG, Purcell AW, McCluskey J, Rossjohn J. 2002. The 1.5 Å crystal structure of a highly selected antiviral T cell receptor provides evidence for a structural basis of immunodominance. *Structure* 10:1521–32
11. Garboczi DN, Ghosh P, Utz U, Fan QR, Biddison WE, Wiley DC. 1996. Structure of the complex between human T-cell receptor, viral peptide and HLA-A2. *Nature* 384:134–41
12. Garcia KC, Degano M, Pease LR, Huang M, Peterson PA, et al. 1998. Structural basis of plasticity in T cell receptor recognition of a self peptide-MHC antigen. *Science* 279:1166–72
13. Ding YH, Smith KJ, Garboczi DN, Utz U, Biddison WE, Wiley DC. 1998. Two human T cell receptors bind in a similar diagonal mode to the HLA-A2/Tax peptide complex using different TCR amino acids. *Immunity* 8:403–11
14. Ding YH, Baker BM, Garboczi DN, Biddison WE, Wiley DC. 1999. Four A6-TCR/peptide/HLA-A2 structures that generate very different T cell signals are nearly identical. *Immunity* 11:45–56
15. Reinherz EL, Tan K, Tang L, Kern P, Liu J, et al. 1999. The crystal structure of a T cell receptor in complex with peptide and MHC class II. *Science* 286:1913–21
16. Reiser JB, Darnault C, Guimezanes A, Gregoire C, Mosser T, et al. 2000. Crystal structure of a T cell receptor bound to an allogeneic MHC molecule. *Nat. Immun.* 1:291–97
17. Degano M, Garcia KC, Apostolopoulos V, Rudolph MG, Teyton L, Wilson IA. 2000. A functional hot spot for antigen recognition in a superagonist TCR/MHC complex. *Immunity* 12:251–61
18. Hennecke J, Carfi A, Wiley DC. 2000. Structure of a covalently stabilized complex of a human αβ T-cell receptor, influenza HA peptide and MHC class II molecule, HLA-DR1. *EMBO J.* 19:5611–24
19. Luz JG, Huang M, Garcia KC, Rudolph MG, Apostolopoulos V, et al. 2002. Structural comparison of allogeneic and syngeneic T cell receptor-peptide-major histocompatibility

complex complexes: a buried alloreactive mutation subtly alters peptide presentation substantially increasing V_β Interactions. *J. Exp. Med.* 195:1175–86
20. Buslepp J, Wang H, Biddison WE, Appella E, Collins EJ. 2003. A correlation between TCR Vα docking on MHC and CD8 dependence: implications for T cell selection. *Immunity* 19:595–606
21. Stewart-Jones GB, McMichael AJ, Bell JI, Stuart DI, Jones EY. 2003. A structural basis for immunodominant human T cell receptor recognition. *Nat. Immun.* 4:657–63
22. Tynan FE, Borg NA, Miles JJ, Beddoe T, El-Hassen D, et al. 2005. High resolution structures of highly bulged viral epitopes bound to major histocompatibility complex class I. Implications for T-cell receptor engagement and T-cell immunodominance. *J. Biol. Chem.* 280:23900–9
23. Tynan FE, Burrows SR, Buckle AM, Clements CS, Borg NA, et al. 2005. T cell receptor recognition of a 'super-bulged' major histocompatibility complex class I-bound peptide. *Nat. Immunol.* 6:1114–22
24. Kjer-Nielsen L, Clements CS, Purcell AW, Brooks AG, Whisstock JC, et al. 2003. A structural basis for the selection of dominant αβ T cell receptors in antiviral immunity. *Immunity* 18:53–64
25. Chen JL, Stewart-Jones G, Bossi G, Lissin NM, Wooldridge L, et al. 2005. Structural and kinetic basis for heightened immunogenicity of T cell vaccines. *J. Exp. Med.* 201:1243–55
26. Hennecke J, Wiley DC. 2001. Structure of a complex of the human αβ-T cell receptor HA1.7, Influenza HA peptide, and MHC class II molecule, HLA-DR4 (DRA*0101, DRB*0401)—insight into TCR cross-restriction and alloreactivity. *J. Exp. Med.* 195:571–81
27. Hahn M, Nicholson MJ, Pyrdol J, Wucherpfennig KW. 2005. Unconventional topology of self peptide-major histocompatibility complex binding by a human autoimmune T cell receptor. *Nat. Immun.* 6:490–96
28. Maynard J, Petersson K, Wilson DH, Adams EJ, Blondelle SE, et al. 2005. Structure of an autoimmune T cell receptor complexed with class II peptide-MHC: insights into MHC bias and antigen specificity. *Immunity* 22:81–92
29. Li Y, Huang Y, Lue J, Quandt JA, Martin R, Mariuzza RA. 2005. Structure of a human autoimmune TCR bound to a myelin basic protein self-peptide and a multiple sclerosis-associated MHC class II molecule. *EMBO J.* 24:2968–79
30. Reiser JB, Darnault C, Gregoire C, Mosser T, Mazza G, et al. 2003. CDR3 loop flexibility contributes to the degeneracy of TCR recognition. *Nat. Immun.* 4:241–47
31. Reiser JB, Gregoire C, Darnault C, Mosser T, Guimezanes A, et al. 2002. A T cell receptor CDR3β loop undergoes conformational changes of unprecedented magnitude upon binding to a peptide/MHC class I complex. *Immunity* 16:345–54
32. Garcia KC, Teyton L, Wilson IA. 1999. Structural basis of T cell recognition. *Annu. Rev. Immunol.* 17:369–97
33. Garcia KC. 1999. Molecular interactions between extracellular components of the T-cell receptor signaling complex. *Immunol. Rev.* 172:73–85
34. Garcia KC, Degano M, Speir JA, Wilson IA. 1999. Emerging principles for T cell receptor recognition of antigen in cellular immunity. *Rev. Immunogenet.* 1:75–90
35. Wang J, Reinherz EL. 2000. Structural basis of cell-cell interactions in the immune system. *Curr. Opin. Struct. Biol.* 10:656–61
36. Rudolph MG, Wilson IA. 2002. The specificity of TCR/pMHC interaction. *Curr. Opin. Immunol.* 14:52–65

37. Rudolph MG, Luz JG, Wilson IA. 2002. Structural and thermodynamic correlates of T-cell signaling. *Annu. Rev. Biophys. Biomol. Struct.* 31:121–49
38. Allison TJ, Garboczi DN. 2002. Structure of γδ T cell receptors and their recognition of non-peptide antigens. *Mol. Immunol.* 38:1051–61
39. Falk K, Rotzschke O, Stevanovic S, Jung G, Rammensee HG. 1991. Allele-specific motifs revealed by sequencing of self-peptides eluted from MHC molecules. *Nature* 351:290–96
40. Rudensky AY, Mazel SM, Yurin VL. 1990. Presentation of endogenous immunoglobulin determinant to immunoglobulin-recognizing T cell clones by the thymic cells. *Eur. J. Immunol.* 20:2235–39
41. van Bleek GM, Nathenson SG. 1991. The structure of the antigen-binding groove of major histocompatibility complex class I molecules determines specific selection of self-peptides. *Proc. Natl. Acad. Sci. USA* 88:11032–36
42. Fremont DH, Matsumura M, Stura EA, Peterson PA, Wilson IA. 1992. Crystal structures of two viral peptides in complex with murine MHC class I H-2K^b. *Science* 257:919–27
43. Madden DR, Garboczi DN, Wiley DC. 1993. The antigenic identity of peptide-MHC complexes: a comparison of the conformations of five viral peptides presented by HLA-A2. *Cell* 75:693–708
44. Stern LJ, Wiley DC. 1994. Antigenic peptide binding by class I and class II histocompatibility proteins. *Structure* 2:245–51
45. Speir JA, Stevens J, Joly E, Butcher GW, Wilson IA. 2001. Two different, highly exposed, bulged structures for an unusually long peptide bound to rat MHC class I RT1-A^a. *Immunity* 14:81–92
46. Zeng Z, Castaño AR, Segelke BW, Stura EA, Peterson PA, Wilson IA. 1997. Crystal structure of mouse CD1: An MHC-like fold with a large hydrophobic binding groove. *Science* 277:339–45
47. Zajonc DM, Elsliger MA, Teyton L, Wilson IA. 2003. Crystal structure of CD1a in complex with a sulfatide self antigen at a resolution of 2.15 Å. *Nat. Immun.* 4:808–15
48. Zajonc DM, Crispin MD, Bowden TA, Young DC, Cheng TY, et al. 2005. Molecular mechanism of lipopeptide presentation by CD1a. *Immunity* 22:209–19
49. Koch M, Stronge VS, Shepherd D, Gadola SD, Mathew B, et al. 2005. The crystal structure of human CD1d with and without α-galactosylceramide. *Nat. Immun.* 6:819–26
50. Batuwangala T, Shepherd D, Gadola SD, Gibson KJ, Zaccai NR, et al. 2004. The crystal structure of human CD1b with a bound bacterial glycolipid. *J. Immunol.* 172:2382–88
51. Gadola SD, Zaccai NR, Harlos K, Shepherd D, Castro-Palomino JC, et al. 2002. Structure of human CD1b with bound ligands at 2.3 Å, a maze for alkyl chains. *Nat. Immun.* 3:721–26
52. De Libero G, Mori L. 2005. Recognition of lipid antigens by T cells. *Nat. Rev. Immunol.* 5:485–96
53. Van Rhijn I, Zajonc DM, Wilson IA, Moody DB. 2005. T-cell activation by lipopeptide antigens. *Curr. Opin. Immunol.* 17:222–29
54. Sullivan BA, Nagarajan NA, Kronenberg M. 2005. CD1 and MHC II find different means to the same end. *Trends Immunol.* 26:282–88
55. Moody DB, Zajonc DM, Wilson IA. 2005. Anatomy of CD1-lipid antigen complexes. *Nat. Rev. Immunol.* 5:387–99
56. Rudolph MG, Wingren C, Crowley MP, Chien YH, Wilson IA. 2004. Combined pseudo-merohedral twinning, non-crystallographic symmetry and pseudo-translation in a monoclinic crystal form of the γδ T-cell ligand T10. *Acta Cryst.* D60:656–64

57. Wingren C, Crowley MP, Degano M, Chien Y, Wilson IA. 2000. Crystal structure of a γδ T cell receptor ligand T22: a truncated MHC-like fold. *Science* 287:310–14
58. Wolan DW, Teyton L, Rudolph MG, Villmow B, Bauer S, et al. 2001. Crystal structure of the murine NK cell-activating receptor NKG2D at 1.95 Å. *Nat. Immun.* 2:248–54
59. Vance RE, Tanamachi DM, Hanke T, Raulet DH. 1997. Cloning of a mouse homolog of CD94 extends the family of C-type lectins on murine natural killer cells. *Eur. J. Immunol.* 27:3236–41
60. Lanier LL. 2005. NKG2D in innate and adaptive immunity. *Adv. Exp. Med. Biol.* 560:51–56
61. Hamerman JA, Ogasawara K, Lanier LL. 2005. NK cells in innate immunity. *Curr. Opin. Immunol.* 17:29–35
62. Vivier E, Tomasello E, Paul P. 2002. Lymphocyte activation via NKG2D: towards a new paradigm in immune recognition? *Curr. Opin. Immunol.* 14:306–11
63. Stephens HA. 2001. MICA and MICB genes: Can the enigma of their polymorphism be resolved? *Trends Immunol.* 22:378–85
64. Yamamoto K, Fujiyama Y, Andoh A, Bamba T, Okabe H. 2001. Oxidative stress increases MICA and MICB gene expression in the human colon carcinoma cell line (CaCo-2). *Biochim. Biophys. Acta* 1526:10–12
65. Tieng V, Le Bouguenec C, du Merle L, Bertheau P, Desreumaux P, et al. 2002. Binding of *Escherichia coli* adhesin AfaE to CD55 triggers cell-surface expression of the MHC class I-related molecule MICA. *Proc. Natl. Acad. Sci. USA* 99:2977–82
66. Li P, Willie ST, Bauer S, Morris DL, Spies T, Strong RK. 1999. Crystal structure of the MHC class I homolog MIC-A, a γδ T cell ligand. *Immunity* 10:577–84
67. Li P, McDermott G, Strong RK. 2002. Crystal structures of RAE-1β and its complex with the activating immunoreceptor NKG2D. *Immunity* 16:77–86
68. Liu Y, Xiong Y, Naidenko OV, Liu JH, Zhang R, et al. 2003. The crystal structure of a TL/CD8αα complex at 2.1 Å resolution: implications for modulation of T cell activation and memory. *Immunity* 18:205–15
69. Claverie JM, Prochnicka-Chalufour A, Bougueleret L. 1989. Implications of a Fab-like structure for the T-cell receptor. *Immunol. Today* 10:10–14
70. Davis MM, Bjorkman PJ. 1988. T-cell antigen receptor genes and T-cell recognition. *Nature* 334:395–402
71. Li H, Lebedeva MI, Llera AS, Fields BA, Brenner MB, Mariuzza RA. 1998. Structure of the Vδ domain of a human γδ T-cell antigen receptor. *Nature* 391:502–6
72. Morita CT, Beckman EM, Bukowski JF, Tanaka Y, Band H, et al. 1995. Direct presentation of nonpeptide prenyl pyrophosphate antigens to human γδ T cells. *Immunity* 3:495–507
73. Belmant C, Espinosa E, Poupot R, Peyrat MA, Guiraud M, et al. 1999. 3-Formyl-1-butyl pyrophosphate, a novel mycobacterial metabolite activating human γδ T cells. *J. Biol. Chem.* 274:32079–84
74. Chien YH, Jores R, Crowley MP. 1996. Recognition by γδ T cells. *Annu. Rev. Immunol.* 14:511–32
75. Moody DB, Besra GS, Wilson IA, Porcelli SA. 1999. The molecular basis of CD1-mediated presentation of lipid antigens. *Immunol. Rev.* 172:285–96
76. Allison TJ, Winter CC, Fournie J, Bonneville M, Garboczi DN. 2001. Structure of a human γδ T-cell antigen receptor. *Nature* 411:820–24
77. Yewdell JW, Haeryfar SM. 2005. Understanding presentation of viral antigens to $CD8^+$ T cells in vivo: the key to rational vaccine design. *Annu. Rev. Immunol.* 23:651–82

78. Melief CJ. 2005. Escort service for cross-priming. *Nat. Immun.* 6:543–44
79. Norbury CC, Basta S, Donohue KB, Tscharke DC, Princiotta MF, et al. 2004. CD8+ T cell cross-priming via transfer of proteasome substrates. *Science* 304:1318–21
80. Connolly ML. 1993. The molecular surface package. *J. Mol. Graph.* 11:139–41
81. Wang JH, Reinherz EL. 2002. Structural basis of T cell recognition of peptides bound to MHC molecules. *Mol. Immunol.* 38:1039–49
82. Hulsmeyer M, Chames P, Hillig RC, Stanfield RL, Held G, et al. 2005. A major histocompatibility complex-peptide-restricted antibody and T cell receptor molecules recognize their target by distinct binding modes: crystal structure of human leukocyte antigen (HLA)-A1-MAGE-A1 in complex with FAB-HYB3. *J. Biol. Chem.* 280:2972–80
83. Sim BC, Travers PJ, Gascoigne NR. 1997. Vα3.2 selection in MHC class I mutant mice: evidence for an alternate orientation of TCR-MHC class I interaction. *J. Immunol.* 159:3322–29
84. Gil D, Schamel WW, Montoya M, Sanchez-Madrid F, Alarcon B. 2002. Recruitment of Nck by CD3ε reveals a ligand-induced conformational change essential for T cell receptor signaling and synapse formation. *Cell* 109:901–12
85. Hennecke J, Wiley DC. 2001. T cell receptor-MHC interactions up close. *Cell* 104: 1–4
86. Speir JA, Garcia KC, Brunmark A, Degano M, Peterson PA, et al. 1998. Structural basis of 2C TCR allorecognition of H-2L^{d} peptide complexes. *Immunity* 8:553–62
87. Guimezanes A, Barrett-Wilt GA, Gulden-Thompson P, Shabanowitz J, Engelhard VH, et al. 2001. Identification of endogenous peptides recognized by in vivo or in vitro generated alloreactive cytotoxic T lymphocytes: distinct characteristics correlated with CD8 dependence. *Eur. J. Immunol.* 31:421–32
88. Rudolph MG, Speir JA, Brunmark A, Mattsson N, Jackson MR, et al. 2001. The crystal structures of K^{bm1} and K^{bm8} reveal that subtle changes in the peptide environment impact thermostability and alloreactivity. *Immunity* 14:231–42
89. Kjer-Nielsen L, Dunstone MA, Kostenko L, Ely LK, Beddoe T, et al. 2004. Crystal structure of the human T cell receptor CD3εγ heterodimer complexed to the therapeutic mAb OKT3. *Proc. Natl. Acad. Sci. USA* 101:7675–80
90. Argaet VP, Schmidt CW, Burrows SR, Silins SL, Kurilla MG, et al. 1994. Dominant selection of an invariant T cell antigen receptor in response to persistent infection by Epstein-Barr virus. *J. Exp. Med.* 180:2335–40
91. Al-Lazikani B, Lesk AM, Chothia C. 2000. Canonical structures for the hypervariable regions of T cell αβ receptors. *J. Mol. Biol.* 295:979–95
92. Sherman LA, Chattopadhyay S. 1993. The molecular basis of allorecognition. *Annu. Rev. Immunol.* 11:385–402
93. Moss DJ, Burrows SR, Silins SL, Misko I, Khanna R. 2001. The immunology of Epstein-Barr virus infection. *Philos. Trans. R. Soc. London Ser. B.* 356:475–88
94. Bhat TN, Bentley GA, Boulot G, Greene MI, Tello D, et al. 1994. Bound water molecules and conformational stabilization help mediate an antigen-antibody association. *Proc. Natl. Acad. Sci. USA* 91:1089–93
95. Malby RL, Tulip WR, Harley VR, McKimm-Breschkin JL, Laver WG, et al. 1994. The structure of a complex between the NC10 antibody and influenza virus neuraminidase and comparison with the overlapping binding site of the NC41 antibody. *Structure* 2:733–46
96. Moss DJ, Burrows SR, Baxter GD, Lavin MF. 1991. T cell-T cell killing is induced by specific epitopes: evidence for an apoptotic mechanism. *J. Exp. Med.* 173:681–86

97. Lehner PJ, Wang EC, Moss PA, Williams S, Platt K, et al. 1995. Human HLA-A0201-restricted cytotoxic T lymphocyte recognition of influenza A is dominated by T cells bearing the Vβ17 gene segment. *J. Exp. Med.* 181:79–91
98. Lawson TM, Man S, Williams S, Boon AC, Zambon M, Borysiewicz LK. 2001. Influenza A antigen exposure selects dominant $V\beta17^+$ TCR in human $CD8^+$ cytotoxic T cell responses. *Int. Immunol.* 13:1373–81
99. Arzt S, Petit I, Burmeister WP, Ruigrok RW, Baudin F. 2004. Structure of a knockout mutant of influenza virus M1 protein that has altered activities in membrane binding, oligomerisation and binding to NEP (NS2). *Virus Res.* 99:115–19
100. Wilson IA, Stanfield RL. 2005. MHC restriction: slip-sliding away. *Nat. Immun.* 6:434–35
101. He XL, Radu C, Sidney J, Sette A, Ward ES, Garcia KC. 2002. Structural snapshot of aberrant antigen presentation linked to autoimmunity: the immunodominant epitope of MBP complexed with $I\text{-}A^u$. *Immunity* 17:83–94
102. Adams EJ, Chien YH, Garcia KC. 2005. Structure of a γδ T cell receptor in complex with the nonclassical MHC T22. *Science* 308:227–31
103. Wilson IA, Stanfield RL. 2001. Unraveling the mysteries of γδ T cell recognition. *Nat. Immun.* 2:579–81
104. Reich Z, Boniface JJ, Lyons DS, Borochov N, Wachtel EJ, Davis MM. 1997. Ligand-specific oligomerization of T-cell receptor molecules. *Nature* 387:617–20
105. Li P, Morris DL, Willcox BE, Steinle A, Spies T, Strong RK. 2001. Complex structure of the activating immunoreceptor NKG2D and its MHC class I-like ligand MICA. *Nat. Immun.* 2:443–51
106. Gao GF, Tormo J, Gerth UC, Wyer JR, McMichael AJ, Stuart DI, et al. 1997. Crystal structure of the complex between human CD8αα and HLA-A2. *Nature* 387:630–34
107. Kern PS, Teng MK, Smolyar A, Liu JH, Liu J, et al. 1998. Structural basis of CD8 coreceptor function revealed by crystallographic analysis of a murine CD8αα ectodomain fragment in complex with $H\text{-}2K^b$. *Immunity* 9:519–30
108. Gangadharan D, Cheroutre H. 2004. The CD8 isoform CD8αα is not a functional homologue of the TCR co-receptor CD8αβ. *Curr. Opin. Immunol.* 16:264–70
109. Wang J, Meijers R, Xiong Y, Liu J, Sakihama T, et al. 2001. Crystal structure of the human CD4 N-terminal two domain fragment complexed to a class II MHC molecule. *Proc. Natl. Acad. Sci. USA* 98:10799–804
110. Wu H, Kwong PD, Hendrickson WA. 1997. Dimeric association and segmental variability in the structure of human CD4. *Nature* 387:527–30
111. Manolios N, Letourneur F, Bonifacino JS, Klausner RD. 1991. Pairwise, cooperative and inhibitory interactions describe the assembly and probable structure of the T-cell antigen receptor. *EMBO J.* 10:1643–51
112. Koning F, Maloy WL, Coligan JE. 1990. The implications of subunit interactions for the structure of the T cell receptor-CD3 complex. *Eur. J. Immunol.* 20:299–305
113. Grakoui A, Bromley SK, Sumen C, Davis MM, Shaw AS, et al. 1999. Immunological synapse: A molecular machine controlling T cell activation. *Science* 285:221–27
114. Davis SJ, van der Merwe PA. 2001. The immunological synapse: required for T cell receptor signalling or directing T cell effector function? *Curr. Biol.* 11:R289–91
115. Davis SJ, van der Merwe PA. 2003. TCR triggering: co-receptor-dependent or -independent? *Trends Immunol.* 24:624–26
116. Bromley SK, Burack WR, Johnson KG, Somersalo K, Sims TN, et al. 2001. The immunological synapse. *Annu. Rev. Immunol.* 19:375–96

117. Berkhout B, Alarcon B, Terhorst C. 1988. Transfection of genes encoding the T cell receptor-associated CD3 complex into COS cells results in assembly of the macromolecular structure. *J. Biol. Chem.* 263:8528–36
118. Wang N, Wang B, Salio M, Allen D, She J, Terhorst C. 1998. Expression of a CD3ε transgene in CD3ε(null) mice does not restore CD3γ and δ expression but efficiently rescues T cell development from a subpopulation of prothymocytes. *Int. Immunol.* 10:1777–88
119. Kappes DJ, Alarcon B, Regueiro JR. 1995. T lymphocyte receptor deficiencies. *Curr. Opin. Immunol.* 7:441–47
120. Kim KS, Sun ZY, Wagner G, Reinherz EL. 2000. Heterodimeric CD3εγ extracellular domain fragments: production, purification and structural analysis. *J. Mol. Biol.* 302:899–916
121. Call ME, Pyrdol J, Wiedmann M, Wucherpfennig KW. 2002. The organizing principle in the formation of the T cell receptor-CD3 complex. *Cell* 111:967–79
122. Sun ZJ, Kim KS, Wagner G, Reinherz EL. 2001. Mechanisms contributing to T cell receptor signaling and assembly revealed by the solution structure of an ectodomain fragment of the CD3εγ heterodimer. *Cell* 105:913–23
123. Manolios N, Kemp O, Li ZG. 1994. The T cell antigen receptor α and β chains interact via distinct regions with CD3 chains. *Eur. J. Immunol.* 24:84–92
124. Manolios N, Li ZG. 1995. The T cell antigen receptor β chain interacts with the extracellular domain of CD3-γ. *Immunol. Cell Biol.* 73:532–36
125. Arnett KL, Harrison SC, Wiley DC. 2004. Crystal structure of a human CD3-ε/δ dimer in complex with a UCHT1 single-chain antibody fragment. *Proc. Natl. Acad. Sci. USA* 101:16268–73
126. Call ME, Wucherpfennig KW. 2005. The T cell receptor: critical role of the membrane environment in receptor assembly and function. *Annu. Rev. Immunol.* 23:101–25
127. Call ME, Wucherpfennig KW. 2004. Molecular mechanisms for the assembly of the T cell receptor-CD3 complex. *Mol. Immunol.* 40:1295–305
128. Call ME, Pyrdol J, Wucherpfennig KW. 2004. Stoichiometry of the T-cell receptor-CD3 complex and key intermediates assembled in the endoplasmic reticulum. *EMBO J.* 23:2348–57
129. Engelman DM. 2003. Electrostatic fasteners hold the T cell receptor-CD3 complex together. *Mol. Cell* 11:5–6
130. Backstrom BT, Muller U, Hausmann B, Palmer E. 1998. Positive selection through a motif in the αβ T cell receptor. *Science* 281:835–38
131. Ghendler Y, Smolyar A, Chang HC, Reinherz EL. 1998. One of the CD3epsilon subunits within a T cell receptor complex lies in close proximity to the Cβ FG loop. *J. Exp. Med.* 187:1529–36
132. Rudd PM, Wormald MR, Stanfield RL, Huang M, Mattsson N, et al. 1999. Roles for glycosylation of cell surface receptors involved in cellular immune recognition. *J. Mol. Biol.* 293:351–66
133. Choudhuri K, Wiseman D, Brown MH, Gould K, van der Merwe PA. 2005. T-cell receptor triggering is critically dependent on the dimensions of its peptide-MHC ligand. *Nature* 436:578–82
134. Margulies DH. 1997. Interactions of TCRs with MHC-peptide complexes: a quantitative basis for mechanistic models. *Curr. Opin. Immunol.* 9:390–95
135. Alam SM, Davies GM, Lin CM, Zal T, Nasholds W, et al. 1999. Qualitative and quantitative differences in T cell receptor binding of agonist and antagonist ligands. *Immunity* 10:227–37

136. Alam SM, Travers PJ, Wung JL, Nasholds W, Redpath S, et al. 1996. T-cell-receptor affinity and thymocyte positive selection. *Nature* 381:616–20
137. Lyons DS, Lieberman SA, Hampl J, Boniface JJ, Chien Y, et al. 1996. A TCR binds to antagonist ligands with lower affinities and faster dissociation rates than to agonists. *Immunity* 5:53–61
138. Boniface JJ, Reich Z, Lyons DS, Davis MM. 1999. Thermodynamics of T cell receptor binding to peptide-MHC: evidence for a general mechanism of molecular scanning. *Proc. Natl. Acad. Sci. USA* 96:11446–51
139. Garcia KC, Tallquist MD, Pease LR, Brunmark A, Scott CA, et al. 1997. αβ T-cell receptor interactions with syngeneic and allogeneic ligands: affinity measurements and crystallization. *Proc. Natl. Acad. Sci. USA* 94:13838–43
140. Willcox BE, Gao GF, Wyer JR, Ladbury JE, Bell JI, et al. 1999. TCR binding to peptide-MHC stabilizes a flexible recognition interface. *Immunity* 10:357–65
141. Wu LC, Tuot DS, Lyons DS, Garcia KC, Davis MM. 2002. Two-step binding mechanism for T-cell receptor recognition of peptide MHC. *Nature* 418:552–56
142. Baker BM, Turner RV, Gagnon SJ, Wiley DC, Biddison WE. 2001. Identification of a crucial energetic footprint on the α1 helix of human histocompatibility leukocyte antigen (HLA)-A2 that provides functional interactions for recognition by tax peptide/HLA-A2-specific T cell receptors. *J. Exp. Med.* 193:551–62
143. Baker BM, Ding YH, Garboczi DN, Biddison WE, Wiley DC. 1999. Structural, biochemical, and biophysical studies of HLA-A2/altered peptide ligands binding to viral-peptide-specific human T-cell receptors. *Cold Spring Harbor Symp. Quant. Biol.* 64:235–41
144. Wilson IA. 1999. Class-conscious TCR? *Science* 286:1867–68
145. Chlewicki LK, Holler PD, Monti BC, Clutter MR, Kranz DM. 2005. High-affinity, peptide-specific T cell receptors can be generated by mutations in CDR1, CDR2 or CDR3. *J. Mol. Biol.* 346:223–39
146. McCoy AJ, Chandana-Epa V, Colman PM. 1997. Electrostatic complementarity at protein/protein interfaces. *J. Mol. Biol.* 268:570–84
147. Rudd PM, Elliott T, Cresswell P, Wilson IA, Dwek RA. 2001. Glycosylation and the immune system. *Science* 291:2370–76
148. Mitra AK, Celia H, Ren G, Luz JG, Wilson IA, Teyton L. 2004. Supine orientation of a murine MHC class I molecule on the membrane bilayer. *Curr. Biol.* 14:718–24
149. Viola A. 2001. The amplification of TCR signaling by dynamic membrane microdomains. *Trends Immunol.* 22:322–27
150. Vogt AB, Spindeldreher S, Kropshofer H. 2002. Clustering of MHC-peptide complexes prior to their engagement in the immunological synapse: lipid raft and tetraspan microdomains. *Immunol. Rev.* 189:136–51
151. Berman HM, Westbrook J, Feng Z, Gilliland G, Bhat TN, et al. 2000. The Protein Data Bank. *Nucleic Acids Res.* 28:235–42
152. Bjorkman PJ, Saper MA, Samraoui B, Bennett WS, Strominger JL, Wiley DC. 1987. The foreign antigen binding site and T cell recognition regions of class I histocompatibility antigens. *Nature* 329:512–18
153. Hennecke J, Wiley DC. 2002. Structure of a complex of the human α/β T cell receptor (TCR) HA1.7, influenza hemagglutinin peptide, and major histocompatibility complex class II molecule, HLA-DR4 (DRA*0101 and DRB1*0401): insight into TCR cross-restriction and alloreactivity. *J. Exp. Med.* 195:571–81

154. CCP4. 1994. The Collaborative Computational Project Number 4, suite programs for protein crystallography. *Acta Cryst.* D50:760–63
155. McDonald IK, Thornton JM. 1994. Satisfying hydrogen bonding potential in proteins. *J. Mol. Biol.* 238:777–93
156. Sheriff S, Hendrickson WA, Smith JL. 1987. Structure of myohemerythrin in the azidomet state at 1.7/1.3 Å resolution. *J. Mol. Biol.* 197:273–96

Annual Review
of Immunology

Volume 24, 2006

Contents